

**A LASER-BASED ASSESSMENT OF ROAD CONSTRUCTION  
AGGREGATE SHAPE AND TEXTURE PROPERTIES AND THEIR  
RELATIONSHIP WITH MATERIAL SHEAR STRENGTH, A PILOT  
STUDY**

By

**I.J. Breytenbach**

**Thesis submitted in partial fulfilment of the requirements for the degree Doctor of  
Philosophy Scientia (Engineering Geology) in the Department of Geology, Faculty of  
Natural and Agricultural Sciences, University of Pretoria, South Africa**

**February 2016**

## Declaration

I, Izak Johannes Breytenbach, hereby declare that the work presented in this thesis is my own unless referenced otherwise. I also declare that this work has not been submitted at any other institute for any degree, examination or other purpose.

---

Signed

---

Date

## Abstract

Experimental research was undertaken to exploit the use of an innovative laser scanning tool and to apply the equipment to the study of (G1) road construction aggregate obtained from crushed rock quarry sources. The aim of the research was to better quantify particle shape and surface texture characteristics and an attempt was made to relate these to the shear strength properties of the materials investigated. By obtaining a better understanding of the effects that particle shape and texture have on the shear strength properties of a material, the overall efficiency of construction aggregate may be improved. Physical material properties and possible effects related to the (geological) origin of the materials were also considered.

In order to assess the particle data obtained from scan results, models were derived which could *sort individual particles in order, based on their shape and/or surface texture*. These models were created by experimental modelling of physical particle properties (i.e. dimensions, volume and surface area) obtained from scan results. A total of 1149 particles' scan data were collected. After experimentation, at least two working concept models were proposed using the scan data, one of which was ultimately abandoned as the model was affected by the elongation (i.e. shape) of particles. The second model proved to be better than the first and was further refined to develop a reference system for each particle size to enable comparison of particle textures.

After developing the comparative models described above, the *aggregate texture value (ATV)* was conceived and refined. A system was developed whereby an *aggregate texture value* was derived for the elongated and regular constituents of an aggregate sample, after separating particle data based on the particles' shape. The *aggregate texture value* weighed in the average model value calculated based on the grading analysis of a particular sample as well as the percentage of elongated particles in a specific size constituent of a sample.

The newly developed *aggregate texture value* was then related to limited tri-axial shear test results to establish whether there is a correlation between the parameter and the shear strength properties of the aggregate.

Findings indicate that the models developed and the newly derived *aggregate texture value* hold significant potential in better quantifying the shear behaviour of aggregates. While this research is based on a limited sample size and data, it is considered a pilot project and the preliminary results justify further, extensive data accumulation and model refinement.



## Acknowledgements

I would like to acknowledge the following people for contributions made to this research thesis:

- The Strategic Research Project, SRP TA 2011-001, *Improvement of pavement performance through better material characterisation using laser and numerical technologies*.
- Laboratory and technical staff of the Built Environment division at the CSIR, who assisted with material tests. The contributions of David Molebalo, Dave Ventura, Alan Crawford, Alfred Nkuna and Richard Mathibela are gratefully acknowledged.
- Melinda de Swardt, Daleen Hartmann, Cathy Barnard and Troné Stander at the University of Pretoria, for very effectively assisting with administrative issues.
- Julius Komba, for his valuable contribution and numerous (late night) discussions regarding our mutual interest in this research. You raised many ideas and assisted with numerous aspects such as literature research, data accumulation and scanning techniques/advice, to name but a few. Your insight and passion for your research is an inspiration to those around you.
- Dr Joseph Anochie-Boateng, for continued enthusiasm and thought-provoking conversations about the project.
- Prof Phil Paige-Green, for continued patience, input and advice despite significant pressures related to other obligations. Thank you for allowing me to benefit from your decades of experience and assisting in countless regards. Your contribution to our discipline is unequalled.

- Prof Louis van Rooy, for guidance, assistance and opportunities throughout my academic career and for contributions to the engineering geological profession in South Africa.
- Dr Robert Leyland for support, assistance and insight into many aspects of this research project, as well as sharing a general passion for engineering geology.
- Renet de Ridder for assistance with drawing and general support throughout the project, both professionally and personally.
- My family, for their support throughout the years. Thanks in particular to my parents (Frans and Mariette) for providing me with opportunities in life from which I could benefit. I hope that this thesis can in some small way serve as compensation for all you have done for me.
- Klem Carsten for motivation and support when it was needed most. Thanks Uncle Dad.
- My wife Anria, for her contribution and help with data processing. I also appreciate your continued support throughout the time it took me to complete this project and your patience when I spent late nights, weekends and holidays in the laboratory for months on end. You honour me with your devotion.

## Table of Contents

Declaration.....	2
Abstract.....	3
Acknowledgements.....	5
List of Symbols and Abbreviations.....	16
1. Introduction.....	17
1.1 Motivation for Research .....	17
1.2 Aim of Research .....	19
2. Literature Review.....	20
2.1 Flakiness Index .....	21
2.1.1 Flakiness Index Test Description.....	21
2.1.2 Criticism of the Flakiness Index .....	22
2.2 Effects of Particle Shape and Surface Texture .....	24
2.2.1 Particle Shape and Surface Texture .....	24
2.3 Inherent Influences on Particle Shape and Texture .....	26
2.3.1 Geological Origin.....	26
2.3.2 The Effects of Micro-cracking.....	29
2.4 External Influences on Particle Shape and Texture .....	30
2.4.1 Effects of Blasting.....	30
2.4.2 Pre-Crushing and Crushing.....	32
2.4.3 Grain Crushing.....	33
2.5 Advanced Methods of Assessing Particle Shape Properties.....	35
2.5.1 Angularity Index .....	36
2.5.2 Aggregate Imaging System.....	37
2.5.3 Image Analysis.....	38
2.5.4 Principal Component Analyses.....	39
2.5.5 Laser Profiling .....	40
2.5.6 Videographer - Shadowgraph .....	41
2.5.7 Videographer - Automation .....	43
2.5.8 Laser Scanning.....	43

3 Methodology .....	45
3.1 Introduction.....	45
3.2 Sample Selection.....	46
3.3 Sample Preparation .....	47
3.3.1 Concept of Sample Preparation for Laboratory Analyses .....	47
3.3.2 Synthesis of Samples One to Five .....	48
3.3.3 Synthesis of Sample Six.....	49
3.3.4 Microscope Thin Section of Fines Substitute Mixture .....	50
3.4 Laboratory Tests .....	51
3.4.1 Grading Analysis .....	51
3.4.2 Compaction Properties.....	52
3.4.3 Sample Preparation and Vibration Table Compaction .....	53
3.4.4 Multi-Stage Tri-axial Tests .....	55
3.4.5 Tri-axial Tests .....	57
3.5 Mineralogy Review.....	59
3.6 Laser Scanning.....	59
3.6.1 Equipment and Data Capture .....	59
3.6.2 Sample Selection for Scanning .....	60
3.6.3 Data Application and Processing.....	62
4. Results and Analysis .....	65
4.1 Laboratory Sample Preparation .....	65
4.1.1 Sample Synthesis .....	65
4.1.2 Control Grading .....	66
4.2.2 Particle Crushing.....	67
4.2 Practical Aspects Related to Particle Scanning .....	69
4.2.1 Advantages of Scanner System.....	69
4.2.2 Limitations of Scanner System .....	70
4.3 Model Development.....	71
4.3.1 Working Model One .....	73
4.3.2 Working Model Two.....	78
4.3.3 Comparison of Models.....	83
4.4 Detailed Models .....	86
4.4.1 Data Analyses .....	86

4.4.2 Model Development Procedure .....	90
4.5 Method Application .....	110
4.6 Influence of Different Material Types .....	124
4.7 Shear Strength Properties of G1 Aggregate .....	131
4.7.1 Tri-axial Tests .....	131
4.7.2 Mohr-Coulomb Failure Criteria and Mohr Circles .....	131
4.8 Comparison between Multi-Stage and Conventional Tri-axial Tests .....	142
5 Application .....	152
5.1 Model Application – Modified Dolerite .....	152
5.1.1 Flakiness Index .....	152
5.1.2 Particle Texture .....	154
5.2 Correlation Between Shear Strength Properties and Particle Properties .....	157
6 Conclusions and Findings .....	164
6.1 Particle Grain Crushing .....	164
6.2 Development and Application of Scanner-based Models .....	164
6.2.1 Scanner Properties and Attributes .....	164
6.2.2 Preliminary Models .....	165
6.2.3 Working Scanner-based Models .....	166
6.3 Flakiness Index .....	167
6.4 Shear Strength Properties .....	168
6.4.1 Shear Strength of Aggregate .....	168
6.4.2 Aggregate Texture Value and Shear Strength Properties .....	169
6.4.3 The Use of Multi-Stage Tri-Axial Tests .....	170
6.5 Final Conclusion .....	170
7 Recommendations and Further Work .....	172
7.1 Data Base Compilation .....	172
7.2 Flakiness Index .....	173
7.3 Aggregate Texture Value and Shear Strength Properties .....	173
7.4 Multi-Stage Tri-Axial Test Method .....	174
8 References .....	175

Addendum B: Thin Section Review of Rock Structures ..... 180

### **Addenda Included on Compact Disk:**

The following Addenda are contained on a compact disc is the rear cover of this thesis:

Addendum A: CSIR Laboratory Results for Bulk Sample Analyses

Addendum C: Scan Data (Rapidform Software required to view data)

Addendum D: Master Data Set

Addendum E: Data for “6.7mm Example”

Addendum F: Data for “9.5mm Example”

Addendum G: Data for “Tillite Comparison”

Addendum H: Data for *aggregate texture value* calculation

## List of Figures

Figure 2.1 Three shape parameters (after Anochie-Boateng <i>et al.</i> , 2011a) .....	26
Figure 2.2 Typical production procedure.....	31
Figure 2.3 Grain size distribution before and after compaction (Zeghal, 2009).....	34
Figure 2.4 Experimental equipment setup used by Fernlund (2005).....	38
Figure 2.5 Laser profiling setup used by Kim <i>et al.</i> (2003).....	40
Figure 2.6 The VDG40 scanning system (Descantes <i>et al.</i> , 2003).....	42
Figure 2.7 Laser scanning equipment up at CSIR (from Anochie-Boateng <i>et al.</i> , 2010) .....	44
Figure 3.1 Experimental procedure for laboratory tests .....	46
Figure 3.2 Vibration table equipment (Vibramech VT 600 – 550) .....	54
Figure 3.3 Tri-axial test equipment.....	56
Figure 3.4 Flow Chart of Tri-Axial Test Sample Preparation and Testing .....	58
Figure 4.1 Flattened particles with blind areas .....	71
Figure 4.2 Histogram (%) for regular particles (V/A) .....	87
Figure 4.3 Histogram (%) for elongated particles (V/A).....	88
Figure 4.4 Histogram (%) for regular particles' elongation .....	89
Figure 4.5 Histogram (%) for elongated particles' elongation .....	89
Figure 4.6 Particle ranges for 26.5 mm particles .....	125
Figure 4.7 Particle ranges for 19.0 mm particles .....	126
Figure 4.8 Particle ranges for 13.2 mm particles .....	127
Figure 4.9 Particle ranges for 9.5 mm particles .....	128
Figure 4.10 Particle ranges for 6.7 mm particles .....	129
Figure 4.11 Particle ranges for 4.75 mm particles .....	130
Figure 4.12 Mohr-Coulomb failure criterion for sample 1, quartzite .....	133
Figure 4.13 Mohr-Coulomb failure criterion for sample 2, granite .....	134
Figure 4.14 Mohr-Coulomb failure criterion for sample 3, quartz porphyry .....	135
Figure 4.15 Mohr-Coulomb failure criterion for sample 4, tillite.....	136
Figure 4.16 Mohr-Coulomb failure criterion for sample 5, hornfels.....	137
Figure 4.17 Mohr-Coulomb failure criterion for sample 6, dolerite.....	138
Figure 4.18 Mohr-Coulomb failure criteria at sample failure (after Craig, 1997)....	140

Figure 4.19 Comparative Mohr-Coulomb failure criteria for sample 1, quartzite....	144
Figure 4.20 Comparative Mohr-Coulomb failure criteria for sample 2, granite .....	145
Figure 4.21 Comparative Mohr-Coulomb failure criteria for sample 3, quartz porphyry.....	146
Figure 4.22 Comparative Mohr-Coulomb failure criteria for sample 4, tillite .....	147
Figure 4.23 Comparative Mohr-Coulomb failure criteria for sample 5, hornfels.....	148
Figure 4.24 Comparative Mohr-Coulomb failure criteria for sample 6, dolerite .....	149
Figure 5.1 Flakiness index vs. shear strength .....	161
Figure 5.2 Flakiness index vs. Internal Angle of Friction .....	163



## List of Tables

Table 2.1 Test requirements for flakiness index (from Method B3, THM1, 1986) ....	23
Table 3.1 Grading specification for G1 crushed stone base and sub-base (from COLTO, 1998).....	48
Table 3.2 Summary of scanned particles .....	61
Table 4.1 Sample grading (% passing sieve sizes) .....	65
Table 4.2 Grading comparison for sample 2 (granite).....	67
Table 4.3 Grading for samples before and after compaction and multi-stage tri-axial tests .....	68
Table 4.4 All 6.7 mm particles (V/A) × (EV).....	74
Table 4.5 Elongated 6.7 mm particles (V/A×EV) .....	76
Table 4.6 Regular 6.7 mm particles (V/A×EV).....	77
Table 4.7 All 6.7 mm particles (V/A).....	80
Table 4.8 Elongated 6.7 mm particles (V/A).....	81
Table 4.9 Regular 6.7 mm particles (V/A) .....	82
Table 4.10 Method comparison for regular 6.7 mm particles.....	84
Table 4.11 Method comparison for elongated 6.7 mm particles .....	85
Table 4.12 Particle selection for 9.5 mm model .....	92
Table 4.13 Model for regular 9.5 mm particles .....	93
Table 4.14 Model for elongated 9.5 mm particles .....	94
Table 4.15 Particle selection for 4.75 mm model .....	95
Table 4.16 Model for regular 4.75 mm particles .....	96
Table 4.17 Model for elongated 4.75 mm particles .....	97
Table 4.18 Particle selection for 6.7 mm model .....	98
Table 4.19 Model for regular 6.7 mm particles .....	99
Table 4.20 Model for elongated 6.7 mm particles .....	100
Table 4.21 Particle selection for 13.2 mm model .....	101
Table 4.22 Model for regular 13.2 mm particles .....	102
Table 4.23 Model for elongated 13.2 mm particles .....	103
Table 4.24 Particle selection for 19.0 mm model .....	104
Table 4.25 Model for regular 19.0 mm particles .....	105

Table 4.26 Model for elongated 19.0 mm particles .....	106
Table 4.27 Particle selection for 26.5 mm model .....	107
Table 4.28 Model for regular 26.5 mm particles .....	108
Table 4.29 Model for elongated 26.5 mm particles .....	109
Table 4.30 Summary of representative particle selection for tillite.....	111
Table 4.31 Regular particles comparison for 26.5 mm tillite .....	112
Table 4.32 Elongated particles comparison for 26.5 mm tillite.....	113
Table 4.33 Regular particles comparison for 19.0 mm tillite .....	114
Table 4.34 Elongated particles comparison for 19.0 mm tillite.....	115
Table 4.35 Regular particles comparison for 13.2 mm tillite .....	116
Table 4.36 Elongated particles comparison for 13.2 mm tillite.....	117
Table 4.37 Regular particles comparison for 9.5 mm tillite .....	118
Table 4.38 Elongated particles comparison for 9.5 mm tillite.....	119
Table 4.39 Regular particles comparison for 6.7 mm tillite .....	120
Table 4.40 Elongated particles comparison for 6.7 mm tillite.....	121
Table 4.41 Regular particles comparison for 4.75 mm tillite .....	122
Table 4.42 Elongated particles comparison for 4.75 mm tillite.....	123
Table 4.43 Load summary for Mohr circles .....	132
Table 4.44 Summary of shear strength properties deduced from Mohr circles.....	139
Table 4.45 Summary of calculated values and graph values of shear strength parameters .....	141
Table 4.46 Shear strength of samples (at approximately 41 kPa confining pressure) .....	142
Table 4.47 Comparative Summary of shear strength properties deduced from Mohr circles .....	150
Table 4.48 Comparative Shear strength of samples (approximately 41 kPa confining pressure).....	151
Table 5.1 Derivation of the flakiness index using scan data (dolerite).....	154
Table 5.2 Analysis of dolerite sample.....	156
Table 5.3 Shear strength data considered for analysis.....	159
Table 5.4 Summary data for correlation analysis .....	160
Table 5.5 Correlation matrix of test parameters (assuming flakiness index of bulk samples) .....	160

## List of Equations

$\tau = c + \sigma_n \tan \phi$ (Equation 2.1) .....	20
$\tau = \sigma_n \tan \phi$ (Equation 2.2) .....	21
Flakiness Index = $(M_p / M_t) \times 100$ (Equation 2.3) .....	22
$ARD_{Total} = (ARD_{Sample} \times \% \text{ aggregate}) + (ARD_{Quartzite} \times \% \text{ crusher dust})$ ..... (Equation 3.1)	52
$BRD_{Total} = (BRD_{Sample} \times \% \text{ aggregate}) + (BRD_{Quartzite} \times \% \text{ crusher dust})$ (Equation 3.2)	53
Elongation Value = $(\text{Width}) / (\text{Depth})$ (Equation 3.3) .....	63
Elongation Value = $(D_l) / (D_s)$ (Equation 3.4) .....	63
Model Value = $(\text{Volume} / \text{Area}) \times \text{Elongation Value}$ ..... (Equation 4.1)	73
Model Value = $\text{Volume} / \text{Area}$ (Equation 4.2).....	78
$\sigma_1 = \Delta \sigma_1 + \sigma_3$ (Equation 4.3) .....	131
$\tau = c + \sigma_n \tan \phi$ (Equation 4.4) .....	140
$\tau_f = \frac{1}{2}(\sigma'_1 - \sigma'_3) \sin 2\theta$ (Equation 4.5).....	140
$\sigma'_f = \frac{1}{2}(\sigma'_1 + \sigma'_3) + \frac{1}{2}(\sigma'_1 - \sigma'_3) \cos 2\theta$ (Equation 4.6).....	140
$\theta = 45^\circ + (\phi'/2)$ (Equation 4.7) .....	141
Aggregate texture value = $\sum (\text{Weighted } V/A) \times (\% \text{ of Fraction}) \times \text{Grading}$ (Equation 5.1) .....	155

## List of Symbols and Abbreviations

10 % FACT	10 % Fines Aggregate Crushing Value
ACV	Aggregate Crushing Value
AI	Angularity Index
AIMS	Aggregate Imaging System
ARD	Apparent Relative Density
ATV	<i>Aggregate Texture Value</i>
BRD	Bulk Relative Density
c	Cohesion
CSIR	Council for Scientific and Industrial Research
DIT	Digital Image Technology
EV	Elongation Value
FI	Flakiness Index
LASS	Laser-based Aggregate Scanning System
MDD	Maximum dry density
OMC	Optimum moisture content
$\tau$	Shear strength
$\tau_f$	Peak shear strength
$\sigma_1, \sigma_3$	Principal stresses
$\sigma_n$	Normal stress
$\sigma_f$	Normal stress upon sample failure plane
$\phi$	Friction angle

# 1. Introduction

## 1.1 Motivation for Research

At present the Standard Specifications for Road and Bridge Works for State Road Authorities, COLTO (1998), which is used in the South African road construction industry, makes little direct provision for assessing the *surface properties of crushed rock materials* which may affect the material's *shear strength properties*. The material specification for G1 aggregate is summarised on Table 3602/1 (page 3600-2) of COLTO (1998) and makes reference to only two attributes related to particle shape or texture:

- Flakiness Index: “*Flakiness index, determined in accordance with TMH1 method B3, shall not exceed 35 on each of the -26,5 + 19 mm fraction and the -19 + 13,2 mm fraction.*”
- Fractured Faces: “*All faces shall be fractured faces.*”

To date the shortcomings of assessing particle shape and texture properties comprehensively have been emphasised by many authors and the difficulty of deriving a single parameter to quantify these properties has been emphasised (e.g. Semmelink, 1991). This has specific reference to crushed rock materials to be utilised for base (or even sometimes sub-base material) in road construction. The COLTO (1998) specifications make provision for the shape of the aggregate (in terms of the flakiness index) as well as crushing properties of the aggregate material, such as aggregate crushing value (ACV) and 10 % Fines Aggregate Crushing Value (10 % FACT). Criticism has been raised, however, against the conventional means of assessing the plate-based flakiness index (Anochie-Boateng, 2010; Fernlund, 2005). The fundamental problem seems to stem from the fact that to date new methods or equipment have not been able to effectively refine or study the particle texture and/or shape properties.

In addition, no consideration is given to the impact the crushing equipment or process used in the quarry for production of the aggregate has on the surface texture of the

rock aggregate or the relationship between this and the performance of the material in roads, both during construction and in-service. The main reason for this is the difficulty in quantifying surface texture, an issue which appears to plague the industry on a worldwide level. With all of the above in mind, it is clear that there is a lack of comprehensive quantification and/or evaluation of the surface textural properties of a material used in road layer works, more specifically, crushed rock aggregates.

Assessment of the shear strength properties of construction materials has also been somewhat limited to date. This is largely due to the fact that the shear strength properties of any given aggregate will be affected by the shape and texture of the particles making up the sample. Equipment for quantifying the shear strength of aggregate materials is also of limited availability. This research therefore seeks to address both issues by investigating particles properties and shear strength properties with the aid of new equipment.

In order to address the shortcomings described above, a new approach was developed towards assessing crushed rock aggregate used for G1 material in road construction in South Africa. *The motivation behind the research was to develop an accurate method of assessing particle shape and texture properties*, which has not been achieved in the South African industry before. Experimental research was undertaken to determine whether a new approach could be developed which was successful or promising enough to justify the pursuit of further, extensive research. The research was further expanded to determine whether the newly derived method could be related to the shear strength properties of the G1 materials, with *the motivation being that a better understanding of shear strength properties would improve pavement engineering*.

This research overlaps and shares interests with a number of current research projects being conducted by the Council for Scientific and Industrial Research (CSIR) in South Africa, utilising a new and innovative three dimensional laser-based scanning system to study the shape and surface properties of construction materials. The research carried out here, as well as associated research being conducted by the CSIR, share a number of common goals and utilise some of the same bulk crushed rock material samples.

## 1.2 Aim of Research

A number of primary and secondary objectives are to be achieved during this research which can be summarised as follows:

- **Primary objectives:**
  - The application of a new laser-based scanner to quantify aggregate particle surface texture and shape properties and *sort particles based on these properties*. This objective, if successful, should improve the current lack of detailed assessment of particle shape and surface texture properties in the South African industry.
  - The derivation of a *single descriptive parameter* which can classify a given aggregate sample material, based on its particle shape and surface texture.
  - Assessing the relationship (if any) between the above-mentioned parameter and the shear strength properties (derived from tri-axial shear tests) of the aggregate.
  
- **Secondary objectives:**
  - Identifying and applying the main advantages of the new laser-based scanning method.
  - The compilation of comparative models which can be used to evaluate or compare any given aggregate particle (in a specified size range).
  - Assessment of particle crushing during compaction.
  - Comparing multiple-stage tri-axial test results with conventional static (i.e. single-load) tri-axial test results and assessing the main differences and limitations of the multi-stage method.

## 2. Literature Review

Existing literature sources outlining experimental methods to determine particle shape or texture characteristics of aggregate materials are reviewed. Although the majority of these methods are only briefly described a range of aggregate properties which may affect the shape and texture properties of the crushed aggregate materials tested are identified.

In essence, the strength of an aggregate material used in road layer-work construction can be related to its shear strength properties (in combination with its compacted density and prevailing moisture content). Adequate shear strength is required to ensure satisfactory performance of aggregate in layer works (Maree, 1979). The shear strength properties are related to Coulomb's Law, as applied to general soil mechanics and is discussed extensively by Cernica (1982). The shear strength of a material, as described by the Mohr-Coulomb failure criteria, can be calculated as indicated in Equation 2.1:

$$\tau = c + \sigma_n \tan \phi \quad (\text{Equation 2.1})$$

where

$\tau$  = shear strength

$c$  = cohesion

$\sigma_n$  = normal stress at sample failure

$\phi$  = internal friction angle

Considering the nature and composition of a crushed rock aggregate material, one would expect that such a material would have very little or no cohesion, though this is seldom the case in reality. Subsequently the shear strength would therefore largely be a function of the friction angle at a specific normal load (not considering the effects of confining pressure). The material properties affecting the strength of a crushed rock aggregate can therefore be fundamentally simplified to those properties affecting only the friction angle as shown below.



$$\tau = \sigma_n \tan \phi \quad (\text{Equation 2.2})$$

where

$\tau$  = shear strength

$\sigma_n$  = normal stress at sample failure / on the failure plane

$\phi$  = internal friction angle

These properties are a function of both the material type and the crushing process.

## 2.1 Flakiness Index

### 2.1.1 Flakiness Index Test Description

Requirements for G1 base material sourced from crushed rock are comprehensive. One of the requirements in the COLTO (1998) specification is that a potential material should have a flakiness index below 35 % for the fractions -26.5 mm to 19.0 mm and -19.0 mm to 13.2 mm. In this research the term *flakiness index* is as applied in the South African context and determined using the plate-based method described by method B3 of the TMH1 (1986) technical specification, also referred to by the COLTO (1998) specification. Also, the requirements state that all faces of aggregate must be fractured faces and the material should be sourced from a sound rock source (i.e. approved quarry), clean and sound mine dump rock or clean and sound boulders. In terms of aggregate shape or texture, only the flakiness index is specified in the listed requirements. The flakiness index of a material has a significant effect on its constructability and properties. The requirement for fractured faces is to ensure an adequate roughness of the aggregate surface, which contributes to the shear strength of the material in service.

The flakiness index is determined by test method B3 described in the 1986 TMH1 (now replaced by SANS 3001-AG4: 2009), as applied to coarse aggregate materials. The said method states the following definition of the flakiness index:

*“The Flakiness Index of a coarse aggregate is the mass of particles in that aggregate, expressed as a percentage of the total mass of that aggregate, which will pass the slot or slots of specified width for the appropriate size fraction, as given in Table 1 below. The width of the slots is half that of the sieve openings through which each of the fractions passes”.*

Mathematically the flakiness index is calculated as follows:

$$\text{Flakiness Index} = (M_p / M_t) \times 100 \quad (\text{Equation 2. 3})$$

where

$M_p$  is the total mass of aggregate passing the slots

$M_t$  is the total mass of the test sample

The flakiness index is determined for the particle sizes indicated in Table 2.1. The remainder of the material larger or smaller than the fraction concerned is screened out (by sieve screening) and discarded. SANS 3001-AG4: 2009 follows a similar method, but sieve sizes have been modified to the new standard sieve sizes prescribed in the SANS 3001 test series.

### *2.1.2 Criticism of the Flakiness Index*

The main motivation for developing alternative methods of assessing particle shape and texture characteristics is that the flakiness index on its own is deemed – in essence – too empirical and simple (Anochie-Boateng *et al.*, 2011a). Lees (*in* Semmelink, 1991) also advises that a limit or specification for the flakiness index should not be applied for specific purposes without considering the distribution of its dimensions. This is further supported by Semmelink (1991), who recommends that the flakiness index should be considered in conjunction with properties such as maximum particle size and the material grading.

**Table 2.1** Test requirements for flakiness index (from Method B3, THM1, 1986)

1		2	3	4	5
Size of fraction to be gauged (sieve size) (mm)		Retained	Minimum length of slot (mm)	Width of slot (subject to a tolerance of 0,10 mm) (mm)	Appropriate mass of test sample passing sieves in Column 1 (kg)
Passing					
75.0	63.0		150.0	37.5	5
63.0	53.0		126.0	31.5	5
53.0	37.5		106.0	26.5	5
37.5	26.5		75.0	18.75	5
26.5	19.0		53.0	13.25	4
19.0	13.2		38.0	9.5	3.5
13.2	9.5		26.4	6,6	2
9.5	6.7		19.0	4.75	1
6.7	4.75		13.4	3.35	0.5

In addition to the above, the test methods involved are subjective, time-consuming, labour-intensive and show poor repeatability (Anochie-Boateng *et al.*, 2010). The current procedure of using a screened sample is plagued by the fact that the sieve screen analysis results (and therefore the material fractions used for the test) are affected by the particle shape itself (Fernlund, 2005). For example, an elongated particle may pass through a specific screen in a vertical orientation, but be retained if it is orientated horizontally.

A literature review by Rao *et al.* (2003) concluded that past research has not considered the difference between angularity and surface texture, but rather simplified the shape properties of materials. Rao *et al.* (2002), for example, developed the Angularity Index which can apparently distinguish crushed stone from gravel sources during processing. Their research identified a relationship between the Angularity Index and the friction angle of a material, where an increase in the Angularity Index corresponds to an increase in the friction angle.

Whilst it is unanimously supported that shape properties of particles should be considered (Räisänen and Mertamo, 2004), it is argued that mechanical tests simply do not describe the material behaviour unambiguously. A number of technical or procedural shortcomings were identified as far as the flakiness index is concerned. Among these is that particles with a flat shape may become segregated within the sample itself, resulting in unrepresentative results or that particles may pass through the crusher without being crushed due to their “flaky” shape (Räisänen and Mertamo, 2004). This may present a massive misrepresentation of a material’s quality when considering in addition, that thin or elongated particles break more easily than, for example, cubical particles (Miskovsky *et al.*, 2004). Other research also states that an increase in flakiness index is associated with a decrease in tensile strength and that variation in the flakiness indices are related to the type of crusher used (Ling *et al.*, 2010). Although this may seem valid and even logical, the statement is not substantiated and it seems particularly over-simplified.

## **2.2 Effects of Particle Shape and Surface Texture**

### *2.2.1 Particle Shape and Surface Texture*

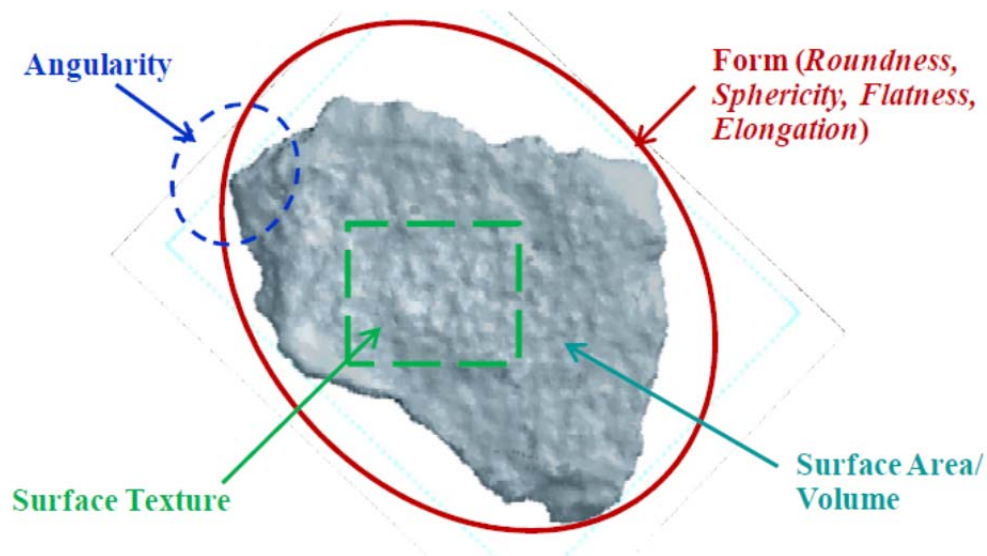
In the South African context there is a distinct preference to exploit sources of hard bedrock for crushing and production of high quality aggregate. In contrast to this, Descantes *et al.* (2006) for instance state that 40 % of annual aggregate production in France is sourced from alluvial deposits which are processed (i.e. crushed) in order to produce more angular material. The preference for angular materials is related directly to their performance under shear (i.e. shear strength). This is supported by Semmelink (1991) which states that at the same porosity, so-called “angular” materials have superior strength to rounded or sub-rounded materials, but that compacting the former also requires more effort.

The particular shape and size of an aggregate particle affects the strength and performance of road layer works (Rao *et al.*, 2002; Semmelink, 1991). The angularity and texture of aggregate influence the shear strength, with the general assumption being that an increase in angularity and texture results in an increase in particle

interlock and also improves load transfer through the aggregate (Rao *et al.*, 2002; Rao *et al.*, 2003). Semmelink (1991) stated that the shape and texture properties which result in a resistance to shearing, subsequently also increase the resistance to compaction. This also applies to the use of aggregate in concrete, where the aggregate cannot simply be considered to be an inert filler material (Dunlevey and Stephens, 1996), but contributes to the overall strength.

It is clear from the above that crushed bedrock is preferred to rounded alluvial materials. Rough and angular materials provide better shear strength than rounded or smooth materials (Rao *et al.*, 2002). Whilst the particle shape and texture appear to be dominant factors dictating aggregate strength, it is often oversimplified by the assumption that a very angular material with coarse texture will produce a high quality aggregate (Ling *et al.*, 2010) without considering other influencing parameters (e.g. secondary minerals, degree of weathering, rock strength, etc.).

Anochie-Boateng and Komba (2010) indicated that a rough aggregate surface and large specific surface area are preferred for asphalt aggregate to elongated, rounded or smooth aggregate. This seems to make sense as a rough surface would increase shear resistance and an increase in surface area would further increase the shear resistance. Recent work by Anochie-Boateng *et al.* (2011a) on the use of three dimensional (3D) laser scanning technology to determine the flakiness index of aggregates concluded that there is a need for accurate and automated procedures to determine flakiness index of aggregates used in roads. They indicated that human errors associated with the traditional methods to accurately quantify and analyse aggregate shape properties could be reduced. Anochie-Boateng *et al.* (2011a) described three shape parameters, namely particle form, particle angularity and particle surface texture, as shown in Figure 2.1.



**Figure 2.1** Three shape parameters (after Anochie-Boateng *et al.*, 2011a)

## 2.3 Inherent Influences on Particle Shape and Texture

The apparent oversimplification of particle shape parameter determination has become the focus of numerous research projects in recent times. This section discusses some of the influencing parameters when considering the particle shape and texture of aggregate. Emphasis will be placed on material properties in this section, whilst the following section will discuss external influences.

### 2.3.1 Geological Origin

In the modern aggregate industry, the effects of geological parameters are often underestimated or even disregarded entirely. This has been mentioned by Tons and Goetz (1967) who studied different materials (e.g. rounded gravel, slag, crushed limestone, etc.) with similar grading properties. Discussions of a number of

parameters and effects related specifically to geology follows, but the effects of cracking or micro-cracking are not included and are discussed in a separate section.

Perhaps one of the most critical aspects often overlooked when considering potential sources of material for aggregate production is the geological origin of the material. Quite simply all rock materials cannot be considered to be similar. Even the same rock type occurring at two different localities may differ, sometimes fundamentally, depending on the geological formation, placement, crystallisation (e.g. fine-grained vs. coarse-grained) and any later structural or metamorphic effects. This can be illustrated by considering tillite occurring at two different localities, deposited under similar sedimentological processes (Dunlevey and Stephenson, 1995). The behaviour of the two materials may prove to differ fundamentally (when the matrix and inclusions in the tillite are different) due to the subsequent difference in physical properties.

The geological nature of the material also affects the ultimate outcome of blasting during production, a matter often overlooked when planning blasting operations (Räisänen and Mertamo, 2004). The authors emphasised that the texture, mineralogy, joints and micro-cracks affect the outcome of blasting and ultimately also influence the crushing properties of the material. This is supported by Miskovsky *et al.* (2004) who state that the mechanical properties of a material are a function of the rock mineralogy, structure, texture, grain size, grain boundaries and micro-cracks. Mineralogy and mineral fabric are listed as affecting parameters by Dunlevey and Stephens (1996), although this was specifically for aggregates used in concrete. It was noted by the same authors during earlier research that the flakiness index of metamorphosed materials tends to increase due to anisotropic stress fields experienced by the rock mass during metamorphism (Dunlevey and Stephens, 1994).

Weinert (1980) placed emphasis on mineralogical properties and indicated that apart from the mineral composition, the size, shape, arrangement (i.e. interlock) and bond between minerals all affects the nature of the rock material. He found that the bond between minerals affect the overall rock strength and on a macro scale rock chemistry, rock structure, rock texture, the effects of stratification and rock deformation (e.g. folding or faulting) have significant influences. Finally, Weinert

(1980) observed that coarse-grained rock materials disintegrate more easily – by means of both weathering and crushing – than finer grained rock materials.

Geological parameters are also regarded as the determining factor in material strength and mechanical properties in hard, unweathered rock. Räsänen and Mertamo (2004) considered a granitic example where the strength of the material is affected by the distribution of dark minerals, the material grain size, the rock body's massive texture, intergrowth in the rock texture, complex grain boundaries, the modal composition, alteration and a lack of micro-cracks. The authors discussed the effects of alteration as a positive attributing factor, in that it may overgrow mineral cleavages and minor cracks, thereby reducing preferential cracking along these planes and effectively increasing the cohesion between mineral grains.

Other case-specific studies have also been conducted which show apparent correlations between geological properties and material performance. A number of examples follow:

- Miskovsky *et al.* (2004) found that an increase in feldspar content in granitoid aggregate samples investigated corresponded to a decreased strength against impact. They also found that the resistance to mechanical impact increases with an increased mica content, diminishing grain size and irregular grain boundaries.
- Ling *et al.* (2010) studied properties of basalt, limestone, granite and gneiss. They stated that physical properties of the aggregate are improved by abundant fine to medium mineral grains, emphasising the role of quartz and feldspar (which contradicts Miskovsky *et al.*, 2004). Interlocking grain boundaries and intergrowth are also listed as positive attributes. The authors singled out schistose layers as a possible contributor resulting in an increased flakiness.
- The depositional environment of sedimentary (and some metamorphic) materials was discussed by Dunlevey and Stephens (1994). They found that alternating bands within sandstone were variable and that lenses of shale also occurred, which is not uncommon in sedimentary materials. The authors continued to discuss the effects of metamorphism on sandstone material and



found that certain grains may be completely destroyed by metamorphism and grains may be homogenised by recrystallization. The latter even occurred in the pore spaces of the original material. Their findings indicated that metamorphism not only modified the mineralogy of the metamorphosed material, but effectively fuses or “welds” mineral grains together.

- Dunlevey and Stephens (1995) also studied tillite materials and concluded that variability occurs due to differences in mineralogy, weathering and the material’s diagenetic history.

### 2.3.2 *The Effects of Micro-cracking*

Mgangira (2008) discussed the importance of a material’s micro-structural character. The majority of literature in this regard concentrates on the effects of micro-cracks or micro-fractures. The occurrence of micro-cracking may result from a number of events, both natural and otherwise. With specific reference to crushed aggregate, the latter is mostly associated with the effects of blasting, which is a science of its own, as well as localised stresses resulting from the crushing process.

The formation of micro-cracks originating from natural causes may find its origin in a number of ways, mostly as a result of the rock material experiencing some form of stress. For example, stress-related micro-cracks may result from tectonic or intrusive events, rapid magma cooling or metamorphic deformation. The implications of micro-cracks, however, have considerable consequences for a proposed source of crushed aggregate if the micro-cracking is well manifested.

The general consensus is that an increase in micro-cracks results in a decreased material strength (Miskovsky *et al.*, 2004; Kujundžić *et al.*, 2008; Weinert, 1980; Räisänen and Mertamo, 2004). In essence the micro-cracks prevailing within the rock present a preferred route along which a material will break during blasting or crushing as described by Griffith’s crack theory (Griffith, 1921); hence the more micro-cracks present, the better the chances of material breakage or crack formation/propagation.

Considering the above, one might speculate that theoretically, the occurrence of micro-cracks may induce elongated aggregate. Bedrock subjected to deformation by, for example, the intrusion of an adjacent dyke may experience preferential stress-orientated micro-cracking which may be similarly orientated (due to the stresses and deformation associated with the force of the intruding body). Upon processing, the rock material would then show preferential breakage along these orientated micro-cracks resulting in aggregate particles that are elongated.

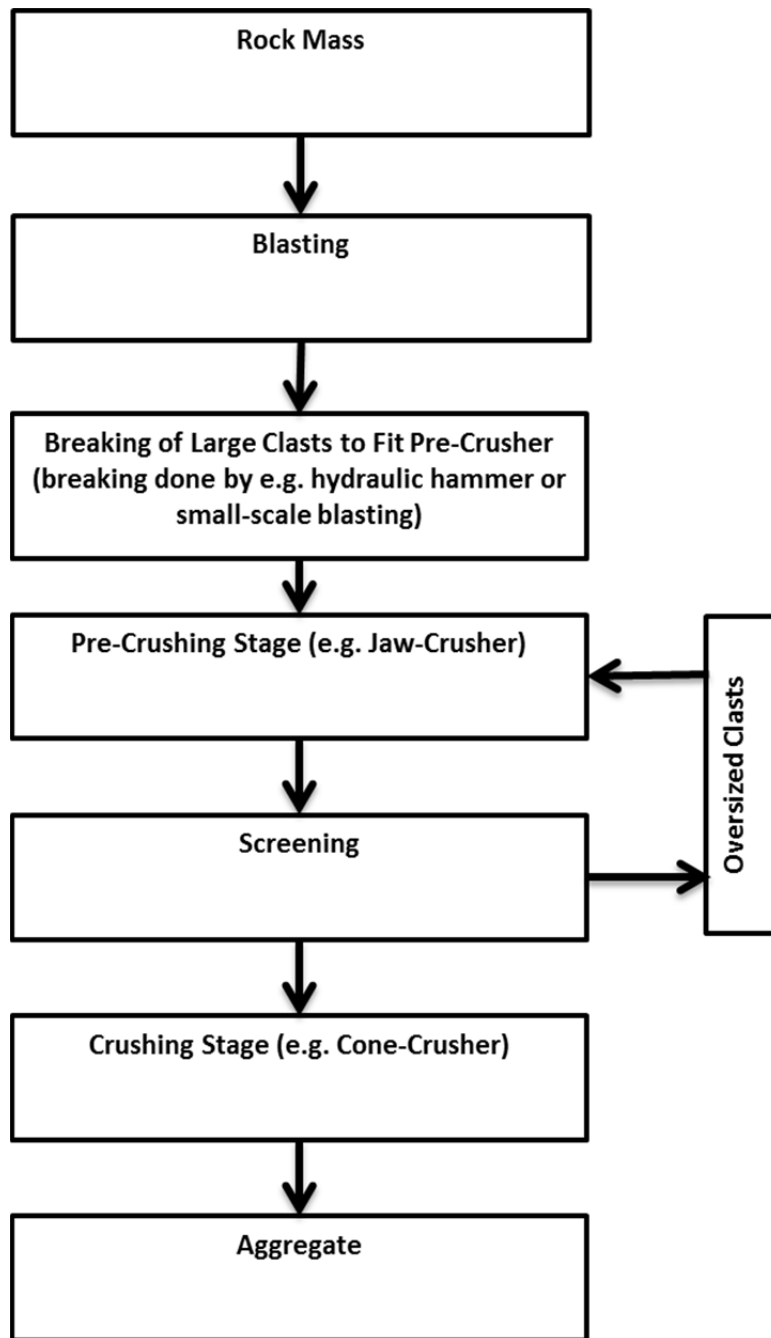
It is also logical that in an unweathered rock mass, the micro-cracks would present a preferred area for chemical decomposition to commence, resulting in enhanced weathering along the joints. However, the opposite also applies in that such micro-cracks would present the most likely place where alterations, recrystallization or hydrothermal activity would occur. Whilst these features will still be weaker than unweathered bedrock, they will be more competent than open cracks.

## **2.4 External Influences on Particle Shape and Texture**

Factors other than the rock material which affect the particle shape characteristics are mostly associated with aggregate production. Whilst the exact procedure and number of crushing stages may vary, Figure 2.2 illustrates the typical production procedure followed in an aggregate production plant

### *2.4.1 Effects of Blasting*

Blasting is one of a few external influences that affect the particle shape and texture, other than the crushing procedure itself. Blasting is a science in its own right, but has a profound effect on the mechanical properties of aggregate produced (Kujundžić *et al.*, 2008). In general an increase in the amount of explosives and an increase in detonation speeds correspond with a reduction in a rock material's resistance to crushing and fragmentation (Kujundžić *et al.*, 2008).



**Figure 2.2** Typical production procedure

Kujundžić *et al.* (2008) stated that blasting of bedrock effectively fragments the material by seismic wave movement through the medium. The aim of blasting is to fragment the bedrock into pieces that would fit pre-crusher equipment (Räisänen and Mertamo, 2004) without requiring expensive additional (secondary) breaking.

The rock hardness determines the required fragmentation energy (Kujundžić *et al.*, 2008) and according to Räsänen and Mertamo (2004) some rock materials sustain more stress than others. The impact of blasting is two-fold; firstly blasting determines the aggregate size distribution of the blasted material (i.e. the size of broken rock) and secondly, blasting induces micro-cracks in the broken rock pieces (Kujundžić *et al.*, 2008). Excessive blasting, or “over-blasting”, results in excessive fine material and unnecessary micro-cracks (Räsänen and Mertamo, 2004), as well as the propagation of existing micro-cracks (Miskovsky, 2004). Considering the effects of micro-cracks discussed in section 2.3.2 it is sensible then that the minimum blasting energy be used to achieve fragmentation in order to prevent excessive micro-cracking (Kujundžić *et al.*, 2008).

#### 2.4.2 Pre-Crushing and Crushing

As mentioned at the beginning of section 2.4, rock blasting is followed by processing of the fragmented rock mass. Whilst the procedure and number of stages may vary between different producers, blasting and material extraction from the blast area is usually followed by pre-crushing; however not all the clasts fragmented by blasting necessarily fit the pre-crusher or crusher. The various crushing procedures greatly affect the shape and mechanical properties of the final aggregate produced (Ling *et al.*, 2010).

Generally there are two methods of reducing the size of blast spoils to fit pre-crushing. Whilst small scale blasting is sometimes used, hydraulic hammers are also used frequently to reduce the size of oversized blast spoils. Kujundžić *et al.* (2008) studied the effects of jaw crushing equipment and hydraulic hammers. They concluded the following:

- The hardness of a rock material affects the required crushing energy of a hydraulic hammer more than that of crushing equipment
- Harder rock materials require *less* impact energy for fragmentation than softer materials. This is ascribed to the fact that hard or brittle materials have lower resistance to impact stresses

- Crushing energy required by a jaw-crusher to crush a material is not strongly correlated to the material hardness
- Softer materials are subject to plastic deformation under crushing

Räisänen and Mertamo (2004) also assessed crushing of raw materials, but placed more emphasis on crushing equipment, the relationship between different crushing equipment and crushing procedures than Kujundžić *et al.* (2008). They concluded the following:

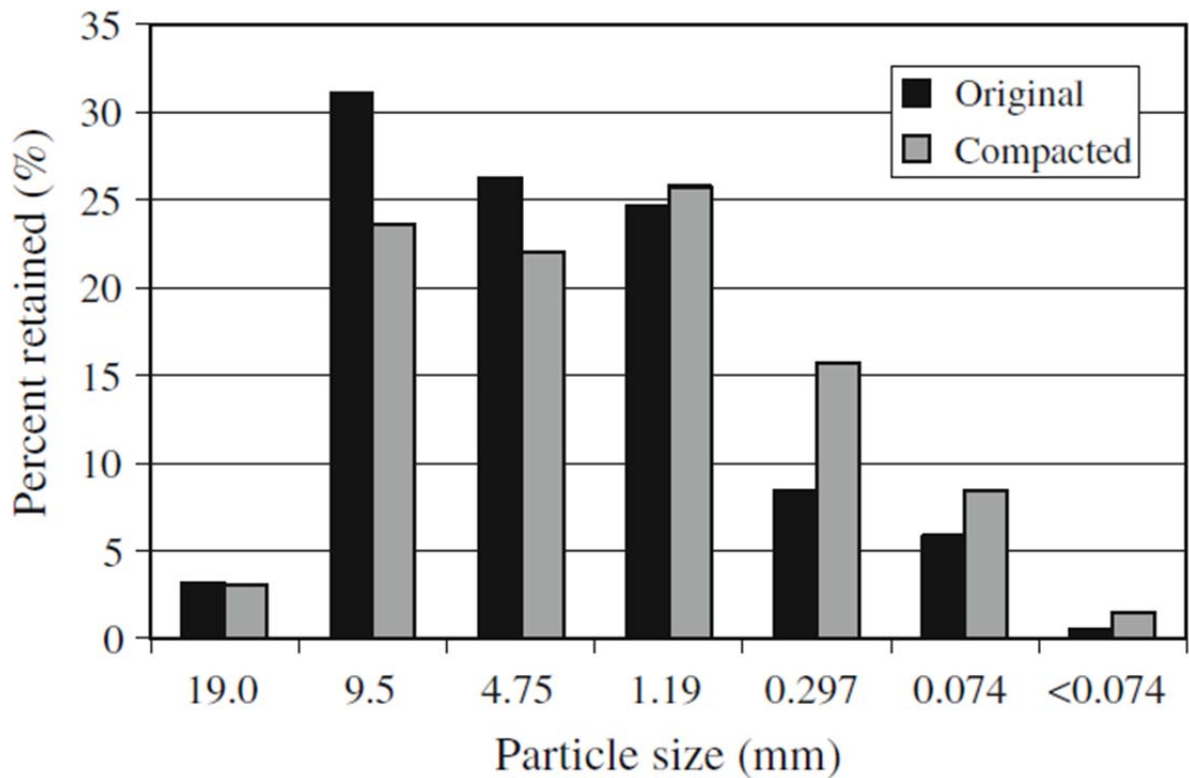
- The longer rock particles are abraded (i.e. crushed) in a crusher, the smoother the aggregate surfaces
- Jaw crushers are better suited for pre-crushing, whilst cone crushers are better suited for later stages of crushing
- Cone-crushers are perhaps more suited for use in laboratory crushing than jaw-crushers
- There is no apparent correlation between the production of laboratory crushers (i.e. jaw-crushers) and industrial, multi-stage crushers
- The resulting particle shape of aggregate depends significantly on the crusher used to produce the aggregate. This results in unreliable data when crushing material with a different crusher to that which is ultimately used in production
- Laboratory crushers tend to produce aggregate with favourably shaped clasts, thereby producing a favourable bias in test results

With the above in mind, it is a known fact in the industry that the shape of aggregate particles can be adjusted almost *ad infinitum* by selecting appropriate crusher types or methods (e.g. choke feeding). For example, vertical shaft impact crushers are often used to ensure that well-shaped aggregate is produced.

### 2.4.3 Grain Crushing

Grain crushing or breakage occurs when a particle breaks under applied shear or compression, which overcomes the material's strength. The process discussed here applies specifically to such breakage during the process of compaction (Zeghal,

2009), i.e. during construction of layer works as opposed to the crushing process discussed in section 2.4.2. Evidence of this was discussed by Zeghal (2009) when investigating material grading before and after construction compaction. A summary of Zeghal’s screen analyses before and after compaction clearly illustrates the alteration in grading due to grain crushing, as depicted in Figure 2.3.



**Figure 2.3** Grain size distribution before and after compaction (Zeghal, 2009)

It is for these reasons that standard specifications for the grading of aggregates are based on the particle size distribution after construction to ensure that the optimum grading in terms of the Fuller-Talbot curves are obtained.

The effects of grain crushing have far reaching consequences, in that they reduce a material’s resilient modulus, thereby increasing permanent deformation (Zeghal, 2009). The particle breakage which occurs during grain crushing could ultimately

result in rutting and compromises the expected service life and carrying capacity of a road (Zeghal, 2009).

According to Arslan *et al.* (2009), particle crushing is the result of confining stress and deformation processes. Particles tend to break when the stresses imposed (e.g. by compaction equipment) exceed the material's indentation strength, threshold abrasive hardness or tensile strength. Of these factors, the authors highlight that particles are often crushed under a critical load which sees tensile failure of the particle. This results in a non-constant volumetric strain when a material is placed under large shear, due to particles crushing, resulting in non-linear Mohr-Coulomb envelopes. Simply stated, the friction angle at high stresses tends to be lower than expected (Arslan *et al.*, 2009). Zeghal (2009) further stated that particle breakage increases with an increase in grain size, angularity, confining pressure and shear stress.

## **2.5 Advanced Methods of Assessing Particle Shape Properties**

The general consensus in industry and research circles is that particle shape and surface texture properties have not been studied or analysed with sufficient precision; however, it is likely that this has been the result of limited suitable methods or equipment being available to achieve this objective. Many authors and researchers have proposed new parameters, indices and equipment which attempt to quantify particle shape and texture properties with varying degrees of success.

The technological advances in recent decades have resulted in many attempts being made to refine the assessment of particle shape properties. In the past decade in particular, methods of automated visual and digital processing have been developed. While these methods add more detail to current approaches, a common drawback in all these methods used is that the scanning procedures are extremely time-consuming and mostly labour-intensive. Whilst the majority of the methods seem promising, the application of some of the proposed technologies to scan aggregate in the volumes produced commercially seems highly unlikely.

Nevertheless, following in this section is a summary of some methods encountered in recent literature which have a common approach or purpose to the research being conducted.

### 2.5.1 Angularity Index

Rao *et al.* (2002) attempted to quantify the angularity of coarse aggregates by means of image analysis. They used the Angularity Index (AI) and not the flakiness index, although both parameters are an indication of the same property (i.e. the angularity of a particle). The aim of their research was partially to find a more effective alternative to the method used by Superpave®. The authors stated that Superpave® recommends the evaluation of angularity of aggregates by means of the ASTM D5821 test procedure which apparently entails the visual examination of each particle whereby the number of crushed faces are counted. This is time-consuming, labour-intensive and subjective and is difficult on smaller particle sizes.

The authors made use of the University of Illinois Aggregate Image Analyser and placed emphasis on crushed stone and rounded gravel, as analysed with the aid of the Mohr-Coulomb formulation of shear strength (refer to Equation 2.1). The results of their research showed that the procedure could differentiate between rounded gravel and crushed stone. Their research shows that the angularity index is not affected by the particle size or orientation and that it also correlates with the materials' angle of internal friction. As part of the analyses, the aspect ratio (i.e. cubical vs. flat vs. elongated), surface texture (i.e. smooth vs. rough) and angularity (i.e. sharp edges or corners vs. rounded) were considered as critical properties for the coarse aggregates used.

Overall the research by Rao *et al.* (2002) showed good results as far as correlation with the materials' friction angle is concerned. One of their conclusions was that the friction angle is affected by a particle's angularity, mineralogy, hardness and gradation but they also stated that the strength of a material is affected by confining pressure.



During later research Rao *et al.* (2003) stated that the angularity of a particle is the result of macro-level properties, while the particle's surface texture is a function of the roughness and irregularities at a micro-level. This seems sensible, although the discussions throughout sections 2.3 and 2.4 suggest that the shape of a particle is dictated to a large extent by the orientation and occurrence of micro-cracks, because these micro-cracks present preferred planes along which breakage can occur.

### 2.5.2 Aggregate Imaging System

Fletcher *et al.* (2002) used a computer automated system to characterise the shape of coarse and fine aggregate particles by means of an Aggregate Imaging System (AIMS). The system is suitable for the analysis of fine and coarse aggregate and can quantify the aggregate texture and angularity, whilst also being able to recognise the three-dimensional form of the aggregate.

The AIMS uses a single camera and backlighting setup, both of which can be moved. According to the authors, this method can perform three specific functions:

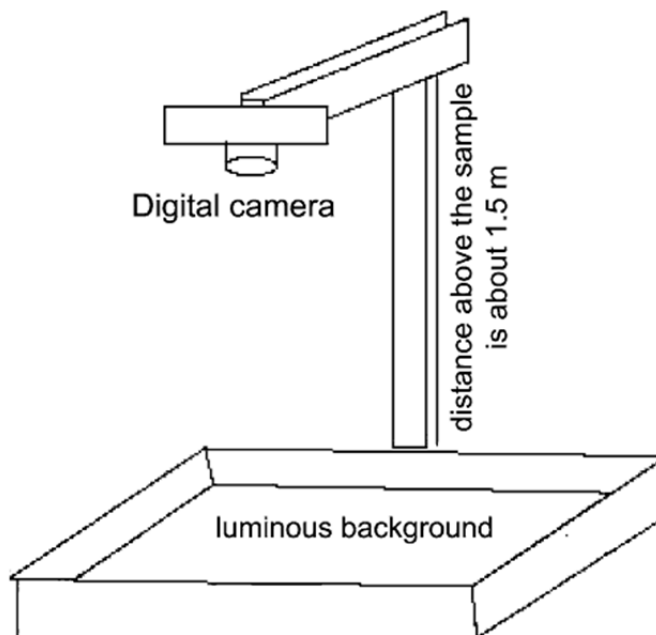
1. The angularity of fine aggregate can be determined. This is inferred from the volume of air voids in a sample which is loosely compacted
2. The angularity of coarse aggregate is inferred from the number of fracture faces that the particle has
3. The relative dimensions of coarse aggregate can be determined and used to identify flat or elongated particles

Whilst it is stated that the test(s) requires a “short time”, little additional information is provided in this regard. Other advantages of this system are that the resolution of analysis can be varied and so too the field of view and lighting scheme and finally, that the entire scanning procedure (which can produce three dimensional results) uses only one camera. On the negative side, this procedure requires the removal of all clasts that do not fall within the scope of analysis (e.g. oversize).

After analyses of fine and coarse aggregates, the authors concluded that the determination of an average angularity (for a given material) is not sufficiently representative to illustrate its performance. They also found a reasonable correlation between the angularity and texture of fine aggregates, despite the fundamental difference of the two properties.

### 2.5.3 Image Analysis

Fernlund (2005) performed image analysis on coarse aggregate in order to assess size distribution in three dimensions. Similar to the work of Fletcher *et al.* (2002) the method utilises a digital camera mounted above the aggregate, with a source of backlighting providing contrast, as depicted in Figure 2.4.



**Figure 2.4** Experimental equipment setup used by Fernlund (2005)

The analysis considers aggregate with a grain size between 10 mm and 50 mm and is said to be for the laboratory environment, specifically as it requires no sieving.

However, the methodology involves stacking individual particles in such a way as to occupy the least possible rectangular space. The particles are then photographed in two positions (i.e. standing up and lying down) in order to obtain the smallest and largest projected areas, thereby allowing the measurement of all three dimensions.

While this method was found to produce more information than conventional sieving, it is hampered by a number of factors:

- Orientating the particles prior to scanning is subjective
- The method of stacking the particles is very time-consuming
- Touching or overlapping aggregate particles hinders aggregate identification by this analysis system
- Particles placed along the periphery of the field of view are subject to a distortion error, particularly if the particles are tall in relation to their other dimensions (i.e. elongated)

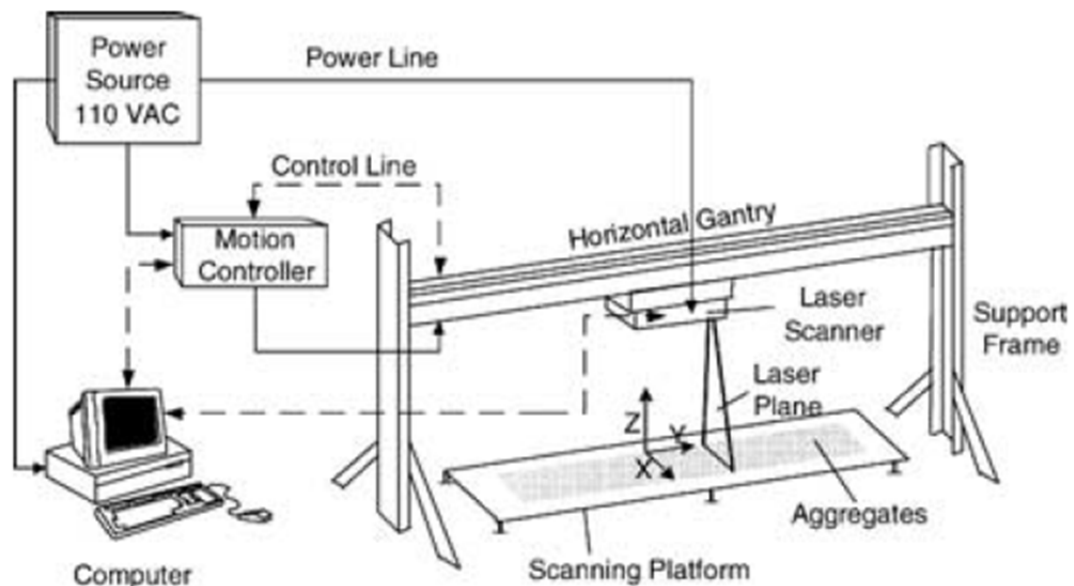
#### *2.5.4 Principal Component Analyses*

Ken *et al.* (2009) proposed an alternative method for determining the shape and size of arbitrary granules. The method is said to determine the shape and size of each particle in two dimensions, using image analyses of backlit particles (as deduced from the text). The authors highlighted that all particles used in their research were convex in shape.

The data obtained from the image analysis were processed by a series of principal component analyses and algorithms. The final outcome of the research was a method that could mathematically determine the (fairly complex) shape of aggregate particles, whilst simultaneously using the processed data to calculate the particle size. Whilst the algorithms discussed fall well beyond the scope of this research, it is impressive to note what the authors achieved through theoretical mathematics and statistics.

### 2.5.5 Laser Profiling

The work of Kim *et al.* (2003) saw processing of aggregate materials by means of a laser profiling setup, depicted in Figure 2.5. Their method focussed on three dimensional segmentation of the aggregate. Whilst the authors discussed digital image technology (DIT), they identified the main stumbling points of the method, i.e. the fact that each particle has to be physically separated from other particles. For example, a number of small particles touching or overlapping may be wrongly assumed as a single, larger particle.



**Figure 2.5** Laser profiling setup used by Kim *et al.* (2003)

The effects of overlapping particles may be overcome, for example, by means of falling particles being scanned; however Kim *et al.* (2003) mean that this is not a feasible method for a number of reasons. Amongst these are that the camera may not be sufficiently fast to capture the moving image, particles may rotate during falling and particles may still overlap during falling by what the authors call the “curtain arrangement” (i.e. one particle falling behind another particle).

Instead, then, Kim *et al.* (2003) developed a laser-based aggregate scanning system (LASS) which is capable of calculating the volume of the aggregate as well as the minimum (square) size opening the aggregate would be able to pass through. This corresponds to an equivalent mesh size. The method uses a Canny edge detector and watershed transformation to analyse the particles and is based on three assumptions:

1. Particles would be orientated in their most stable orientation when scattered randomly
2. A similar specific gravity applies to all particles, provided the material is sourced from the same parent material
3. The volume of the hidden lower part of the particles is proportional to the volume measured by the scanning system

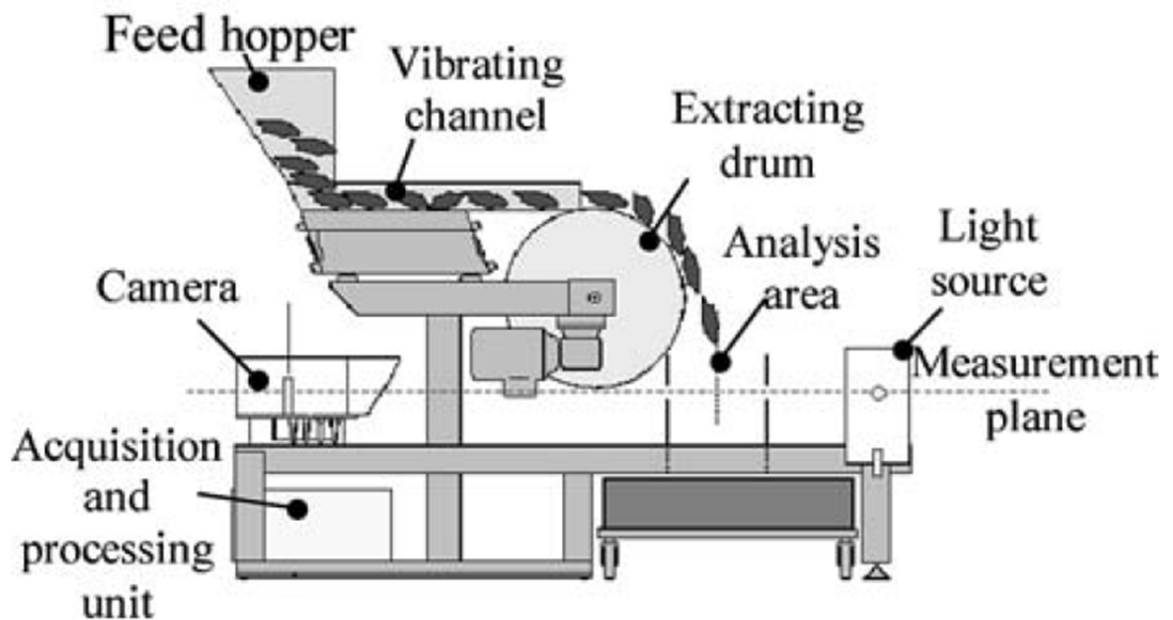
As with the majority of alternative methods, physical separation of particles is required prior to scanning. The authors correctly stated that the effort required to manually pack individual particles counters the main motivation behind automated scanning (i.e. improving analysis and reducing the time required to do so).

Ultimately the method developed showed that despite best efforts, the estimated mesh size calculated still had some shortcomings. The real-life aggregate was judged by the analyses to be retainable on a specific sieve screen size, when in real life the particle passed the specified screen when in a different orientation.

### *2.5.6 Videographer - Shadowgraph*

In the initial research by Descantes *et al.* (2006) using a VDG40 videographer, the emphasis was placed on measuring crushed alluvial gravel aggregate properties. The alluvial materials were considered due to their apparent abundance as sources of crushed rock material in France and the broken surfaces of crushed particles were analysed.

The method developed by Descantes *et al.* (2006) also used a backlit source, referred to as a shadowgraph. The system incorporated a feeder system feeding particles onto a rolling drum. The drum then dropped particles in a controlled fashion to ensure that the biggest surface area of the particle faces the camera when falling past the camera. The camera would then capture the backlit image and process the data. The authors state that the particles move past the measuring area (i.e. the camera) at an accrued speed of 2.6 km/h. The camera then performs successive line-scans at a frequency of 13 kHz. These line scans are then compiled to give a single, scanned image. The entire process is presented graphically in Figure 2.6.



**Figure 2.6** The VDG40 scanning system (Descantes *et al.*, 2003)

The authors used a one kilogram sample of 6/10 mm (i.e. presumably 6 – 10 mm) material which, considering the volumes of crushed aggregate processed during normal quarry production, is miniscule. At first the indicated size and mass of the sample was thought to be erroneous, but the authors later stated that the one kilogram sample comprised 1500 particles. Nevertheless, the sample was apparently adequate to complete the research under consideration. The method is capable of a scanning

resolution of  $0.2 \text{ mm} \times 0.2 \text{ mm}$ ; however, the experimental setup is such that it is deduced that only a two dimensional model can be processed. Once captured, the data can be processed to determine the grading, flatness and elongation of the scanned particles.

This proposed scanning method apparently required less than three minutes to scan a one kilogram sample consisting of roughly 1500 particles and the authors concluded that the results seemed highly repeatable.

### *2.5.7 Videographer - Automation*

Further research undertaken with the VDG40 videographer used a similar approach and equipment to that used by Descantes *et al.* (2006); however the emphasis of the research was shifted to automatically determine the flakiness index of aggregates (Bouquety *et al.*, 2006).

The research undertaken used a database of 122 samples, each consisting of roughly 500 particles. The two-dimensional results produced by this method assume that each particle is a rotational ellipsoid (i.e. similar in two of its three dimensions). This is necessary to calculate the particle volume. The authors stated that the aggregate shape depends strongly on the petrography and processing of the material and generally observed that elongated particles are also flat.

It was concluded that there was a very good agreement between the manually tested flakiness indices and the estimated flakiness indices.

### *2.5.8 Laser Scanning*

The current work at the CSIR by Anochie-Boateng and his co-researchers has demonstrated that modern 3D laser based applications can be adapted and used to accurately measure the surface properties of rock aggregates used in road construction (Anochie-Boateng *et al.*, 2010; Anochie-Boateng *et al.*, 2011b). These researchers have developed surface area properties of aggregates used in five typical South

African asphalt mixes. It was found that existing methods underestimate the surface area of the aggregate particles by between 10 % and 30 %, depending on the type of asphalt mix. This may have large implications for the calculation of the correct bitumen film thickness of these asphalt mixes, commonly used on most surfaced roads worldwide.

Figure 2.7 shows a photograph of the 3D laser scanning device currently under development at CSIR and used in this research. The laser device has been calibrated to determine basic shape properties of conventional and non-conventional aggregates used in pavements. This device has also been evaluated at the CSIR for accuracy and repeatability (Anochie-Boateng *et al.*, 2010). In addition, the capacity and precision of the laser scanning device to accurately measure surface properties of irregular objects was also verified through measurement of volume of aggregates (Anochie-Boateng *et al.*, 2012).



**Figure 2.7** Laser scanning equipment up at CSIR (from Anochie-Boateng *et al.*, 2010)



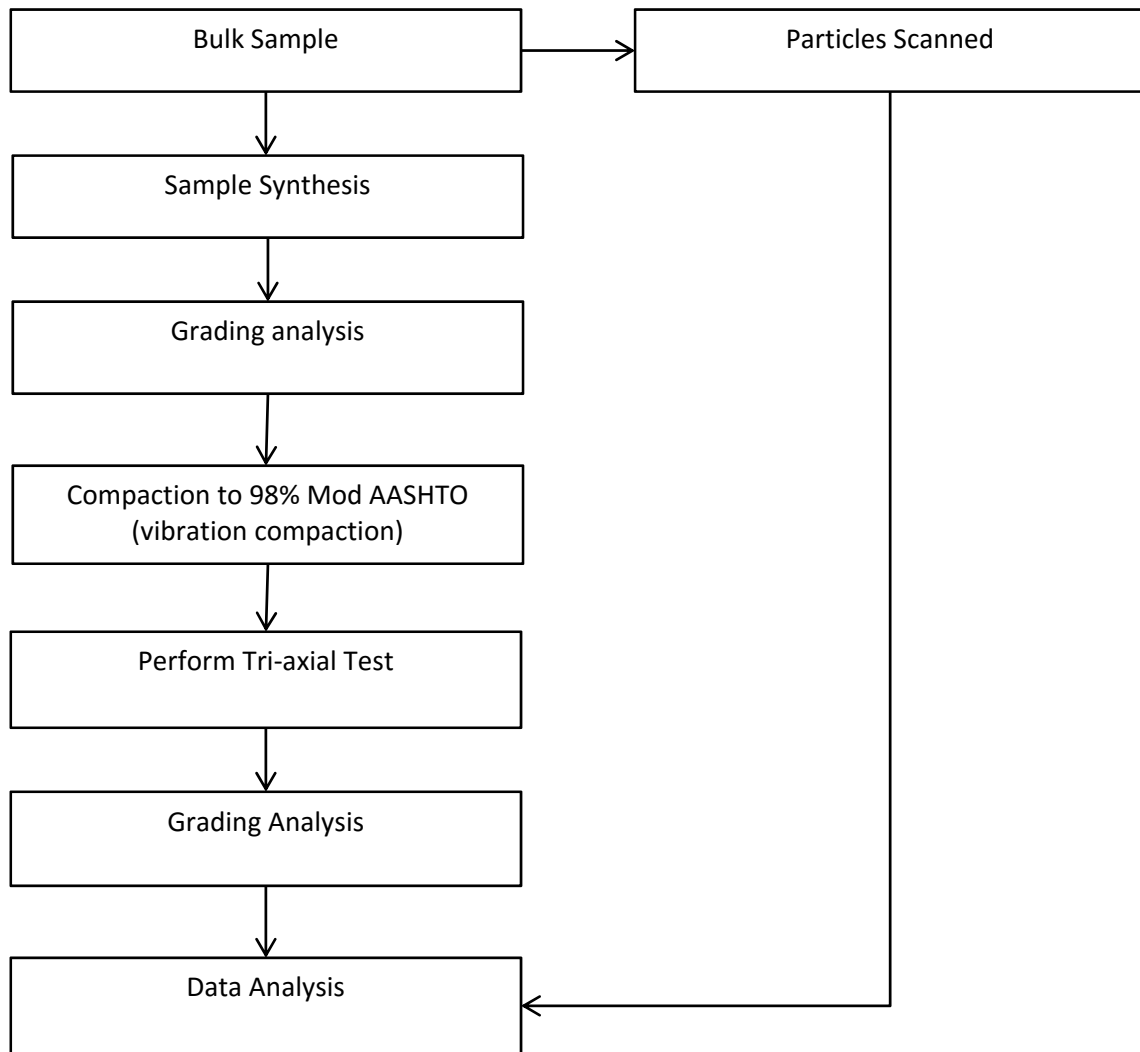
## 3 Methodology

### 3.1 Introduction

A set of standard material tests was performed on the bulk samples collected for the project. The results of the six sample materials used in laboratory analyses are included in Addendum A. It must be clearly noted that these results were obtained on bulk samples collected and that these properties may not necessarily represent the individual components of the synthesised and/or modified samples used during test evaluations. Similarly, sample selection for particle scanning was done from the bulk samples and will be discussed in more detail later. The laboratory tests performed on the bulk material samples included the following:

- Bulk grading analyses – modified after Method B4 (TMH1, 1986).
- Flakiness index - Method B3 (TMH1, 1986).
- Aggregate Crushing Value (ACV) – Method B1 (TMH1, 1986).
- 10 % Fines Aggregate Crushing Value (10 % FACT) – Method B2 (TMH1, 1986).
- Aggregate Impact Value (AIV) – BS812 Part 112.
- Polished Stone Value (PSV) – SABS 848.
- Bulk Relative Density (BRD) on +4.75 mm – Method B14 (TMH1, 1986).
- Apparent Relative Density (ARD) on +4.75 mm – Method B15 (TMH1, 1986).
- Water Absorption – Methods B14 and B15 (TMH1, 1986).

After the above-mentioned tests were completed, the aggregate samples were subjected to the experimental procedures derived for this research. The test procedure followed during the specialised laboratory testing is summarised in Figure 3.1.



**Figure 3.1** Experimental procedure for laboratory tests

### 3.2 Sample Selection

This research overlaps on-going research on the same aggregates conducted by the Built Environment division of the CSIR. Whilst the CSIR research project investigated approximately twenty different geological materials, this research project is concerned with only six materials of different geological and regional origin for laboratory analyses.

Crushed rock aggregate samples were retrieved from commercial sources or quarries used for road construction (i.e. road side quarries) as part of on-going road rehabilitation/construction operations. The material available from these sources was restricted and also had to be shared with other initiatives and research efforts at the CSIR. Materials used as G1 crushed aggregate were preferred. Samples were collected from stockpile sources and where available, boulders of the source material were also taken (for coring and UCS tests). The samples selected for this project included:

- Sample 1: Quartzite aggregate (Magaliesberg Formation, Pretoria Group, Transvaal Supergroup – collected in Pretoria, Gauteng).
- Sample 2: Granite aggregate (Johannesburg Dome – collected in Midrand, Gauteng).
- Sample 3: Quartz porphyry aggregate (Makwassie Formation, Ventersdorp Supergroup – collected near Wolmaransstad, North West).
- Sample 4: Tillite aggregate (Dwyka Group, Karoo Supergroup – collected near Verulam, Kwazulu-Natal).
- Sample 5: Hornfels aggregate (Tygerberg Formation, Malmesbury Group – Durbanville, Western Cape).
- Sample 6: Modified dolerite aggregate (Karoo Supergroup – collected in Trichardt, Mpumalanga).

### **3.3 Sample Preparation**

#### *3.3.1 Concept of Sample Preparation for Laboratory Analyses*

It was contemplated that a means would have to be derived to remove the variability of the test samples resulting from the properties of the materials' fine constituents as the aim of this research is focussed on the effects of the aggregate particles and not the material "fines". The variability of the fine constituent will be discussed in more detail later.

The most practical way to eliminate any variation in material properties induced by the finer components was to remove the finer constituents from the sample completely and replace them with a uniform, inert fines mix from a single source. The same size fractions would have to be replaced in each sample in order to allow a direct comparison.

In order to simulate the ideal grading of the samples tested, the COLTO specifications were consulted as applicable for G1 crushed base and sub-base material. The specification on grading is summarised in Table 3.1.

**Table 3.1** Grading specification for G1 crushed stone base and sub-base (COLTO, 1998)

<b>Nominal Aperture size of sieve (mm)</b>	<b>% passing sieve, by mass</b>
37.5	100
26.5	84 – 94
19.0	71 – 84
13.2	59 – 75
4.75	36 – 53
2.00	23 – 40
0.425	11 – 24
0.075	4 - 12

### *3.3.2 Synthesis of Samples One to Five*

As mentioned in the previous section, the fine constituent was substituted by a single source's material. The limitations of scanning equipment used for particle analyses came into play when selecting the particle constituents to be replaced. Considering the resolution of scanning and the preferred range of scanning (for this investigation) it was decided that the materials passing the 4.75 mm screen would be replaced with a controlled mix. Conversely, only particles retained on the 4.75 mm screen and larger (but also passing the 37.5 mm screen) would be considered.

Samples one through five were oven dried for 24 hours at 105 °C and sieved in bulk, separating the samples into their respective size components. Particles passing the 4.75 mm screen were then returned to the bulk sample and each of the remaining fractions (-37.5 mm to +4.75 mm) retained. These fractions were then mixed in a ratio compliant with the specification given in Table 3.1. A total sample mass between 14 kg and 16 kg was selected in order to provide a suitable volume of material for tri-axial tests, with a small additional percentage, should it be required.

With the above-mentioned grain sizes being accounted for, the fine material constituent (i.e. passing 4.75 mm screen) was replaced with a quartzite crusher dust mix. The crusher dust mix was also composed to comply with the specified grading shown in Table 3.1. Quartzite was selected as the donor material, as it was deemed to be the most inert source of available crusher dust at the time of the project. In theory the quartzite crusher dust also includes miniscule deleterious components or impurities (e.g. smectite group minerals, etc.). A bulk sample of roughly 90kg was collected and sieved into its particle size components after oven drying.

### *3.3.3 Synthesis of Sample Six*

Sample six (dolerite) was synthesised differently from the remaining samples. It was anticipated that all the materials used qualified as G1 crushed rock material and should therefore comply with specifications for such a material. Subsequently it was accepted that these materials should have similar properties, including an acceptable flakiness index. It was therefore expected that the shear strength properties of the sample materials may be very similar, specifically as far as the shape (i.e. flakiness index) of the samples is concerned.

With the above in mind, it was decided to synthesise sample six with a different approach. It was already known that the material fulfilled the requirements and specifications for use as a crushed rock source, including an acceptable flakiness index, etc. In order to assess the effects of an elevated (i.e. high) flakiness index, sample six was given a skewed (i.e. elevated) flakiness index to assess comments by Semmelink (1991) that an excessive flakiness index causes a reduced density in a

material due to reduced “packability” of particles. This, in turn, *causes a reduction in material strength.*

Whereas the remaining samples were graded using a standard sieve stack, sample six was graded using the addition of sieves with apertures of 9.5 mm and 6.7 mm with the specific aim of modifying the flakiness index with relative ease. Considering the method of determining the flakiness index (refer to Table 2.1), sample six was divided into the particle size constituents (after oven drying) by means of conventional sieving. The respective particle sizes were then processed with the aid of a flakiness index plate in order to deliberately include more elongated particles in the sample than would be accepted by the COLTO specification (i.e. the material was specifically mixed to have a high flakiness index). Each particle included in this sample was fitted through the flakiness index plate manually in order to get an exact flakiness index value.

The sample was further mixed in a similar manner to the remaining samples, in that the particle constituents smaller than 4.75 mm were replaced with a crusher dust mix which was pre-determined and sourced from quartzite crusher dust.

#### *3.3.4 Microscope Thin Section of Fines Substitute Mixture*

In order to investigate the mixture of fine materials substituted in the synthesised samples, a small sample of each of the four sizes substituted was taken for analysis. A thin section was made from particles or dust of each of the four fractions to allow study under the microscope. The general aim was to assess – if possible – the shape of the particles of different size components. The thin sections were studied with the aid of a Leica DM750P microscope but delivered relatively insignificant information with little difference between the size fractions. The matter will not be discussed further.

### 3.4 Laboratory Tests

The following describes experimental procedure used during material testing in the laboratory. The procedure followed during scanning is discussed in a separate section.

#### 3.4.1 Grading Analysis

Grading analyses were performed prior to compaction and tri-axial tests, as well as after the completion of the tests. The aim of the grading analyses was simply to establish whether the materials had been altered during testing (i.e. compaction and tri-axial tests) and if so, to what extent. The main alteration expected was that of particle crushing (refer to section 2.4.3).

The matter was complicated slightly by the fact that a sample of between 12 kg and 16 kg was mixed to be used for the tri-axial test, but not all of the material was consumed and some was left over. In order to assess the potential grading changes, grading analyses were done on all samples (except sample six) at the following stages:

- A control grading analysis after sample synthesis, before vibrating table compaction. Grading analysis was done on oven-dried samples of the entire sample (12-16 kg)
- A grading analysis was performed on the remaining materials not used for the tri-axial sample. The remainder had to be oven dried again as the material was moist from sample preparation
- Grading analysis was done after tri-axial testing, again after oven-drying

The grading was compared for the sample used for the tri-axial tests (i.e. the total original grading minus the material not used for the tri-axial sample) before the test and again after the test. Seeing as the emphasis of this research lies with the particles retained on the 4.75 mm screen and larger, the grading analyses considered only these grain sizes, and not the fine particles substituted into the samples. The screens used include the nominal apertures described in Table 3.1.

This exercise was not done for sample six. While it would have been interesting to assess whether elongated particles are more susceptible to particle crushing, it proved impracticable to repeat the grading analysis for the sample due to the volume of elongated particles. The particles do not grade well (i.e. fit through sieve apertures) which resulted in an inaccurate reflection of the grading. It should be noted that this problem was not an issue when mixing the sample, as the elongated particles were sourced from the sieved bulk sample which did not comprise excessive numbers of elongated particles deliberately included in the final test sample.

### 3.4.2 Compaction Properties

In order to determine the optimum moisture content (OMC) and maximum dry density (MDD), COMPACT software was used. COMPACT was developed by the CSIR and was done so to predict compactibility (and bearing capacities) of untreated granular soils. The two attributes calculated (i.e. MDD and OMC) were required for compaction of the samples to a simulated 98 % Mod AASHTO density.

Input parameters used for the calculation of MDD and OMC included the grading of each prepared sample, as well as the apparent relative density (ARD) and bulk relative density (BRD). All samples were non-plastic and appropriate values were used for Atterberg limit input in software analyses. Some modification was required to compensate for the substitution of the finer constituents; however the quartzite crusher dust sourced for these purposes was from the same source (i.e. quarry) used as sample one. The ARD and BRD values were taken from the test results done on the bulk samples (as part of the larger CSIR research project). This data was then applied to calculate a weighted ARD and BRD for each sample. The aggregate and crusher dust were calculated as a percentage of the total sample mass and used to calculate weighted values as follows:

$$ARD_{\text{Total}} = (ARD_{\text{Sample}} \times \% \text{ aggregate}) + (ARD_{\text{Quartzite}} \times \% \text{ crusher dust})$$

(Equation 3.1)

and



$$\text{BRD}_{\text{Total}} = (\text{BRD}_{\text{Sample}} \times \% \text{ aggregate}) + (\text{BRD}_{\text{Quartzite}} \times \% \text{ crusher dust})$$

(Equation 3.2)

### 3.4.3 Sample Preparation and Vibration Table Compaction

In order to prepare samples for tri-axial tests, the materials had to be compacted. Numerous methods of compaction were considered; however ultimately the vibration table compaction was selected as it is the most commonly used method for this particular (i.e. large diameter) tri-axial test in South Africa. The method of using the vibration table for compaction (including method development and calibration) was refined by Semmelink (1991) and based on his research, the method is slightly more effective than the conventional drop hammer equipment used for Modified AASHTO compaction. While this is a debatable issue, such a discussion falls beyond the scope of this research and the method was used as the equipment was readily available. The method of compaction is likely to have little effect on the particle orientation within the sample, when compared with other methods of compaction (Henderson *et al.*, 2011); hence there should be little difference in the final shear strength properties of the sample.

The parameters discussed in the preceding section were used to compact the test samples using a vibration table. The machine used was a Vibramech VT 600 – 550 vibration table which utilises a 50 kg mass load. The method uses a compaction mould which (when fully assembled) is 385 mm high and has an inner diameter of 150 mm. This mould delivers a sample with a length of 300 mm, with the remainder of the mould length stabilising the vibrating mass during compaction. Figure 3.2 shows the equipment used for vibration compaction.

The samples were compacted in the standard way (method A11T in TMH1, 1986). The samples were oven dried for 24 hours after which the necessary mass for the required density was calculated. Water was added to the material (according to OMC calculations) and thoroughly mixed by hand. The moistened and mixed material was then divided into three portions. Each portion was added to the mould in sequence



**Figure 3.2** Vibration table equipment (Vibramech VT 600 – 550)

after the preceding portion had been compacted (which is in slight variance with the method of Semmelink (1991) who preferred compaction in a single layer). Simply stated, each tri-axial test specimen was compacted in three layers. The upper (compacted) surface of the first and second layers were lightly scarified with a metal rod before adding the next portion for compaction, to allow effective particle interlock and to prevent smooth surfaces from forming at the tops of these two layers during compaction. Compaction summaries are included in Addendum A.

#### 3.4.4 Multi-Stage Tri-axial Tests

Shear strength properties were initially assessed using the multi-stage tri-axial test approach. The multi-stage tri-axial test is a method often used to reduce material test costs or when limited sample material is available (as was the case in this research). The test method has the advantage that it effectively uses one sample to perform three tests, instead of three samples as per conventional tri-axial test procedure. The disadvantage of the method is that results are often not reliable and that test data may be very subjective and operator dependent.

The multi-stage tri-axial tests were performed at the CSIR pavement materials laboratory. The tests were performed on the large diameter samples (300 mm height, 150 mm diameter) compacted as discussed previously (after being left to equilibrate for at least 24 hours). The sample itself was sleeved in a *double* rubber membrane which was tested for leaks before the experiments commenced.

The tri-axial apparatus applied its confining pressure to the sample by means of compressed gas in an enclosed Perspex or steel chamber. The normal load is applied via a hydraulically operated piston which applies a controlled (stiff) load (i.e. sudden and catastrophic sample failure is avoided) and uniform strain is maintained. Figure 3.3 shows the test equipment with a sample in the Perspex chamber.

Experimental data was captured (real-time) electronically as the tests proceeded. For each load applied at different confining pressures, the test was allowed to proceed until the loading curve started to “level out” indicating the onset of plastic failure. At this point, it was assumed that failure had initiated (or was imminent) and the test was halted prior to the sample actually failing. The point at which loading is halted is entirely decided by the operator and is therefore often subjective and operator dependent.

The experiments were conducted in four phases. The sample was loaded by applying a confining pressure of 138 kPa. Normal loading continued until the loading curve appeared to level out (i.e. the sample was near failure), as discussed above. The test was then immediately halted, the normal load removed and the confining pressure



**Figure 3.3** Tri-axial test equipment

changed for the next test. This approach was used for confining pressures of approximately 138 kPa, then 103 kPa and finally 41 kPa. Once these tests were complete, the sample was again confined at 138 kPa and was then (normally) loaded until actual sample failure occurred (as for conventional tri-axial tests). Tests with this approach yielded results that could *theoretically* be adjusted (upwards) using the final (i.e. actually failed) test result at 138 kPa to derive the material's shear strength properties with the aid of conventional Mohr circles. It was considered that the actual shear strength would be slightly higher than this prematurely released "failure".

The data of the multi-stage tri-axial tests were imported into Excel® and compiled into spread sheet form for analyses. The normal loads that were applied (given in kN) were processed to yield a stress in kPa (using the cross sectional area of the sample), i.e. principal stresses.

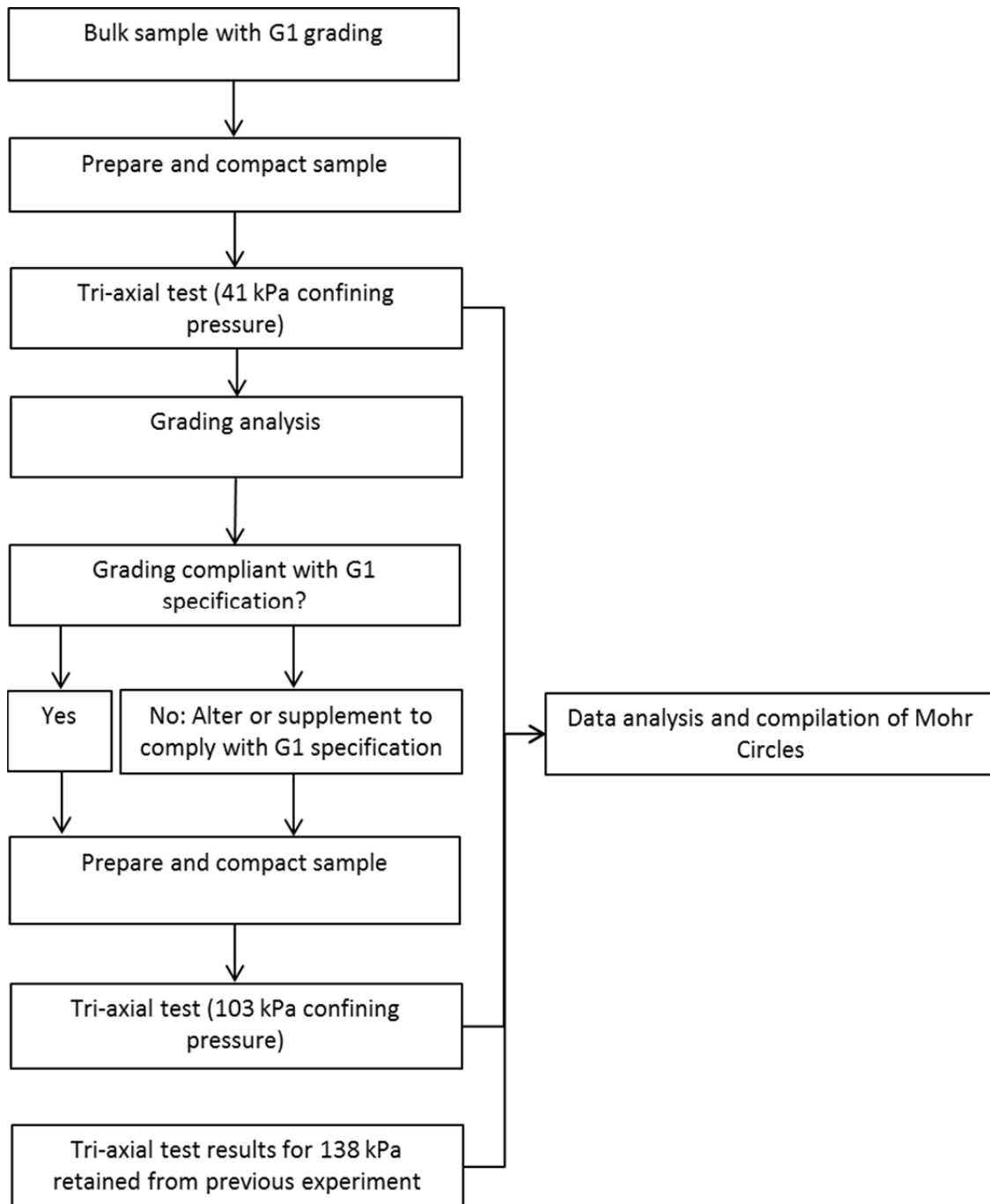
The results obtained were initially processed using Matlab®. An existing software program was used to develop Mohr circles and ultimately deduce the angle of internal friction and cohesion values for each sample. The resulting output was of a poor quality and consequently, Mohr circle data output was later generated using alternative methods. The data will be discussed in detail in chapter 4.

The multi-stage tri-axial test results were deemed to be questionable and had to be evaluated (and ultimately completely disregarded, based on the said evaluation). This is also discussed in a later chapter.

#### 3.4.5 Tri-axial Tests

The tri-axial tests were repeated using the conventional tri-axial test approach after the multi-stage test results proved questionable. Data from the final (i.e. failed at 138kPa confining pressure) multi-stage tri-axial test were retained and conventional tri-axial tests were repeated at two lower confining pressures, respectively.

Samples were prepared and compacted in the same manner as previously described. The limited sample material available necessitated that the same material (but not the same *specimen*) be re-used for the different tests. This, in turn, made it necessary to ensure that the material grading was still compliant with that of a G1 specification material before each test. As a result, the material was oven dried, graded and modified/supplemented (where necessary) from the bulk samples before each tri-axial test. Figure 3.4 summarises the procedure followed. Samples were tested at similar (though not identical) confining pressures to those used for the multi-stage tests to allow a direct comparison between test results at a later stage.



**Figure 3.4** Flow Chart of Tri-Axial Test Sample Preparation and Testing

Once completed, the data obtained from the tri-axial test results were analysed and used to compile Mohr-Coulomb failure criteria (i.e. Mohr circles) from which to derive shear strength properties and ultimately determine the shear strength.



### 3.5 Mineralogy Review

A single rock particle of each of the six test samples was selected and submitted to the Council for Geoscience to prepare a thin section for petrographic analysis. Though a single particle will not be representative of the entire aggregate sample, this step was included as supplementary information. The thin sections were investigated under a microscope using methods commonly applied in mineralogy and petrology; however the emphasis of this evaluation was shifted from the detailed mineralogy to the physical attributes of the rock mass (e.g. mineral interlock, mineral shape, micro-cracking, etc.). The thin sections were investigated using a Leica DM750P microscope. The results have limited significance to this project and are included in Addendum B.

### 3.6 Laser Scanning

#### 3.6.1 Equipment and Data Capture

The research component involving the laser scanning of aggregates was done with an experimental laser system, which is under development at the CSIR. Scanning was done according to the protocol document developed by Anochie-Boateng and Komba (2010), using a Roland LPX 1200 laser scanner with Rapidform XOS™2 software. Details concerning the document and test equipment are currently considered sensitive and may not be discussed in significant detail; however a basic description of the scanning procedure follows.

The process of scanning with the aid of the laser system is done in four main steps:

1. *Scanning*: Scanning of the aggregate was done in stages and at a specified resolution. Particles were generally scanned in two stages in order to obtain data on six aspects (i.e. front, rear, left, right, top and bottom). The first stage of scanning generally covered four faces (i.e. front, rear, left and right) while the second stage involved the top and bottom faces.

2. *Alignment*: After scanning in two (or more) stages, the data acquired had to be aligned in order to represent the entire particle scanned and not just individual scan faces.
3. *Combining Data*: Once the scanned data had been aligned into the proper orientation, the aligned data had to be combined into one object.
4. *Merging Data*: The merging process and model refinement was generally done in one step. Manual and automatic (software) modification and manipulation can be done during this stage. After merging was completed, the data were transformed into and saved as a single object.

Once the object had been completely processed, the software provides an array of data which can be used. For use in this research, only five parameters were considered, namely the object's length, width, height (depth parameter in the software), the surface area and the particle's calculated volume. Dimensions were determined by a "bounding box" which the software fitted on the scanned particle. The merged scan data is included in Addendum C.

### 3.6.2 *Sample Selection for Scanning*

Sample selection for the scanning exercise was mostly done as part of the larger SRP project. The aim was to collect twenty samples of different aggregate materials for scanning; however, at the time of this research only seven materials had been scanned (of nine collected samples). The seven materials that had been scanned were sampled in a specific manner.

Each material was divided into its respective size fractions by screening with the aid of a sieve stack. The particles used for scanning were those retained on the 26.5 mm, 19.0 mm, 13.2 mm, 9.5 mm, 6.7 mm and 4.75 mm screens (particles smaller than 4.75 mm generally did not scan well and were omitted from the research). Some 30 particles were to be selected for each material, from each particle size (i.e. a total of 180 particles per sample); however this did also not fully materialise as 26.5 mm particles were only scanned on some occasions.



The sampling was biased slightly in order to specifically include elongated and/or flattened particles which may not necessarily have been sampled if particles were selected at random. Elongated particles generally had higher sample numbers (i.e. they were sampled and scanned last, Pers. Comm., Komba, 2012). The data obtained from each specimen (i.e. particle) were then amalgamated to deliver datasets for each size fraction, containing the data of all the materials scanned (e.g. a dataset was compiled for 4.75 mm particles, consisting of all seven scanned sources' data). This approach was deemed more sensible in order to assess a greater variety of particle shapes as it was considered that not all particles of similar size would have similar properties (Tons and Goetz, 1967).

After cleaning and oven drying, each particle was scanned using the approach discussed in section 3.6.1. The particles were given a sample number and marked. This was done in case there was a need to refer back to the actual particle at any point during the investigation. Considering all materials and particle sizes, a total of 1149 particles were scanned, as summarised in Table 3.2.

**Table 3.2** Summary of scanned particles

	<b>Quartzite</b>	<b>Granite</b>	<b>Tillite</b>	<b>Hornfels</b>	<b>Recycled Aggregate</b>	<b>Gravel (alluvial)</b>	<b>Dolerite (modified)</b>	<b>Total</b>
<b>26.5 mm</b>	0	22	30	18	0	0	30	100
<b>19.0 mm</b>	30	30	30	30	30	30	30	210
<b>13.2 mm</b>	30	30	30	30	30	30	30	210
<b>9.5 mm</b>	30	30	30	30	30	30	30	210
<b>6.7 mm</b>	30	30	30	30	30	30	30	210
<b>4.75 mm</b>	30	30	30	30	30	30	29	209
<b>Total</b>	150	172	180	168	150	150	179	<b>1149</b>

Using the approach above, particles of the following materials were scanned:

- Quartzite
- Granite
- Hornfels
- Tillite
- Modified dolerite (refer to section 3.3.3)
- Recycled aggregate (referred to in data as “RA”)
- Alluvial gravel (referred to in data as “Gravel”). This material does not constitute a road building aggregate but was sampled and analysed due to its rounded particle shape. As such, it is not strictly applicable or directly comparable in the research context; however the material ultimately yielded invaluable information.

The quartz porphyry sample used in tri-axial tests (as sample 3) was not yet scanned at the time of writing this thesis; hence no scan data is available for the material.

### *3.6.3 Data Application and Processing*

The parameters calculated by the scanner software were entered into an Excel® spread sheet for each particle size scanned (i.e. 26.5 mm, 19.0 mm, 13.2 mm, 9.5 mm, 6.7 mm and 4.75 mm). Descriptive detail was also included to serve as a reference to the scanned sample (i.e. particle numbers were recorded). Data entered into spread sheet format recorded the following:

- Particle number (1 – 30)
- Material type (i.e. sample material e.g. granite)
- Width (mm)
- Height (mm)
- Depth (mm)
- Surface Area (mm<sup>2</sup>)
- Volume (mm<sup>3</sup>)

The data was then revised to ensure that the “Width” column contains the largest measured particle dimension and that the “Depth” column contained the smallest measured particle dimension. The “Height” column contained the intermediate of the three dimensions measured. Revision in this regard was necessary as the scanner’s software did not automatically arrange the dimensions in this order, but rather recorded it based on the scanned particle’s orientation during scanning.

The data arrangement described above was done specifically with the aim of calculating another parameter namely the “Elongation Value”. The flakiness index has previously been assessed using this same laser scanning system by Anochie-Boateng *et al.* (2011a) but the present approach adopted (i.e. using the elongation value) simplified data analysis considerably.

The elongation value used in this research is the ratio between the longest and shortest dimensions of any given particle:

$$\text{Elongation Value} = (\text{Width}) / (\text{Depth}) \quad (\text{Equation 3.3})$$

In more conventional terms, the same equation can also be expressed as:

$$\text{Elongation Value} = (D_l) / (D_s) \quad (\text{Equation 3.4})$$

where

$D_l$  = the longest particle dimension

$D_s$  = the shortest particle dimension

For the purposes of this research, terminology as given in equation 3.3 will be used.

The *elongation value* (EV) was used as a quick reference to identify elongated and/or flattened particles in the data. After a review of the dataset compiled based on the scanned particles’ dimensions, a division was needed to discern between regular (or

cubical) particles and elongated (or flat) particles. For the purposes of this research the limit was set at an elongation value (or ratio) of 2.00. While the selection of this value may be argued, it was deemed the most sensible boundary based on the number of particles which exceeded the dividing value of 2.00. It must be borne in mind that while individual guidelines define elongated particles differently, G1 aggregate materials are specifically produced not to contain large numbers of elongated or flat particles. Using a higher elongation value as divider (e.g.  $EV > 4$ ) would therefore result in very few datasets for elongated particles and would prevent a comparison between difference in shear strength properties of the particles (i.e. elongated vs regular particles).

The final parameter calculated in the spread sheet was the ratio between the particle's volume and its area ( $V/A$ ). The reciprocal of this function was also considered during early analyses; however, it was found that the function ( $V/A$ ) generated a larger range of values which could be used more conveniently than smaller values with numerous decimal increments generated by its reciprocal.

The master data set was used for further analyses. The data (in Excel® spread sheet format) is included in Addendum D.

## 4. Results and Analysis

### 4.1 Laboratory Sample Preparation

#### 4.1.1 Sample Synthesis

The sample preparation was performed in two phases. The first phase consisted of removing the material constituent finer than 4.75 mm, while the second phase involved mixing in a substitute uniform fine material sourced from quartzite crusher dust. The synthesised samples were required to be between 12k g and 16 kg in mass to provide sufficient material for the tri-axial tests and as such, the grading was calculated using this mass in conjunction with the COLTO grading specification. The prepared materials were not fully consumed during the sample preparation for the tri-axial tests as the mass of material required varied depending on the maximum dry density properties calculated for each of the materials. As a result the actual grading of the samples used for tri-axial tests varied slightly from the synthesised (bulk) samples. Table 4.1 illustrates the grading of the six samples prepared and used as source material for tri-axial tests.

**Table 4.1** Sample grading (% passing sieve sizes)

<b>% Passing Sieve (mm)</b>	<b>COLTO specification</b>	<b>Sample 1 (Quartzite)</b>	<b>Sample 2 (Granite)</b>	<b>Sample 3 (Quartz porphyry)</b>	<b>Sample 4 (Tillite)</b>	<b>Sample 5 (Hornfels)</b>	<b>Sample 6 (Modified Dolerite)</b>
37.5	100	100	100	100	100	100	100
26.5	84 – 94	90.82	91.00	88.19	88.98	89.79	89.69
19.0	71 – 84	76.81	76.35	75.13	75.86	76.21	75.89
13.2	59 – 75	65.83	65.15	63.50	64.78	64.93	66.62
4.75	36 – 53	41.87	41.67	39.71	43.04	44.39	41.02
2.00	23 – 40	30.09	29.76	28.07	31.17	31.37	28.21
0.425	11 – 24	14.42	14.18	14.65	15.07	16.04	N/A
0.075	4 - 12	4.26	5.78	5.50	4.00	6.48	N/A

#### *4.1.2 Control Grading*

As part of the assessment of potential particle grain crushing during compaction of test samples (and the actual tri-axial tests), it was proposed to do a grading analysis of each sample before compaction and tri-axial tests, as well as afterwards. This was done for both the multi-stage and conventional tri-axial tests. The argument behind this was that any particle crushing incurred during test sample compaction or testing would be reflected as a difference in grading afterwards. To achieve this, a grading analysis was done after sample synthesis but before compaction and tri-axial tests to serve as a control grading against which to compare subsequent grading analyses done after the tests. This was done for each sample except the modified dolerite sample, which was very difficult to separate repeatedly by sieving due to the deliberate inclusion of abundant elongated particles.

After the first round of verification tests, it became apparent that there was a notable discrepancy in the grading analyses done before and after compaction/testing. The discrepancy was ascribed to the fact that the initial control grading analyses were done on “quartered” samples, where a fraction of the entire sample is extracted and run through the sieve stack. The corresponding grading analyses for the whole sample (as mixed during synthesis) and the quartered (control) sample did not correspond exactly; hence the identification of grading differences would not have been possible. To illustrate the point, Table 4.2 shows the grading analyses for sample 2 (granite) as performed on the entire sample and the quartered sample.

From these results it was apparent that in order to ensure accurate grading information (to verify or disprove particle crushing) the entire bulk sample would have to be graded, as opposed to only a quartered sample. The latter was not sufficiently representative of the bulk sample. With the differences between the two methods of grading identified at a sufficiently early stage, it was decided to abandon quartering for the grading analyses and subsequently the entire sample was graded before and after tri-axial tests to allow an accurate grading comparison.

**Table 4.2** Grading comparison for sample 2 (granite)

<b>% Passing Sieve (mm)</b>	<b>COLTO specification</b>	<b>Entire sample</b>	<b>Quartered sample</b>	<b>% difference</b>
37.5	100	100	100	0
26.5	84 – 94	91.00	81.79	9.21
19.0	71 – 84	76.35	67.24	9.11
13.2	59 – 75	65.15	58.00	7.15
4.75	36 – 53	41.67	37.87	3.8
2.00	23 – 40	29.76	29.76	0
0.425	11 – 24	14.18	14.04	0.14
0.075	4 - 12	5.78	6.49	0.71

#### *4.2.2 Particle Crushing*

The process discussed in the preceding section was analysed by comparing the percentage (by mass) passing each sieve size. The sieve analyses were done after oven-drying the samples to allow direct comparisons with the results prior to tri-axial tests. Table 4.3 illustrates the grading differences between test samples before and after compaction and testing, which resulted from particle crushing during sample compaction or multi-stage tri-axial tests. Similar trends were noted during the conventional tri-axial tests, but data was used to correct the grading and will not be repeated here.

The results of the grading comparisons indicate that some of the samples did show small changes in grading. Sample 2 (granite) showed the largest change in grading, with the largest increase in the fraction passing 26.5 mm. This suggests that particle crushing resulted in this fraction (in particular) being altered. An increase in the percentage passing the screen indicates that some of the particles previously retained on the 26.5 mm screen were broken during compaction or the tri-axial test.

**Table 4.3** Grading for samples before and after compaction and multi-stage tri-axial tests

Passing Screen (mm)	Sample1 (Quartzite)		Sample2 (Granite)		Sample3 (Quartz Porphyry)		Sample4 (Tillite)		Sample5 (Hornfels)	
	Before	After	Before	After	Before	After	Before	After	Before	After
<b>37.5</b>	100	100	100	100	100	100	100	100	100	100
<b>26.5</b>	89	92	89	94	88	87	88	88	88	89
<b>19.0</b>	76	78	78	79	74	74	74	74	76	76
<b>13.2</b>	65	67	67	67	62	63	63	63	64	64
<b>4.75</b>	43	43	44	45	40	41	42	42	42	46

The test results also show that sample 4 (tillite) showed no difference in grading either after compaction or after the tri-axial test. This would suggest that no particle crushing occurred in this material.

The results brought forth an observation related to the matrix of the rock materials. The general (and unsubstantiated) trend observed here is that coarser grained materials tend to be more susceptible to particle crushing than finer grained materials when subjected to the same compactive effort. Though this observation is not necessarily mutually exclusive, it is clear that the granite sample (sample 2) and the quartzite sample (sample 1) showed larger variations in grading than the samples with comparatively finer grain or mineral/texture sizes. This, however, may not necessarily be simply a function of mineral grain size, but may also be affected by the rock strength, possible micro-fractures, particle shape, etc.

Regardless of the reason for the particle crushing, the effects and manifestation thereof were noted and considered during the remaining investigations. The effects were countered by supplementing the affected particle size fractions from the bulk sample prior to each test to ensure compliance with the COLTO grading specification.



## 4.2 Practical Aspects Related to Particle Scanning

### 4.2.1 Advantages of Scanner System

The scanner system proved to hold many advantages over conventional systems currently used for particle shape analysis and is also considered superior over the systems discussed in the literature review. The main advantage of this method is that it analyses particles' dimensions with great accuracy and delivers results for three dimensional models as opposed to the majority of the existing systems which only provide two dimensional data. This allows the calculation of amongst others, very accurate dimensions, surface areas and particle volumes. These parameters are not recordable when using a backlit system, for example, without making certain assumptions.

The system can scan at a maximum resolution of 0.1 mm which means that the scanned surface can be recorded with great detail. This does also necessitate that the user keeps perspective when processing the data, as it is easy to get occupied trying to refine the models effectively, while working with small particles. For example, when scanning a 4.75 mm particle the model can be zoomed to view a one millimetre section over the display of an entire computer screen; hence the particle can be magnified dramatically. When this happens it is easy to try and rectify very small imperfections or data discrepancies which will ultimately have a miniscule effect on the calculation of the surface area or volume of the particle. Hence, care must be taken not to spend excessive time on model refinement which may produce very little improvement in the data.

The results obtained from the scanning are also more comprehensive and useful than the current approach used to determine the flakiness index (i.e. manually fitting particles through the flakiness index plate). While the results of the particle scanning can identify elongated particles, the method supplies additional information (e.g. dimensions, volume, surface area, etc.) above that obtained from the plate-based method. This information is obtained with little additional effort and serves as an

added bonus as it can be used for an array of complementary analyses that are not possible with current, conventional methods.

#### *4.2.2 Limitations of Scanner System*

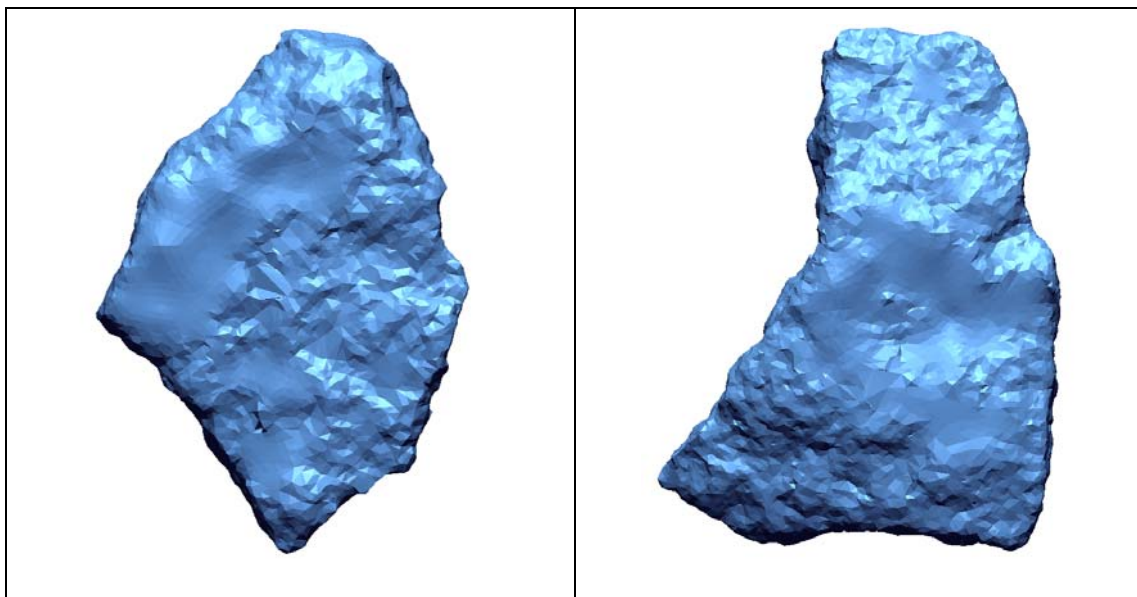
As with the majority of similar systems, the scanning equipment is not without limitations. This applies to both the apparatus and the method.

The biggest limitation of the scanning system is the time required to process the data for a single particle. The scanning time is affected by the size of the particle scanned, as well as the resolution at which it is being scanned. The higher the resolution used, the more time is required for scanning. To put the matter into perspective, scanning and processing (i.e. scan, align, combine and merge) a particle retained on the 26.5 mm screen (and less than 37.5 mm in size) at a resolution of 0.1 mm (in all dimensions) takes approximately one hour. This time includes physically scanning and processing the scan data to deliver a complete model, provided there are no complications. At the other end of the scale, a particle retained on the 4.75 mm screen can be scanned and completed in approximately ten minutes when using the same resolution. Scan time is also dictated by the skill and experience of the operator. With this in mind, it is clear that the procedure is time-consuming and requires a computer-literate operator.

Another limitation of the system is that certain particles are often difficult to orientate into a stable position in the scanner. While cohesive putty (e.g. Prestik®) can be applied to remedy this problem it is not always effective. If the object that is being scanned moves in any way during the scanning process, the scan data will be inaccurate and the faces scanned will not align. In such instances the particles usually have to be scanned again (i.e. the scan must be repeated).

Elongated or flattened particles produce their own problems when scanned. The concept of line-of-sight plays a big role. Highly flattened particles often suffer inaccurate surface area and volume estimates as a result of no line-of-sight. A flattened particle will usually have very limited data points for the large, flat areas due

to the fact that these faces are usually parallel to the scanning laser. Re-orientating the particles to have the flattened faces facing the scanner (i.e. perpendicular to the scanner) often does not work for the reason explained in the preceding paragraph (i.e. instability). The particle tends to move or fall over while the rotating table turns, even if mounted in the very centre of the turntable, which results in some errors. Figure 4.1 illustrates two flattened particles which have blind areas which could not be scanned. The software automatically filled these areas during the merging process; however, the in-filled area is very obvious and results relating to this area are not necessarily accurate.



**Figure 4.1** Flattened particles with blind areas

The scanning equipment is also sensitive to dust and vibrations. While the equipment should be kept in a clean and still environment in a research laboratory, the equipment will suffer much disturbance and dust if used in a commercial laboratory where vibration (e.g. compaction equipment) and dust is abundant.

### 4.3 Model Development

With the scan data available, a number of approaches were attempted to develop a model to rank or arrange particles in terms of their surface texture. The reason for this

is that if a method could be identified which could sort or arrange particles, it would be considerably easier to derive a parameter to describe the shape and/or texture properties of a particle (or material). The approaches attempted were limited to using the particle dimension, volume and surface area data obtained from scan results, as the aim of the research is specifically to exploit the high accuracy of the scanning equipment. Numerous approaches were tried on a trial and error basis and some successes were achieved based on visual observation of the data sorting.

Following initial trials, it was decided to develop a model with ten “reference particles” with which any given aggregate particle could be compared. As the aim of a proposed new system is ultimately to be applied in industry, the method or model should preferably be relatively simple.

It was considered that the two parameters that are most advantageous to this method of scanning (i.e. surface area and volume) would be instrumental in developing a reference system. From initial data experimentation and analyses, it was ultimately concluded that the ratio between the particle’s volume and surface area showed significant potential for differentiating between different particles’ surface texture or surface roughness. It was relatively obvious that the dimensions of each particle also needed to be considered (i.e. elongation). Subsequently data was analysed for individual particle sizes, considering these parameters. Particle sizes considered were those retained on a specific screen (e.g. +26.5 mm, +19.0 mm, +13.2 mm, etc.) and passing the screen normally considered one size larger than these.

It was initially theorised that the two extremes of shear resistance could be related to spheres and cubes. The hypothesis was that a sphere would have the least shear resistance related to shape and surface texture, while a cube would show the best interlock. Theoretical calculations were undertaken, but results soon proved the hypothesis to be erroneous as calculations for cubes and spheres produced identical values when determining the ratio between surface area and particle volume for a specific radius or length. In essence, the calculated value was always a ratio, depending on the dimensions of the object used. Anochie-Boateng *et al.* (2010) also considered spheres and cubes in their research; however more emphasis was placed on the accuracy of the scanning equipment.

After numerous concepts and models were attempted, only two showed potential. These two models were further analysed and tested as concepts and ultimately one model was abandoned in favour of the other. In the following discussion the two methods are described only briefly as they were compiled during the feasibility test stage. Subsequent sections explain the refinement and workings of the selected model in detail.

It was decided that the application of the models being compared would be best illustrated using an example. The +6.7 mm particle size was selected at random for use in this comparison. Datasets (with limited descriptive statistical analyses) for this example are included in Addendum E.

#### *4.3.1 Working Model One*





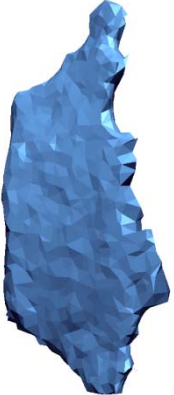



The first working model utilised the parameters volume, surface area and elongation (refer to section 3.6.3) for each particle. The “model value” was calculated as follows:

$$\text{Model Value} = (\text{Volume} / \text{Area}) \times \text{Elongation Value} \quad (\text{Equation 4. 1})$$

Once the model value had been calculated in a spread sheet, the range of values was sorted in ascending order. Ten values (i.e. representative particles) were randomly selected from the data in ascending order. The particle numbers (and material types) were retrieved from the data set and used to compile a model table showing the values/particles. Certain value ranges did not have representative particles due to insufficient data (this was clear from histogram analyses, but will be discussed in detail in section 4.5). Nevertheless, Table 4.4 shows the particles that were identified.

Using the entire data set for a given particle size (6.7 mm in this instance), preliminary analyses seemed promising. Particles appeared to range from relatively rounded at low values to angular at high values. In addition, it was noted that the results were severely affected by the elongation of the particles, which resulted in the selected “model particles” being biased towards including elongated particles.

**Table 4.4** All 6.7 mm particles (V/A) × (EV)

 <p><b>1.409</b> (Tillite 10)</p>	 <p><b>2.115</b> (Tillite 20)</p>	 <p><b>2.817</b> (Dolerite 8)</p>	 <p><b>3.536</b> (Hornfels 28)</p>	 <p><b>4.231</b> (Hornfels 26)</p>
 <p><b>4.936</b> (Granite 24)</p>	 <p><b>5.598</b> (Quartzite 28)</p>	<p>(Insufficient Data)</p>	<p>(Insufficient Data)</p>	 <p><b>7.775</b> (Tillite 28)</p>

As such, the model produced results based more on particle elongation and angularity than actual texture.

In order to address this (or attempt to minimise the effect of elongation on the data), the data were divided into two subsets based on the elongation values of the particles. Data for elongated and “regular” particles had to be analysed separately. The approach previously used was continued here in that particles with an elongation value of 2.00 and more would be considered elongated, while particles with an elongation value of less than 2.00 would be considered “regular” (refer to section 3.6.3).

The data were again sorted while the elongation value was applied to divide the data. To reiterate, elongated particles were accepted to be any particle in which the ratio between the maximum and minimum dimensions was more than 2.00. Once the two datasets were compiled (i.e. one data set for elongated particles and one data set for regular particles), the same (modelling) procedure was followed as discussed at the beginning of this section and ten new particles were identified for each dataset.

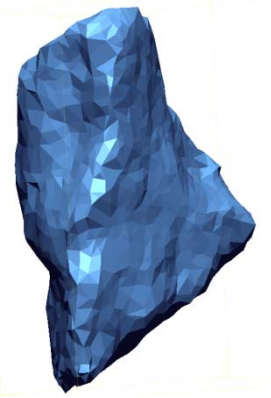


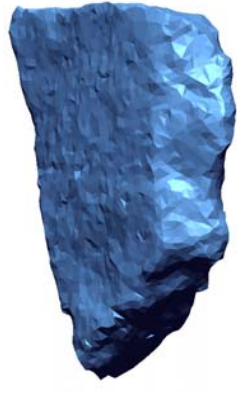

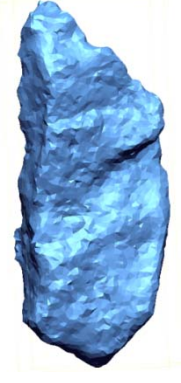


The model calculated for elongated particles (Table 4.5) showed little significant change or sorting in terms of surface texture or roundedness. No discernible increase or decrease was noted in the particle roughness of elongated particles identified for the model. Instead it appeared that the elongation and angularity of the particles again biased the model.

The model derived for regular particles using the same approach showed slightly more promise on initial revision. However, closer inspection showed that these particles too reflected a contrast in elongation and angularity rather than texture. The ten particles selected from the range of values for regular particles are shown in Table 4.6.

The cause of the apparent lack of sorting in the data was identified when the sorted data for the two datasets was reviewed. It was noted that by factoring the elongation value into the calculation, the model values were drastically biased towards elongated




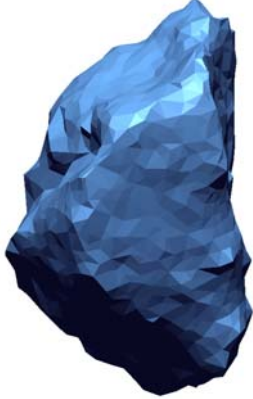




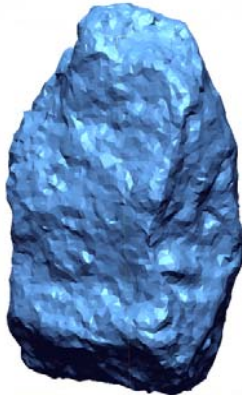
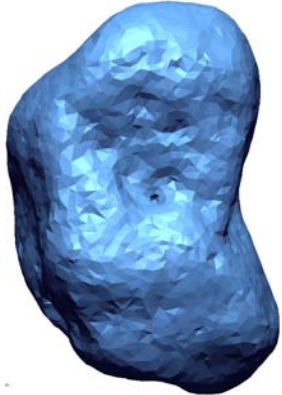


**Table 4.5** Elongated 6.7 mm particles (V/A×EV)

 <p><b>2.103</b> (Hornfels 16)</p>	 <p><b>2.736</b> (Dolerite 11)</p>	 <p><b>3.345</b> (Gravel 21)</p>	 <p><b>4.000</b> (Hornfels 24)</p>	 <p><b>4.630</b> (Granite 28)</p>
 <p><b>5.433</b> (Quartzite 29)</p>	 <p><b>5.600</b> (Quartzite 28)</p>	<p>(Insufficient data)</p>	<p>(Insufficient data)</p>	 <p><b>7.775</b> (Tillite 28)</p>



**Table 4.6** Regular 6.7 mm particles (V/A×EV)

 <p><b>1.409</b> (Tillite 10)</p>	 <p><b>1.584</b> (Granite 9)</p>	 <p><b>1.782</b> (Hornfels 9)</p>	 <p><b>1.965</b> (Tillite 1)</p>	 <p><b>2.154</b> (Quartzite 18)</p>
 <p><b>2.322</b> (Recycled Aggregate 1)</p>	 <p><b>2.541</b> (Gravel 23)</p>	 <p><b>2.706</b> (Gravel 19)</p>	 <p><b>2.774</b> (Granite 12)</p>	 <p><b>3.089</b> (Gravel 28)</p>

particles (i.e. high values). This was the case even for regular particles, but the effect was less amplified. The resulting models would all produce similar results in that limited texture attributes were discerned, but the models emphasised the elongation and associated angularity dramatically.

It was finally concluded that this method did not produce satisfactory results as the model failed to effectively achieve the objective of discriminating between particles based on their surface roughness or texture. The model did, however, show that the elongated nature of particles needed to be considered in analyses or distinctions needed to be made in data to allow analysis of regular and elongated particles.

#### *4.3.2 Working Model Two*

The second working model followed a similar approach to the first model with the exception that the elongation value was omitted from the model calculations. Subsequently the model value was calculated simply as follows:

$$\text{Model Value} = \text{Volume} / \text{Area} \quad (\text{Equation 4. 2})$$

As before, these values were calculated using a spread sheet. In order to compare the approach with the first working model that was derived, all the particle data were considered in this model before further subdivision. The model derived for the entire data range is illustrated in Table 4.7 and clearly shows that it is once more unduly influenced by elongated particles. The model showed the tendency to go from very angular and flattened/elongated particles to very rounded, more regular particles. Though the model in this form was not yet satisfactory, it did show significant improvement over the same stage results for the first working model in that it started discerning particle texture rather than pure particle angularity and/or elongation.











The data were further sorted in ascending order of the elongation value in order to divide the results into two subsets as previously done (i.e. regular particles and elongated particles). The data were again processed using equation 4.2, but this time the analysis was done for regular particles and elongated particles separately.

Analysis of the elongated particles showed that despite no longer factoring the elongation value into calculations, the parameter still affected the results. Table 4.8 shows the model derived for elongated particles and while the model does show significant refinement in texture, the angularity (as a function of elongation) of the particles still greatly affects the outcome of the analysis. The process was further affected by the fact that some of the scan data did not have the same scan density or resolution (e.g. Granite 13 vs. Recycled Aggregate 3 in Table 4.7), resulting in less accurate data (i.e. volume and surface area calculations).

The results of the analysis done on regular particles, however, showed considerable improvement over any of the preceding models. As elongated particles are excluded from this dataset, their effects on the data are largely ascribed to the actual particle texture and less so to the angularity associated with being elongated. That being, angularity is still considered to affect the result but the effects are far less pronounced after removing the elongated particle data.











The model derived for the regular particles is illustrated in Table 4.9. From this table it is clear that the particles range from coarse and angular (i.e. Hornfels 10) to fairly smooth and rounded (i.e. gravel 22). It must be emphasised that while gravel 5 appears smoother and more rounded than gravel 22, it is often the case that some irregularities or angularities of particles are out of sight in the 2-dimensional representation and are not necessarily illustrated on the captured image (i.e. the rear of the image may contain a coarser or rougher area).

**Table 4.7** All 6.7 mm particles (V/A)



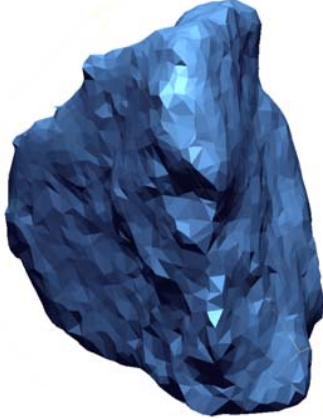





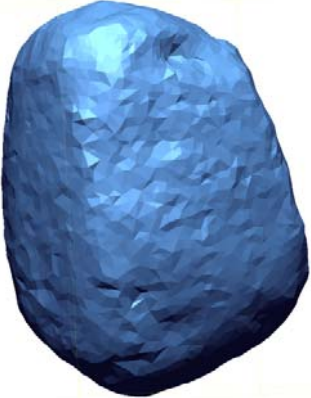
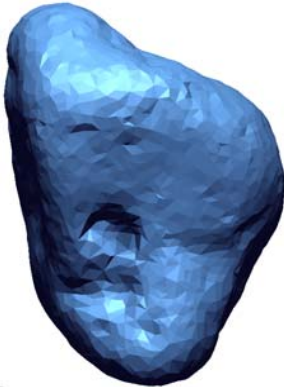
 <p><b>0.675</b> (Hornfels 30)</p>	 <p><b>0.774</b> (Tillite 26)</p>	 <p><b>0.873</b> (Granite 27)</p>	 <p><b>0.981</b> (Hornfels 16)</p>	 <p><b>1.084</b> (Quartzite 15)</p>
 <p><b>1.187</b> (Granite 13)</p>	 <p><b>1.294</b> (Recycled Aggregate 3)</p>	 <p><b>1.385</b> (Gravel 9)</p>	 <p><b>1.490</b> (Recycled Aggregate 12)</p>	 <p><b>1.595</b> (Gravel 29)</p>



**Table 4.8** Elongated 6.7 mm particles (V/A)

 <p><b>0.675</b> (Hornfels 30)</p>	 <p><b>0.774</b> (Tillite 26)</p>	 <p><b>0.873</b> (Granite 27)</p>	 <p><b>0.981</b> (Hornfels 16)</p>	 <p><b>1.084</b> (Quartzite 15)</p>
 <p><b>1.182</b> (Gravel 25)</p>	 <p><b>1.310</b> (Dolerite 25)</p>	 <p><b>1.427</b> (Gravel 15)</p>	 <p><b>1.512</b> (Dolerite 28)</p>	 <p><b>1.595</b> (Gravel 29)</p>

**Table 4.9** Regular 6.7 mm particles (V/A)

 <p><b>0.910</b> (Hornfels 10)</p>	 <p><b>0.981</b> (Hornfels 7)</p>	 <p><b>1.062</b> (Tillite 9)</p>	 <p><b>1.139</b> (Tillite 15)</p>	 <p><b>1.207</b> (Hornfels 9)</p>
 <p><b>1.285</b> (Granite 6)</p>	 <p><b>1.354</b> (Gravel 4)</p>	 <p><b>1.438</b> (Gravel 19)</p>	 <p><b>1.513</b> (Gravel 5)</p>	 <p><b>1.580</b> (Gravel 22)</p>

### 4.3.3 Comparison of Models

From the working models discussed above, two important conclusions were drawn:






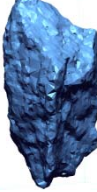
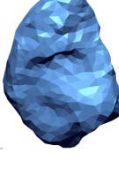



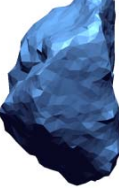

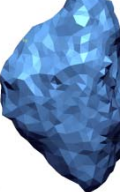
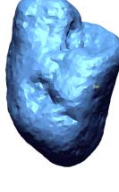


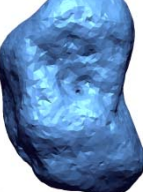
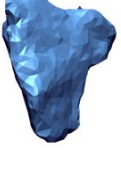





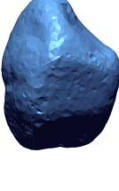

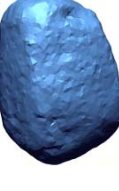
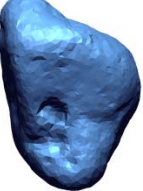
1. The elongation of a particle affects the models greatly. While it is necessary to consider the elongation of the particles, the elongation value should not be factored into calculations as it strongly biases results.
2. Particle texture and angularity are strongly co-dependent and cannot be discerned or separated effectively in the data. The angularity is often affected by the elongation and subsequently the effect can be limited by controlling or limiting the elongation of the particles in analyses.

Table 4.10 and Table 4.11 allow direct comparisons for regular and elongated particles, respectively. Each table shows results for all particles (first row) analysed using only the volume and area. The second row shows results after dividing the data into two subgroups (i.e. regular and elongated) and factoring in the elongation – as done in working model one. The final row shows the results divided into data groups without factoring in elongation, as done in working model two.

With all of the model comparisons considered it was concluded that working model two was better as it showed more refinement than model one and was not as strongly biased by the elongation of the particle. The model is currently relatively effective, but it is considered that it would improve considerably should more data become available.






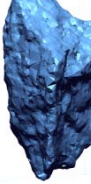











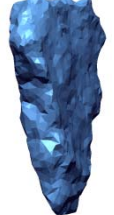
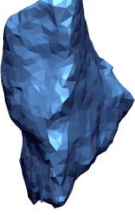

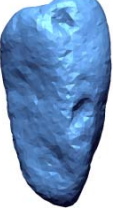

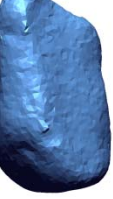

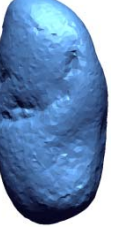
With the above in mind, working model two was selected as the approach to be adopted continuing further in this research. The model described and discussed here was done briefly and will be discussed, expanded, refined and analysed in more detail in the following sections.

**Table 4.10** Method comparison for regular 6.7 mm particles

Method	Rough	→								Smooth
		All Particles (V/A)								
Regular Particles (V/A)×EV										
Regular Particles (V/A)										



**Table 4.11** Method comparison for elongated 6.7 mm particles

Method	Rough	→								Smooth
		All Particles (V/A)								
Elongated Particles (V/A)×EV								(Insufficient data)	(Insufficient data)	
Elongated Particles (V/A)										

## 4.4 Detailed Models

Using the general approach outlined in section 4.3.2, the data were analysed in more detail. The data were considered for individual particle sizes, as the ratio between a particle's surface area and volume differs in range for different particle sizes (e.g. 26.5 mm vs. 4.75 mm). This meant that a model had to be developed for each particle size used for analysis. To illustrate the procedure, consider the data for particles of 9.5 mm size included in Addendum F. Development of the models was done in the following steps:

1. Select particle size (e.g. 9.5 mm) data
2. Sort all data based on elongation value
3. Divide dataset into regular (elongation value  $< 2.00$ ) and elongated (elongation value  $> 2.00$ ) particles
4. Sort datasets (i.e. elongated and regular) according to increasing (V/A) values.
5. Calculate general descriptive statistics, including a histogram analysis for the elongation values and (V/A) to identify gaps in the data set and to determine general attribute ranges
6. Identify minimum and maximum (V/A) values and determine data range
7. Calculate ten equal increments (values) between (and including) the minimum and maximum values
8. Consult the data set for the nearest matching values (i.e. particles) calculated in step seven. The particle with the closest corresponding value with individual increments was selected to graphically represent the model.

At step eight the gaps in data became most apparent as the nearest matching model was often significantly higher or lower in value; or sometimes even absent. This shortcoming will be overcome as more data is obtained.

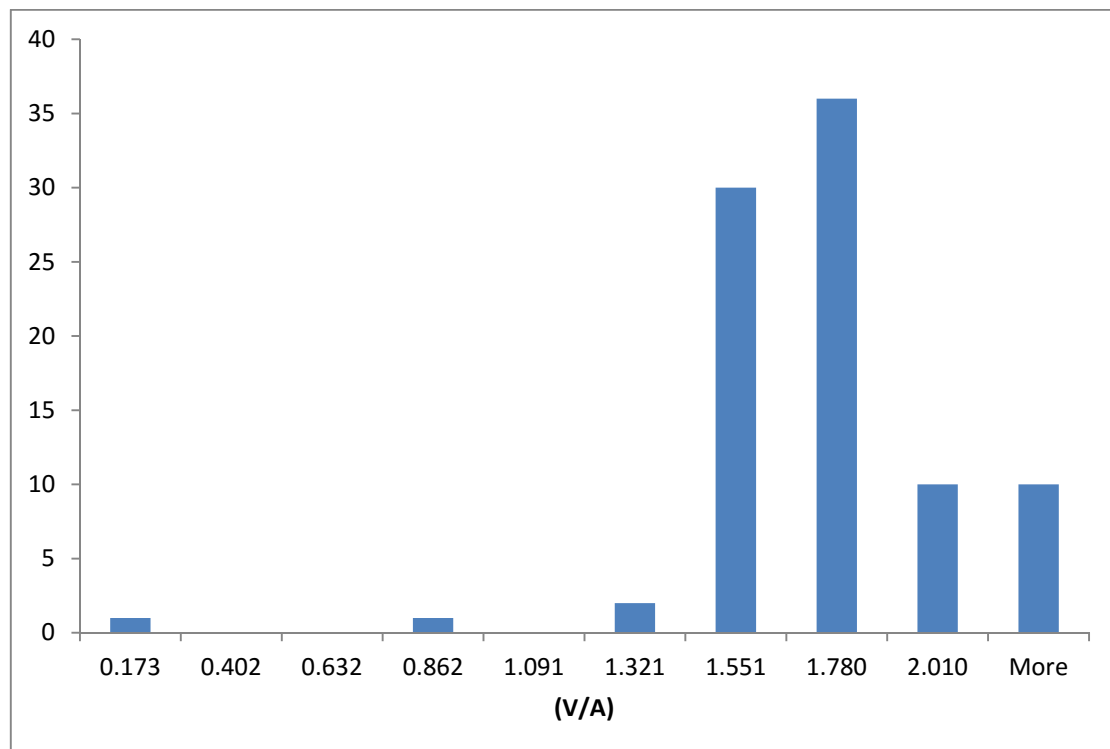
### 4.4.1 Data Analyses

The descriptive statistics and histogram analyses revealed certain deficiencies in the data. The bias in data which was previously discussed (section 3.6.2 – i.e. preferential

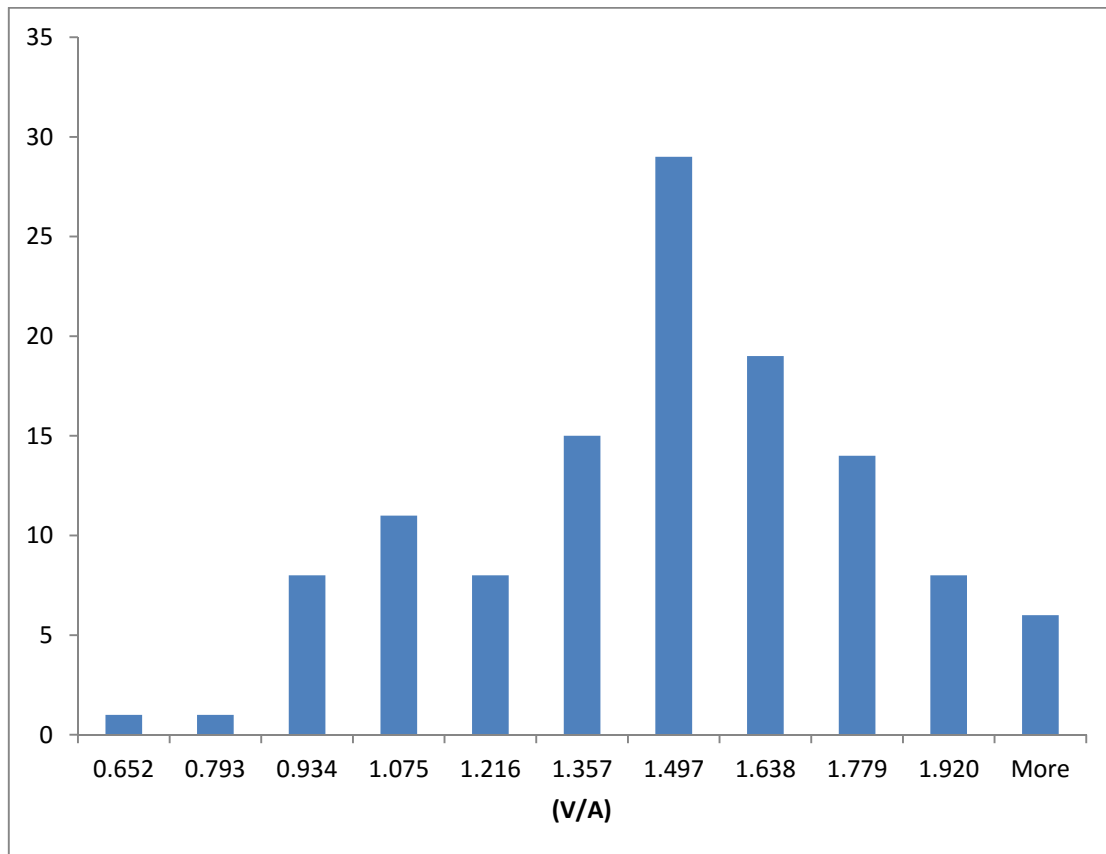
selection of elongated particles) became apparent during the data analyses. More elongated particles were sampled relative to regular particles and this trend was not representative of the bulk sample.

The resulting gaps in the data became even more notable and better illustrated when histograms were compiled. Figure 4.2 shows a histogram compiled for regular particles, while Figure 4.3 shows the histogram for elongated particles when analysing the ratio between the particles' volume and area (V/A).

From the two histograms it is apparent that the elongated particles have a better – or more representative - data range than the regular particles. While it would be ideal to have the entire data range equally represented (i.e. a more normal distribution with no peaks or troughs in the histogram), this is unlikely to ever be achieved. The data for regular particles, though, seems to be concentrated with large gaps and little representative data in between. This will ultimately result in a far better model for the elongated particle data set than the regular particle dataset, as the latter will not contain sufficient data to represent the entire range of values calculated.



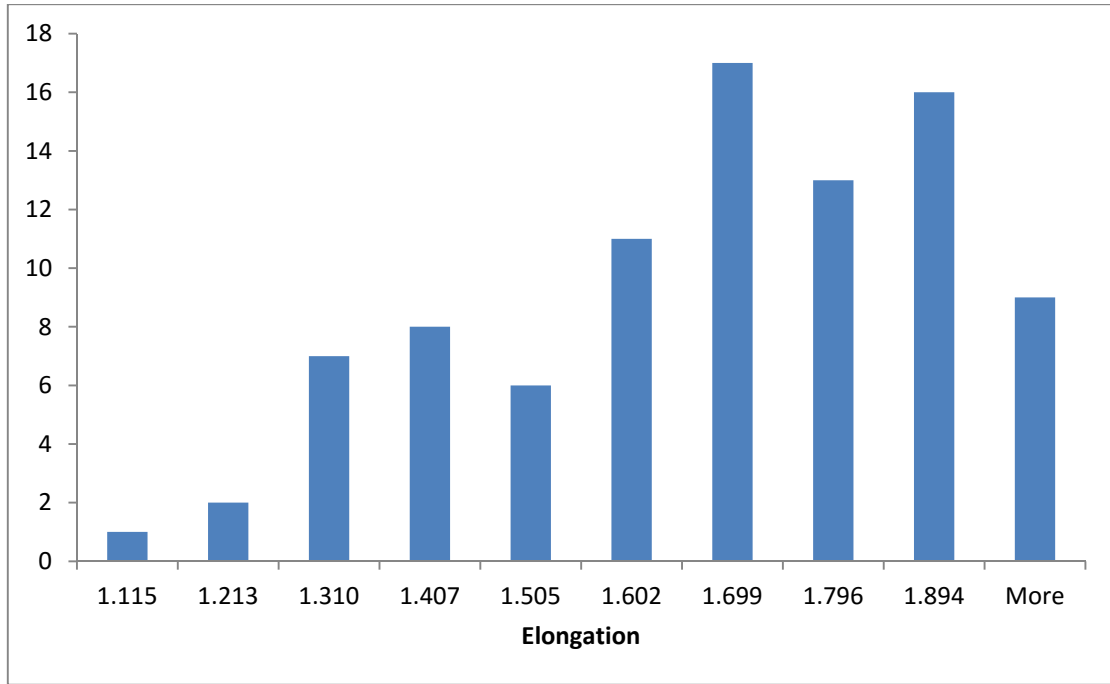
**Figure 4.2** Histogram (%) for regular particles (V/A)



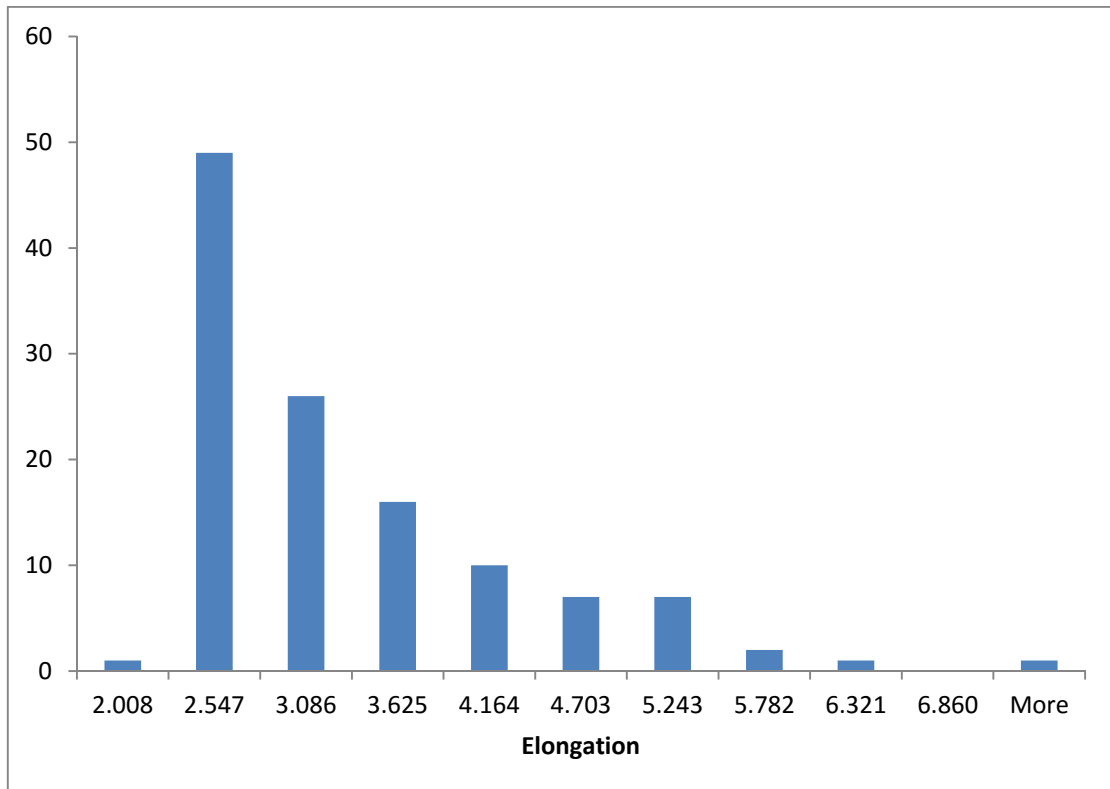
**Figure 4.3** Histogram (%) for elongated particles (V/A)

In addition, the data distribution of the particles' elongation values was also reviewed. Clearly regular particles would have elongation values between 1.00 and 1.99, while elongated particles would have elongation values exceeding 2.00. Figure 4.4 shows a histogram for the regular particles' elongation. It can be deduced that the majority of the particles have slightly more oblate or tabular shapes, with the minority of the particles having elongation values near 1.00 (i.e. cubic shape). By far the majority of the particles have an elongation value between 1.50 and 1.99.

The histogram compiled for the elongation value of the separated elongated particles (Figure 4.5) also shows an interesting distribution. The majority of the particles have elongation values between 2.00 and 3.00 with range (or "bin") counts becoming progressively less as the elongation value increases. At some point the elongation would have been influenced by the grading procedure used when the particle sizes were initially segregated.



**Figure 4.4** Histogram (%) for regular particles' elongation



**Figure 4.5** Histogram (%) for elongated particles' elongation

If one considers the matter logically, a very elongated particle is unlikely to become vertically orientated (even when agitated by the shaker) and would remain in a “flat” orientation. As a result, the particle would never be orientated in such a way that it would actually pass a sieve screen, even though it may be able to do so based on its other two dimensions. This effect is also likely to be more pronounced in larger particles (e.g. 26.5 mm) than in smaller particles, as the latter may still be movable by the shaker’s agitation. Nevertheless, as the particle elongation increases, the chances of such a particle obtaining a suitable orientation to pass the screen are likely to decrease.

Strictly speaking, though, such a scenario should not actually be encountered in the samples used for analyses, as the materials should be largely devoid of excessively elongated particles. Any (excessively) elongated particles that may indeed be included in the sample should comprise only a small constituent of the sample. With this in mind, the bias in sample collection must once more be considered. The composition of sample six, in particular, will disregard this approach as the entire sample was specifically mixed to contain an excessive volume of elongated particles.

#### *4.4.2 Model Development Procedure*

Table 4.12 shows the selection approach while Table 4.13 and Table 4.14 show the models for regular and elongated particles, respectively. The corresponding particles that were selected for the model are highlighted in the data sets (Addendum F).

It is clear from Table 4.13 that data were not available to represent certain ranges of the model. This was a frequent occurrence throughout analyses and is attributed to the fact that the data used for analyses is based on stratified “random” sampling of limited particles. It is anticipated that these data may also not necessarily be sufficient to classify all materials effectively using this system. However, if the data set is expanded, more data would result in more accurate models and may even enable the introduction of extra intervals of roughness (i.e. fifteen or twenty “classes” as opposed to the ten used in this analysis). If the scanning system is used in industry, test data may simply be added to the existing data base and the models revised periodically to

benefit from the new data. It is expected that the models will become more refined and complete with the progressive addition of more data.


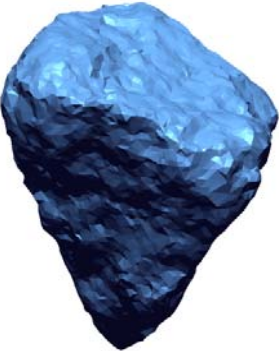
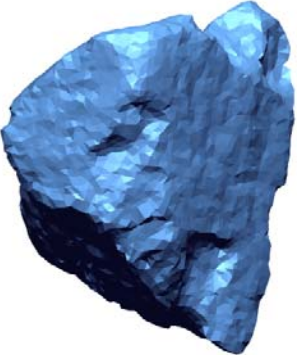
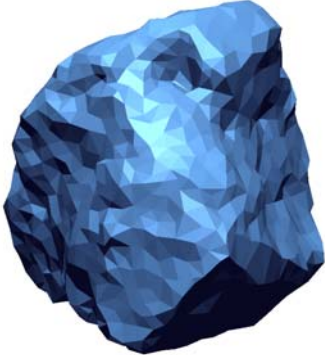

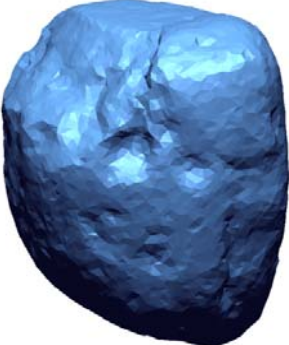

Regardless of the restrictions imposed by the available data set (and occasional variable scan resolutions) the method depicted above was followed through for all particles sizes for which data was available (i.e. 4.75 mm, 6.7 mm, 9.5 mm, 13.2 mm, 19.0 mm and 26.5 mm). Data for the 26.5 mm particles was particularly limited, but included nevertheless. Table 4.15 to Table 4.29 show the resulting models.

**Table 4.12** Particle selection for 9.5 mm model










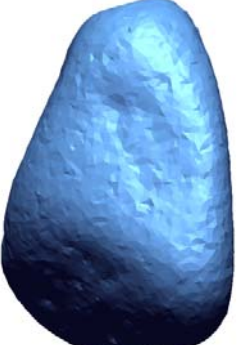
<b>REGULAR PARTICLES</b>		
<b>Minimum V/A</b>	0.173	
<b>Maximum V/A</b>	2.240	
<b>Range</b>	2.067	
<b>Increments Calculated</b>	0.230	
<b>Increment Value</b>	<b>Nearest Match</b>	<b>Sample/Particle Number</b>
0.173	0.173	Hornfels 1
0.402	None	None
0.632	0.745	Granite 8
0.862	None	None
1.091	None	None
1.321	1.320	Hornfels 8
1.551	1.552	Recycled Aggregate 8
1.780	1.777	Quartzite 8
2.010	2.016	Gravel 12
2.240	2.240	Gravel 19
<b>ELONGATED PARTICLES</b>		
<b>Minimum V/A</b>	0.652	
<b>Maximum V/A</b>	2.061	
<b>Range</b>	1.409	
<b>Increments Calculated</b>	0.157	
<b>Increment Value</b>	<b>Nearest Match</b>	<b>Sample/Particle Number</b>
0.652	0.652	Hornfels 30
0.809	0.730	Hornfels 29
0.965	0.949	Quartzite 23
1.122	1.126	Quartzite 30
1.278	1.271	Recycled Aggregate 25
1.435	1.431	Tillite 21
1.591	1.583	Quartzite 12
1.748	1.742	Gravel 25
1.905	1.891	Gravel 22
2.061	2.061	Gravel 27



**Table 4.13** Model for regular 9.5 mm particles

 <p><b>0.173</b> (Hornfels 1)</p>	<p>(Insufficient Data)</p>	 <p><b>0.745</b> (Granite 8)</p>	<p>(Insufficient Data)</p>	<p>(Insufficient Data)</p>
 <p><b>1.320</b> (Hornfels 8)</p>	 <p><b>1.552</b> (Recycled Aggregate 8)</p>	 <p><b>1.777</b> (Quartzite 8)</p>	 <p><b>2.016</b> (Gravel 12)</p>	 <p><b>2.240</b> (Gravel 19)</p>











**Table 4.14** Model for elongated 9.5 mm particles

 <p><b>0.652</b> (Hornfels 30)</p>	 <p><b>0.730</b> (Hornfels 29)</p>	 <p><b>0.949</b> (Quartzite 23)</p>	 <p><b>1.126</b> (Quartzite 30)</p>	 <p><b>1.271</b> (Recycled Aggregate 25)</p>
 <p><b>1.431</b> (Tillite 21)</p>	 <p><b>1.583</b> (Quartzite 12)</p>	 <p><b>1.742</b> (Gravel 25)</p>	 <p><b>1.891</b> (Gravel 22)</p>	 <p><b>2.061</b> (Gravel 27)</p>

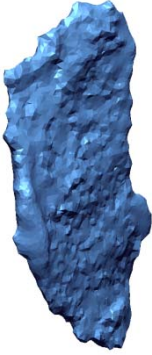





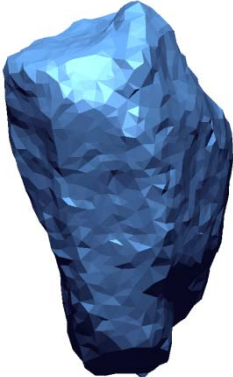

**Table 4.15** Particle selection for 4.75 mm model

<b>REGULAR PARTICLES</b>		
<b>Minimum V/A</b>	0.625	
<b>Maximum V/A</b>	1.162	
<b>Range</b>	0.537	
<b>Increments Calculated</b>	0.060	
<b>Increment Value</b>	<b>Nearest Match</b>	<b>Sample/Particle Number</b>
0.625	0.625	Quartzite 8
0.685	0.715	Quartzite 10
0.744	0.745	Quartzite 3
0.804	0.804	Hornfels 3
0.864	0.866	Granite 8
0.923	0.925	Tillite 1
0.983	0.982	Dolerite 16
1.043	1.041	Hornfels 7
1.102	1.093	Gravel 1
1.162	1.162	Gravel 3
<b>ELONGATED PARTICLES</b>		
<b>Minimum V/A</b>	0.304	
<b>Maximum V/A</b>	1.503	
<b>Range</b>	1.199	
<b>Increments Calculated</b>	0.133	
<b>Increment Value</b>	<b>Nearest Match</b>	<b>Sample/Particle Number</b>
0.304	0.304	Tillite 28
0.437	0.439	Tillite 29
0.570	0.570	Hornfels 28
0.703	0.706	Tillite 25
0.837	0.836	Hornfels 22
0.970	0.970	Granite 21
1.029	1.022	Hornfels 19
1.236	None	None
1.369	None	None
1.503	1.503	Dolerite 6

**Table 4.16** Model for regular 4.75 mm particles

 <p><b>0.625</b> (Quartzite 8)</p>	 <p><b>0.745</b> (Quartzite 10)</p>	 <p><b>0.745</b> (Quartzite 3)</p>	 <p><b>0.804</b> (Hornfels 3)</p>	 <p><b>0.866</b> (Granite 8)</p>
 <p><b>0.925</b> (Tillite 1)</p>	 <p><b>0.982</b> (Dolerite 16)</p>	 <p><b>1.041</b> (Hornfels 7)</p>	 <p><b>1.093</b> (Gravel 1)</p>	 <p><b>1.162</b> (Gravel 3)</p>

**Table 4.17** Model for elongated 4.75 mm particles



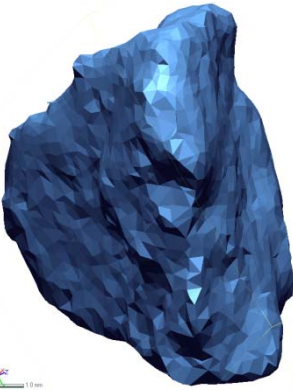

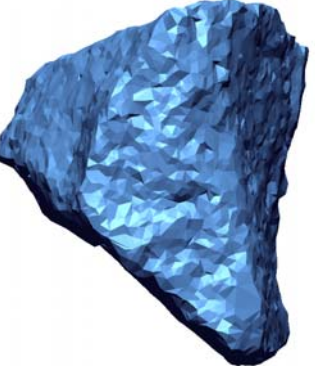

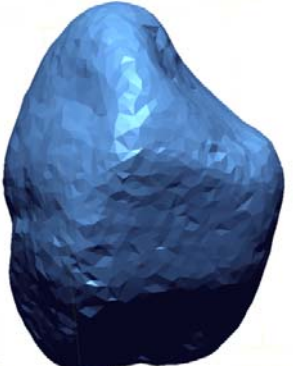
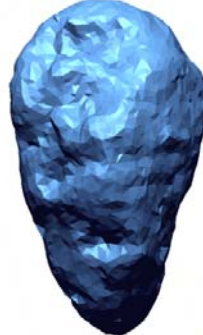

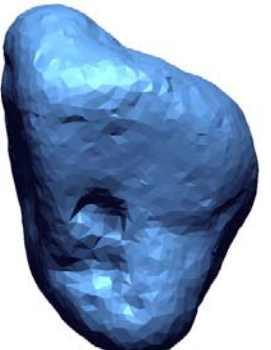
 <p><b>0.304</b> (Tillite 28)</p>	 <p><b>0.439</b> (Tillite 29)</p>	 <p><b>0.570</b> (Hornfels 28)</p>	 <p><b>0.706</b> (Tillite 25)</p>	 <p><b>0.836</b> (Hornfels 22)</p>
 <p><b>0.970</b> (Granite 21)</p>	 <p><b>1.022</b> (Hornfels 19)</p>	<p>(Insufficient Data)</p>	<p>(Insufficient Data)</p>	 <p><b>1.503</b> (Dolerite 6)</p>








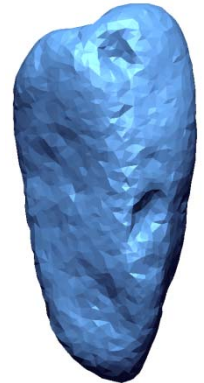
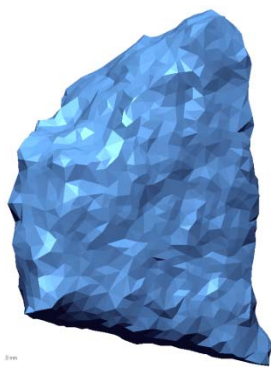



**Table 4.18** Particle selection for 6.7 mm model

<b>REGULAR PARTICLES</b>		
<b>Minimum V/A</b>	0.910	
<b>Maximum V/A</b>	1.580	
<b>Range</b>	0.670	
<b>Increments Calculated</b>	0.074	
<b>Increment Value</b>	<b>Nearest Match</b>	<b>Sample/Particle Number</b>
0.910	0.910	Hornfels 10
0.985	0.981	Hornfels 7
1.059	1.062	Tillite 9
1.134	1.139	Tillite 15
1.208	1.208	Quartzite 2
1.282	1.285	Granite 6
1.357	1.354	Gravel 4
1.431	1.439	Gravel 19
1.506	1.513	Gravel 5
1.580	1.580	Gravel 22
<b>ELONGATED PARTICLES</b>		
<b>Minimum V/A</b>	0.675	
<b>Maximum V/A</b>	1.595	
<b>Range</b>	0.920	
<b>Increments Calculated</b>	0.102	
<b>Increment Value</b>	<b>Nearest Match</b>	<b>Sample/Particle Number</b>
0.675	0.675	Hornfels 30
0.778	0.774	Tillite 26
0.880	0.873	Granite 27
0.982	0.981	Hornfels 16
1.084	1.084	Quartzite 15
1.186	1.182	Gravel 25
1.289	1.284	Dolerite 8
1.391	1.379	Dolerite 30
1.493	1.490	Recycled Aggregate 12
1.595	1.595	Gravel 29

**Table 4.19** Model for regular 6.7 mm particles

 <p><b>0.910</b> (Hornfels 10)</p>	 <p><b>0.981</b> (Hornfels 7)</p>	 <p><b>1.062</b> (Tillite 9)</p>	 <p><b>1.139</b> (Tillite 15)</p>	 <p><b>1.208</b> (Quartzite 2)</p>
 <p><b>1.285</b> (Granite 6)</p>	 <p><b>1.354</b> (Gravel 4)</p>	 <p><b>1.439</b> (Gravel 19)</p>	 <p><b>1.513</b> (Gravel 5)</p>	 <p><b>1.580</b> (Gravel 22)</p>

**Table 4.20** Model for elongated 6.7 mm particles

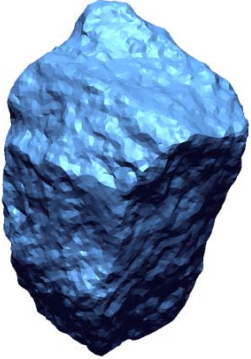
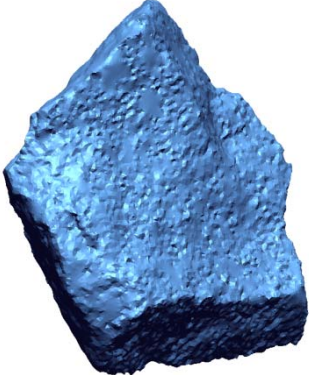
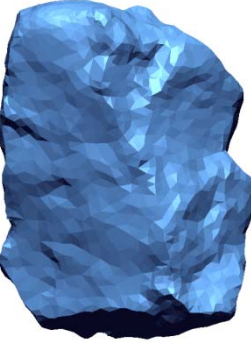

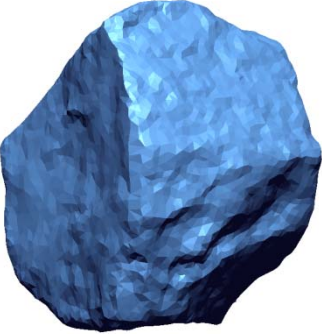
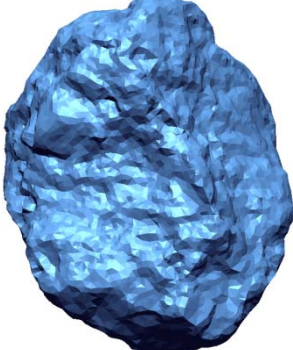
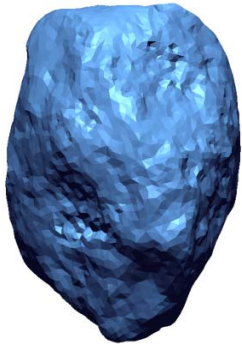
 <p><b>0.675</b> (Hornfels 30)</p>	 <p><b>0.774</b> (Tillite 26)</p>	 <p><b>0.873</b> (Granite 27)</p>	 <p><b>0.981</b> (Hornfels 16)</p>	 <p><b>1.084</b> (Quartzite 15)</p>
 <p><b>1.182</b> (Gravel 25)</p>	 <p><b>1.284</b> (Dolerite 8)</p>	 <p><b>1.379</b> (Dolerite 30)</p>	 <p><b>1.490</b> (Recycled Aggregate 12)</p>	 <p><b>1.595</b> (Gravel 29)</p>



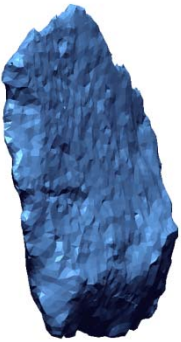


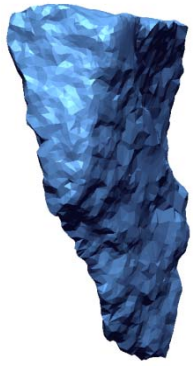
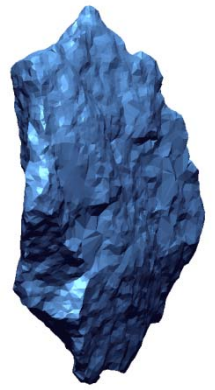
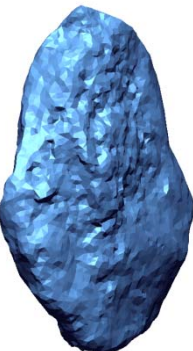
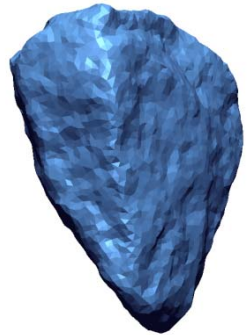

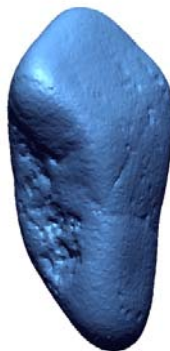
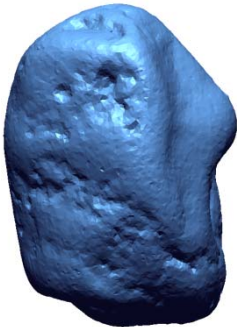
**Table 4.21** Particle selection for 13.2 mm model

<b>REGULAR PARTICLES</b>		
<b>Minimum V/A</b>	0.377	
<b>Maximum V/A</b>	2.917	
<b>Range</b>	2.540	
<b>Increments Calculated</b>	0.282	
<b>Increment Value</b>	<b>Nearest Match</b>	<b>Sample/Particle Number</b>
0.377	0.377	Granite 2
0.659	None	None
0.942	None	None
1.224	None	None
1.506	1.661	Quartzite 22
1.788	1.783	Quartzite 10
2.071	2.066	Quartzite 7
2.353	2.360	Hornfels 9
2.635	2.630	Granite 14
2.917	2.917	Recycled Aggregate 2
<b>ELONGATED PARTICLES</b>		
<b>Minimum V/A</b>	0.815	
<b>Maximum V/A</b>	3.146	
<b>Range</b>	2.331	
<b>Increments Calculated</b>	0.259	
<b>Increment Value</b>	<b>Nearest Match</b>	<b>Sample/Particle Number</b>
0.815	0.815	Quartzite 30
1.074	0.986	Hornfels 29
1.333	1.331	Tillite 29
1.592	1.585	Dolerite 17
1.851	1.853	Dolerite 6
2.110	2.112	Recycled Aggregate 21
2.369	2.362	Recycled Aggregate 13
2.628	2.615	Granite 12
2.887	2.900	Gravel 26
3.146	3.146	Gravel 14

**Table 4.22** Model for regular 13.2 mm particles

 <p><b>0.377</b> (Granite 2)</p>	<p>(Insufficient Data)</p>	<p>(Insufficient Data)</p>	<p>(Insufficient Data)</p>	 <p><b>1.661</b> (Quartzite 22)</p>
 <p><b>1.783</b> (Quartzite 10)</p>	 <p><b>2.066</b> (Quartzite 7)</p>	 <p><b>2.360</b> (Hornfels 9)</p>	 <p><b>2.630</b> (Granite 14)</p>	 <p><b>2.917</b> (Recycled Aggregate 2)</p>

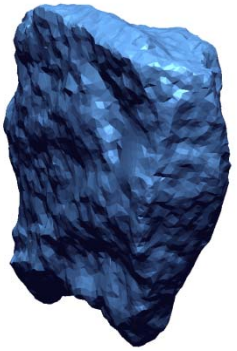
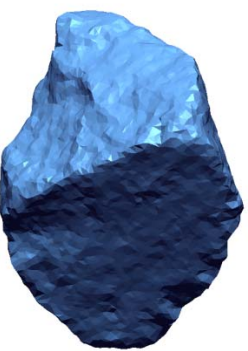
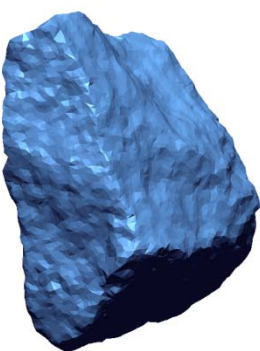
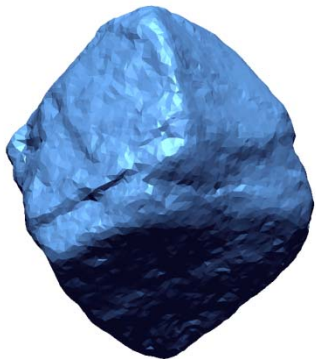
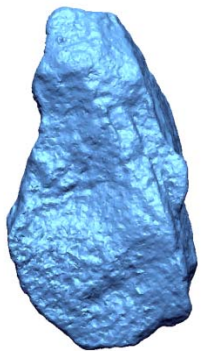
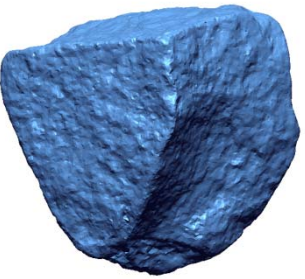
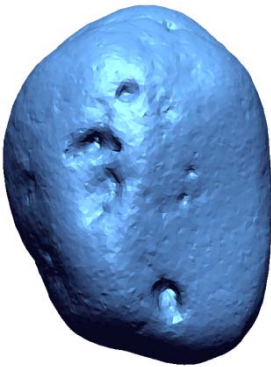
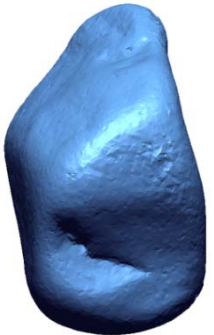
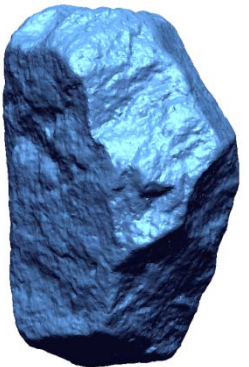
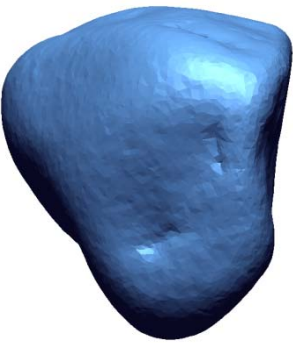
**Table 4.23** Model for elongated 13.2 mm particles

 <p><b>0.815</b> (Quartzite 30)</p>	 <p><b>0.986</b> (Hornfels 29)</p>	 <p><b>1.331</b> (Tillite 29)</p>	 <p><b>1.585</b> (Dolerite 17)</p>	 <p><b>1.853</b> (Dolerite 6)</p>
 <p><b>2.112</b> (Recycled Aggregate 21)</p>	 <p><b>2.362</b> (Recycled Aggregate 13)</p>	 <p><b>2.615</b> (Granite 12)</p>	 <p><b>2.900</b> (Gravel 26)</p>	 <p><b>3.146</b> (Gravel 14)</p>

**Table 4.24** Particle selection for 19.0 mm model


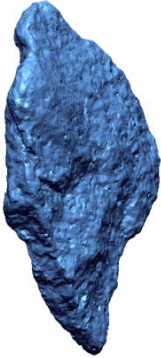

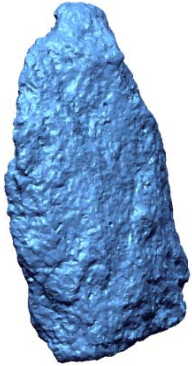
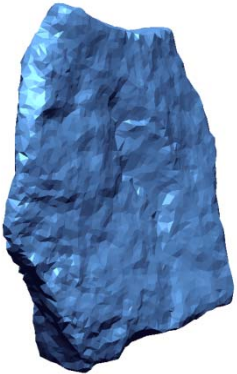
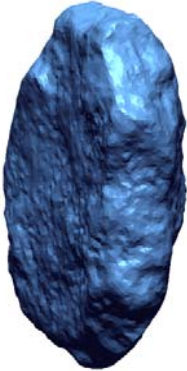
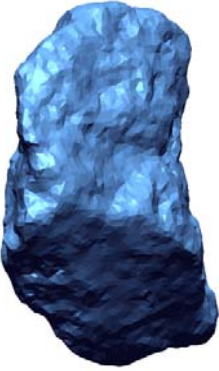
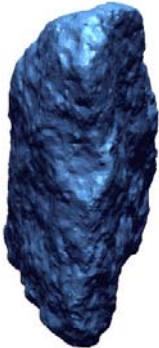
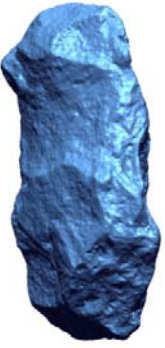
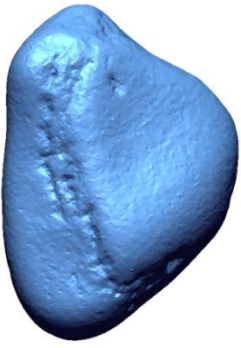
<b>REGULAR PARTICLES</b>		
<b>Minimum V/A</b>	2.204	
<b>Maximum V/A</b>	4.010	
<b>Range</b>	1.806	
<b>Increments Calculated</b>	0.201	
<b>Increment Value</b>	<b>Nearest Match</b>	<b>Sample/Particle Number</b>
2.204	2.204	Dolerite 28
2.405	2.375	Quartzite 18
2.605	2.605	Quartzite 12
2.806	2.808	Hornfels 18
3.007	3.000	Tillite 18
3.207	3.198	Hornfels 3
3.408	3.407	Gravel 7
3.609	3.637	Gravel 18
3.809	3.827	Tillite 19
4.010	4.010	Gravel 29
<b>ELONGATED PARTICLES</b>		
<b>Minimum V/A</b>	1.209	
<b>Maximum V/A</b>	3.621	
<b>Range</b>	2.412	
<b>Increments Calculated</b>	0.268	
<b>Increment Value</b>	<b>Nearest Match</b>	<b>Sample/Particle Number</b>
1.209	1.209	Quartzite 29
1.477	1.505	Granite 29
1.745	1.755	Quartzite 28
2.013	2.022	Granite 28
2.281	2.278	Quartzite 17
2.549	2.550	Recycled Aggregate 12
2.8170	2.825	Granite 16
3.085	3.089	Granite 18
3.353	3.343	Tillite 21
3.621	3.621	Gravel 17

**Table 4.25** Model for regular 19.0 mm particles

 <p><b>2.204</b> (Dolerite 28)</p>	 <p><b>2.375</b> (Quartzite 18)</p>	 <p><b>2.605</b> (Quartzite 12)</p>	 <p><b>2.808</b> (Hornfels 18)</p>	 <p><b>3.000</b> (Tillite 18)</p>
 <p><b>3.200</b> (Hornfels 3)</p>	 <p><b>3.407</b> (Gravel 7)</p>	 <p><b>3.637</b> (Gravel 18)</p>	 <p><b>3.827</b> (Tillite 19)</p>	 <p><b>4.010</b> (Gravel 29)</p>



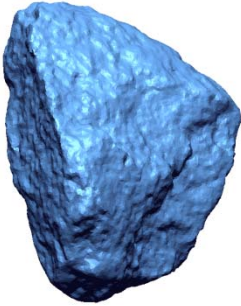
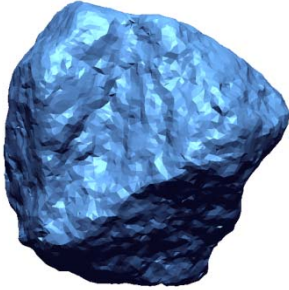
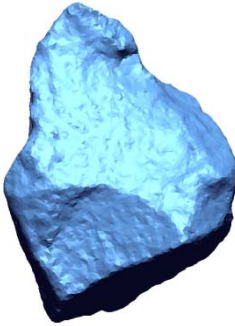
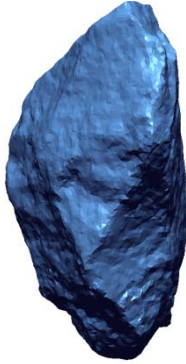
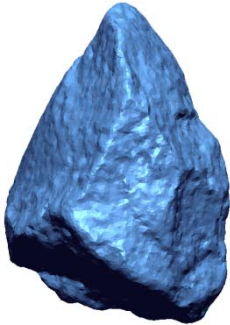
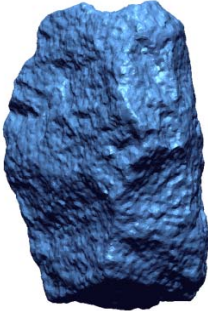
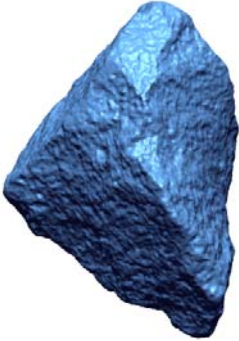
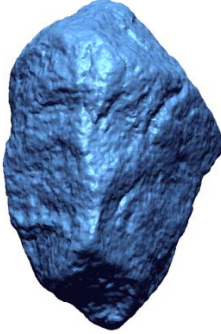
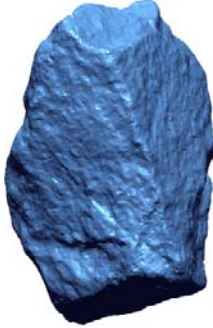
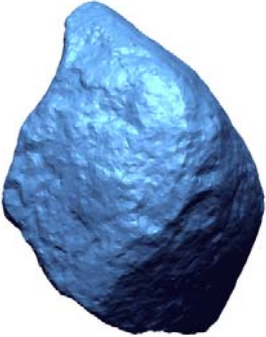
**Table 4.26** Model for elongated 19.0 mm particles

 <p><b>1.209</b> (Quartzite 29)</p>	 <p><b>1.505</b> (Granite 29)</p>	 <p><b>1.755</b> (Quartzite 28)</p>	 <p><b>2.022</b> (Granite 28)</p>	 <p><b>2.278</b> (Quartzite 17)</p>
 <p><b>2.550</b> (Recycled Aggregate 12)</p>	 <p><b>2.825</b> (Granite 16)</p>	 <p><b>3.089</b> (Granite 18)</p>	 <p><b>3.343</b> (Tillite 21)</p>	 <p><b>3.621</b> (Gravel 17)</p>

**Table 4.27** Particle selection for 26.5 mm model

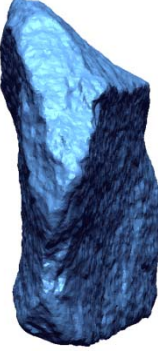

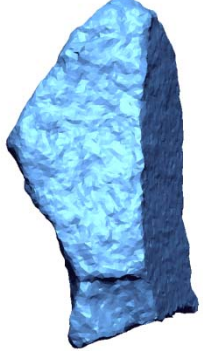

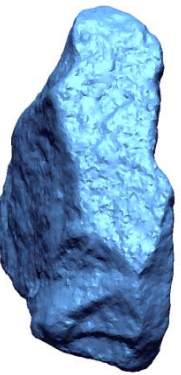
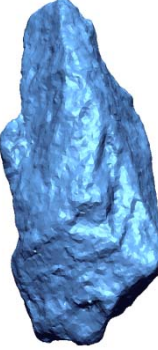
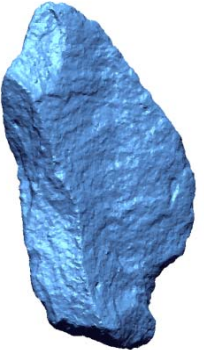
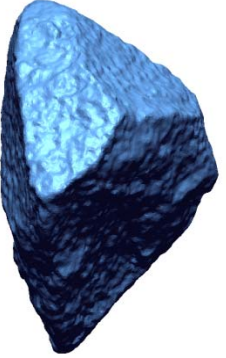
<b>REGULAR PARTICLES</b>		
<b>Minimum V/A</b>	3.303	
<b>Maximum V/A</b>	4.964	
<b>Range</b>	1.661	
<b>Increments Calculated</b>	0.185	
<b>Increment Value</b>	<b>Nearest Match</b>	<b>Sample/Particle Number</b>
3.303	3.303	Dolerite 11
3.488	3.504	Granite 6
3.672	3.663	Hornfels 16
3.857	3.857	Hornfels 6
4.041	4.043	Tillite 9
4.227	4.216	Dolerite 13
4.411	4.455	Dolerite 15
4.596	4.607	Dolerite 6
4.780	4.781	Tillite 23
4.964	4.964	Tillite 15
<b>ELONGATED PARTICLES</b>		
<b>Minimum V/A</b>	3.168	
<b>Maximum V/A</b>	4.796	
<b>Range</b>	1.628	
<b>Increments Calculated</b>	0.181	
<b>Increment Value</b>	<b>Nearest Match</b>	<b>Sample/Particle Number</b>
3.168	3.168	Hornfels 15
3.349	3.349	Granite 16
3.530	3.572	Hornfels 5
3.711	3.702	Tillite 18
3.892	3.918	Tillite 22
4.072	4.007	Tillite 17
4.253	4.200	Tillite 30
4.434	None	None
4.615	None	None
0.181	0.181	Dolerite 1

**Table 4.28** Model for regular 26.5 mm particles

 <p><b>3.303</b> (Dolerite 11)</p>	 <p><b>3.504</b> (Granite 6)</p>	 <p><b>3.663</b> (Hornfels 16)</p>	 <p><b>3.857</b> (Hornfels 6)</p>	 <p><b>4.043</b> (Tillite 9)</p>
 <p><b>4.216</b> (Dolerite 13)</p>	 <p><b>4.455</b> (Dolerite 5)</p>	 <p><b>4.607</b> (Dolerite 6)</p>	 <p><b>4.781</b> (Tillite 23)</p>	 <p><b>4.964</b> (Tillite 15)</p>



**Table 4.29** Model for elongated 26.5 mm particles

 <p><b>3.168</b> (Hornfels 15)</p>	 <p><b>3.349</b> (Granite 16)</p>	 <p><b>3.572</b> (Hornfels 5)</p>	 <p><b>3.702</b> (Tillite 18)</p>	 <p><b>3.918</b> (Tillite 22)</p>
 <p><b>4.007</b> (Tillite 17)</p>	 <p><b>4.200</b> (Tillite 30)</p>	<p>(Insufficient Data)</p>	<p>(Insufficient Data)</p>	 <p><b>4.796</b> (Dolerite 1)</p>

## 4.5 Method Application

The method and models discussed in the previous section can be applied in an attempt to characterise an aggregate material. For this, the tillite sample is utilised to show how the models can be applied to summarise the particle textures of any selected material. This differs from the models in the preceding section where one particle was compared with a standard set of particle data. The aim of this section is to consider the particles of a particular size and material and to simplify their data to a single particle which is deemed most representative of all the particles of a particular size, for that particular material. Simply stated, this is a data reduction exercise, reducing all the particles scanned (for a specific size) to a single data set best representing the sample. The single values can be used to provide a visual reference as illustrated, but will be applied further in subsequent sections. The data for this example is included in Addendum G.

As with previous analyses the data for each particle size is divided into elongated and regular particles. These two subsets are again analysed individually to account for elongation and associated angularity.

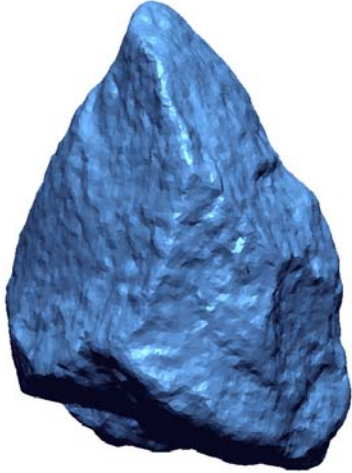
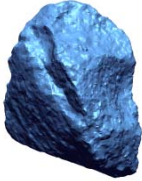
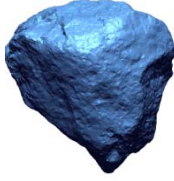


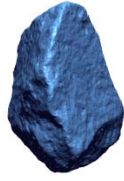
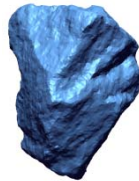
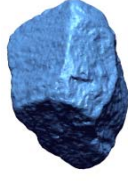
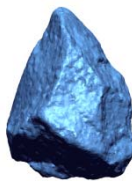

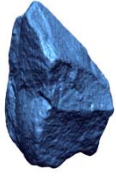
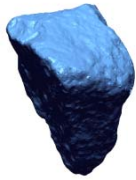
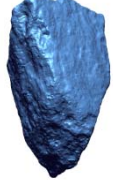
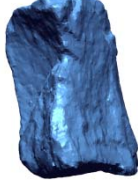
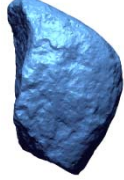
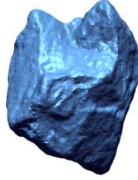
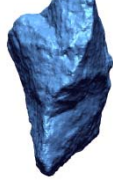
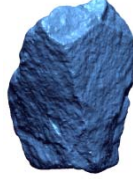

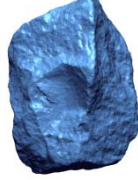
The representative value of  $(V/A)$  for the particle size is found by simply calculating a mean value of the  $(V/A)$ . This is done for regular and elongated particles of each particle size (i.e. 4.75 mm, 6.7 mm, 9.5 mm, 13.2 mm, 19.0 mm and 26.5 mm) and can be easily performed using a spread sheet. This average value is then compared with the models derived in the previous section to identify a single particle with the closest correlating  $(V/A)$  value. Alternatively a closest match can be selected from the source data (i.e. the master dataset), which is more comprehensive and thus likely to provide more accurate results. The particle is assumed to be representative of the cumulative particle data. The percentage of elongated or regular particles is also recorded as an early indicator of the content of elongated particles (i.e. flakiness index). The comparison for the tillite example is summarised in table 4.30 below, based on the models summarised in Table 4.15 to Table 4.29.

**Table 4.30** Summary of representative particle selection for tillite

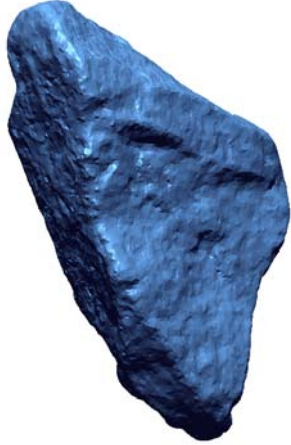











<b>Particles</b>	<b>Average (V/A)</b>	<b>Corresponding Model (V/A)</b>	<b>Model Particle</b>
26.5 mm Regular	4.120	4.043	Tillite 9
26.5 mm Elongated	3.834	3.918	Tillite 22
19.0 mm Regular	3.267	3.200	Hornfels 3
19.0 mm Elongated	2.678	2.550	Recycled Aggregate 12
13.2 mm Regular	2.362	2.360	Hornfels 9
13.2 mm Elongated	2.013	2.112	Recycled Aggregate 21
9.5 mm Regular	1.461	1.552	Recycled Aggregate 8
9.5 mm Elongated	1.253	1.271	Recycled Aggregate 25
6.7 mm Regular	1.185	1.208	Quartzite 2
6.7 mm Elongated	0.922	0.873	Granite 27
4.75 mm Regular	0.837	0.866	Granite 8
4.75 mm Elongated	0.725	0.706	Tillite 25

To allow the reader a visual comparison, Table 4.31 through Table 4.42 show the elongated or regular particles for a particular particle size, as well as its representative model particle, as identified through the procedure described above. Note that the model particle may not necessarily be of the same origin as the sample being assessed. For example, when calculating an “average value” for a tillite, it may happen that the closest match in the data is (for example) a dolerite particle. Hence, the closest match identified may be of a different origin to the material being summarised.

**Table 4.31** Regular particles comparison for 26.5 mm tillite

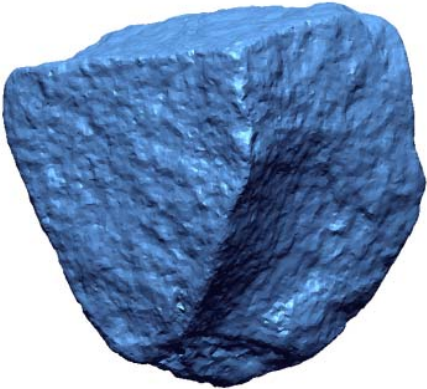
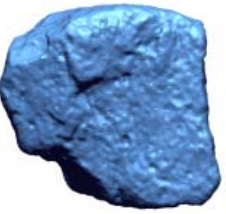
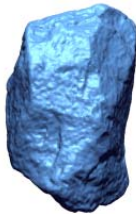
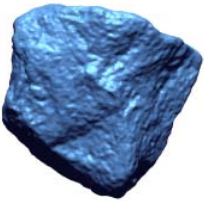
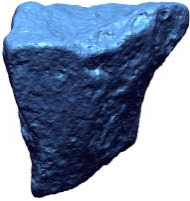
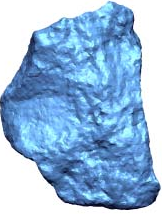

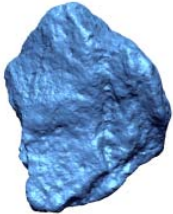

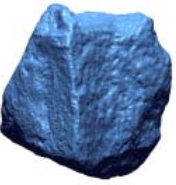
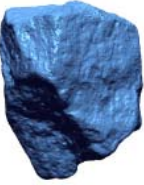
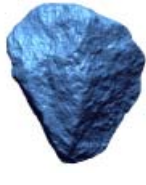


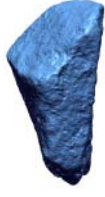
										<p>For <i>regular</i> tillite particles 26.5 mm:  Average (V/A) = 4.120</p> <p>Nearest match in system (left):  Tillite 9 = 4.043</p> <p>19/30 particles = 63 %</p>
 1	 2	 3	 4	 5	 6	 8	 9	 10	 11	
 12	 13	 14	 15	 19	 20	 23	 24	 25		

**Table 4.32** Elongated particles comparison for 26.5 mm tillite

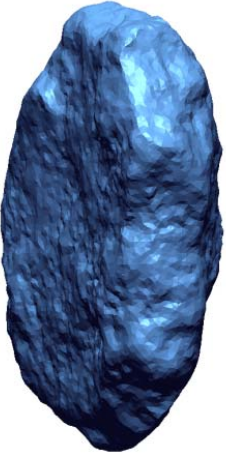









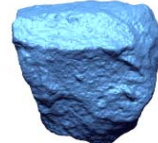


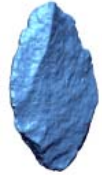


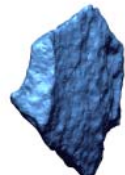
	<p>For <i>elongated</i> tillite particles 26.5 mm:  Average (V/A) = 3.834</p> <p>Nearest match in system (left):  Tillite 22 = 3.918</p> <p>11/30 particles = 37 %</p>				
 7	 16	 17	 18	 21	 22
 26	 27	 28	 29	 30	



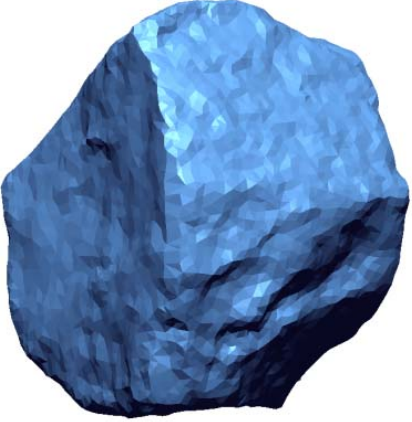
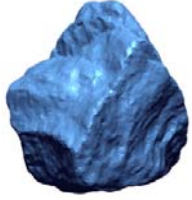
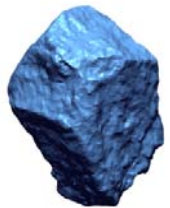

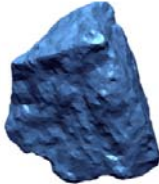

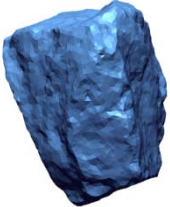
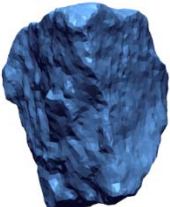

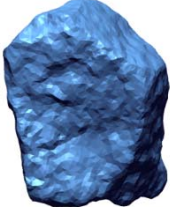
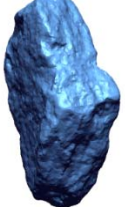
**Table 4.33** Regular particles comparison for 19.0 mm tillite

							<p>For <i>regular</i> tillite particles 19.0 mm:  Average (V/A) = 3.267</p> <p>Nearest match in system (left):  Hornfels 3 = 3.200</p> <p>14/30 particles = 47 %</p>
 <p>1</p>	 <p>2</p>	 <p>3</p>	 <p>4</p>	 <p>5</p>	 <p>6</p>	 <p>7</p>	
 <p>8</p>	 <p>9</p>	 <p>10</p>	 <p>16</p>	 <p>18</p>	 <p>19</p>	 <p>20</p>	

**Table 4.34** Elongated particles comparison for 19.0 mm tillite



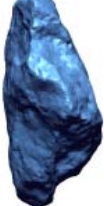

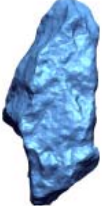

















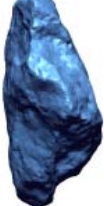

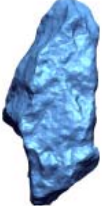















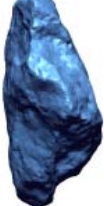

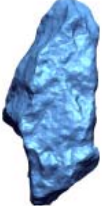
















		<p>For <i>elongated</i> tillite particles 19.0 mm:  Average (V/A) = 2.678</p> <p>Nearest match in system (left):  Recycled Aggregate 12 = 2.550</p> <p>16/30 particles = 53 %</p>					
 11	 12	 13	 14	 15	 17	 21	 22
 23	 24	 25	 26	 27	 28	 29	 30

**Table 4.35** Regular particles comparison for 13.2 mm tillite

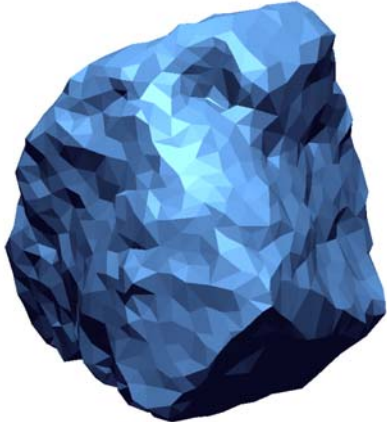
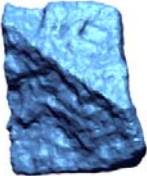


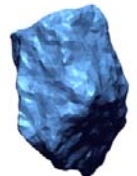
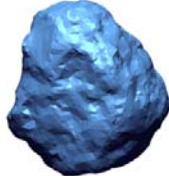

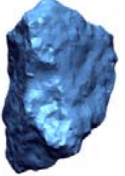

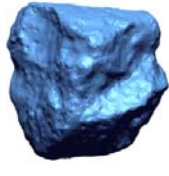
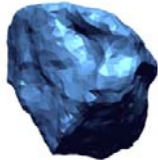
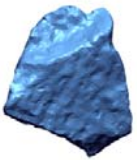
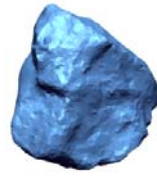


	<p>For <i>regular</i> tillite particles 13.2 mm:  Average <math>(V/A) = 2.362</math></p> <p>Nearest match in system (left):  Hornfels 9 = 2.360</p> <p>10/30 particles = 33 %</p>			
 <p>1</p>	 <p>2</p>	 <p>3</p>	 <p>4</p>	 <p>6</p>
 <p>7</p>	 <p>8</p>	 <p>9</p>	 <p>10</p>	 <p>19</p>



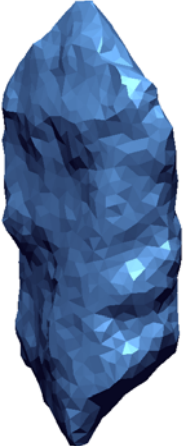











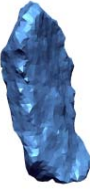




**Table 4.36** Elongated particles comparison for 13.2 mm tillite

		<p>For <i>elongated</i> tillite particles 13.2 mm:  Average (V/A) = 2.013</p> <p>Nearest match in system (left):  Recycled Aggregate 21 = 2.112</p> <p>20/30 particles = 67 %</p>																											
		<table border="1"> <tr> <td> 5</td> <td> 11</td> <td> 12</td> <td> 13</td> <td> 14</td> <td> 15</td> <td> 16</td> <td> 17</td> <td> 18</td> <td> 20</td> </tr> <tr> <td> 21</td> <td> 22</td> <td> 23</td> <td> 24</td> <td> 25</td> <td> 26</td> <td> 27</td> <td> 28</td> <td> 29</td> <td> 30</td> </tr> </table>										 5	 11	 12	 13	 14	 15	 16	 17	 18	 20	 21	 22	 23	 24	 25	 26	 27	 28
 5	 11	 12	 13	 14	 15	 16	 17	 18	 20																				
 21	 22	 23	 24	 25	 26	 27	 28	 29	 30																				

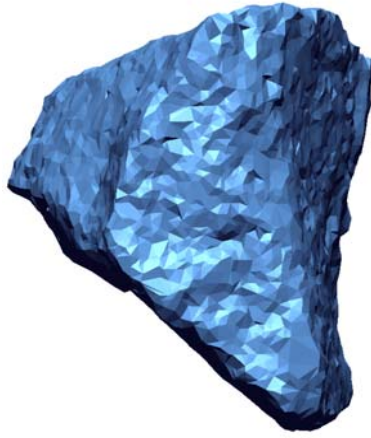


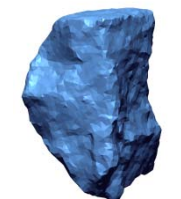
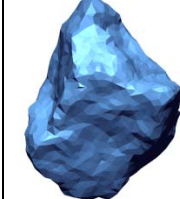

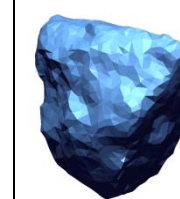
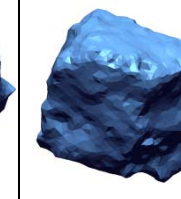
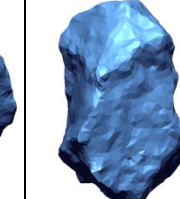
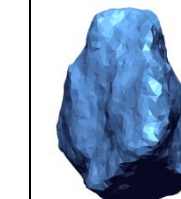

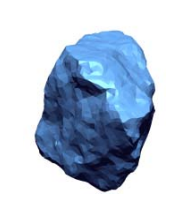

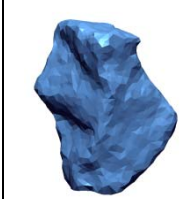
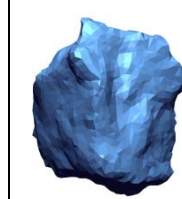
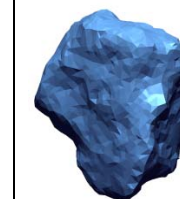
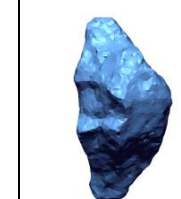

**Table 4.37** Regular particles comparison for 9.5 mm tillite

	<p>For <i>regular</i> tillite particles 9.5 mm:  Average (V/A) = 1.461</p> <p>Nearest match in system (left):  Recycled Aggregate 8 = 1.552</p> <p>14/30 particles = 47 %</p>					
 1	 2	 3	 4	 5	 6	 7
 8	 9	 10	 14	 16	 17	 20












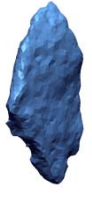


**Table 4.38** Elongated particles comparison for 9.5 mm tillite

		<p>For <i>elongated</i> tillite particles 9.5 mm:  Average (V/A) = 1.253</p> <p>Nearest match in system (left):  Recycled Aggregate 25 = 1.271</p> <p>16/30 particles = 53 %</p>					
 11	 12	 13	 15	 18	 19	 21	 22
 23	 24	 25	 26	 27	 28	 29	 30

**Table 4.39** Regular particles comparison for 6.7 mm tillite



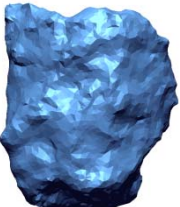


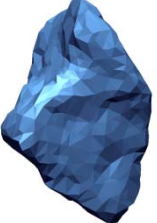


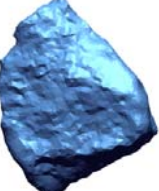






									<p>For <i>regular</i> tillite particles 6.7 mm:  Average (V/A) = 1.185</p> <p>Nearest match in system (left):  Quartzite 2 = 1.208</p> <p>17/30 particles = 57 %</p>
 1	 2	 3	 4	 5	 6	 7	 8	 9	
 10	 12	 13	 15	 16	 17	 18	 20		

**Table 4.40** Elongated particles comparison for 6.7 mm tillite














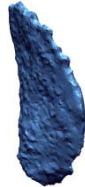


							<p>For <i>elongated</i> tillite particles 6.7 mm:  Average <math>(V/A) = 0.922</math></p> <p>Nearest match in system (left):  Granite 27 = 0.873</p> <p>13/30 particles = 43 %</p>
 11	 14	 19	 21	 22	 23	 24	
 25	 26	 27	 28	 29	 30		



**Table 4.41** Regular particles comparison for 4.75 mm tillite

		<p>For <i>regular</i> tillite particles 4.75 mm:  Average <math>(V/A) = 0.837</math></p> <p>Nearest match in system (left):  Granite 8 = 0.866</p> <p>14/30 particles = 47 %</p>				
 1	 2	 3	 4	 5	 6	 7
 8	 9	 10	 16	 18	 19	 20

**Table 4.42** Elongated particles comparison for 4.75 mm tillite

		<p>For <i>elongated</i> tillite particles 4.75 mm:  Average (V/A) = 0.725</p> <p>Nearest match in system (left):  Tillite 25 = 0.706</p> <p>16/30 particles = 53 %</p>													
		 11		 12		 13		 14		 15		 17		 21	
 23		 24		 25		 26		 27		 28		 29		 30	

## 4.6 Influence of Different Material Types

An indication was required of whether there is a correlation between different material types used in the investigation and the range of model values calculated for each. Any existing trends observed in the calculated data could potentially be related back to the material type (or more likely, the crushing procedure applied). To achieve such an indication, model values for each material and size fraction was plotted to allow a visual comparison with other models. Figure 4.6 through 4.11 shows plots for particles sizes from 26.5 mm to 4.75 mm for regular and elongated particles.

From the results it is clear that there are no clear trends as far as the calculated values and material types are concerned. None of the materials showed a specific cluster of values which would suggest that particles resemble each other very closely. The data for each material covered a range of values, though these ranges differed from one material to the next.

A few general observations were made from the graphs:

- The granite sample contained a data outlier on two occasions (i.e. 13.2 mm regular particles and 9.5 mm regular particles). In both instances one particle had a significantly lower calculated value than the remaining granite particles. In the case of the 13.2 mm particle, the value was even lower than the remaining data for the entire 13.2 mm dataset.
- For 26.5 mm particles (both regular and elongated) the tillite had the highest calculated values, suggesting that the particles may be the most rounded or smoothest in the dataset.
- For 13.2 mm particles (regular and elongated) the quartzite tended to have the lowest calculated values. This would suggest that the particles would be the most angular or coarse in the dataset.

It would appear from the graphs that no specific trends prevail, but that the different materials simply have different ranges in calculated model values.



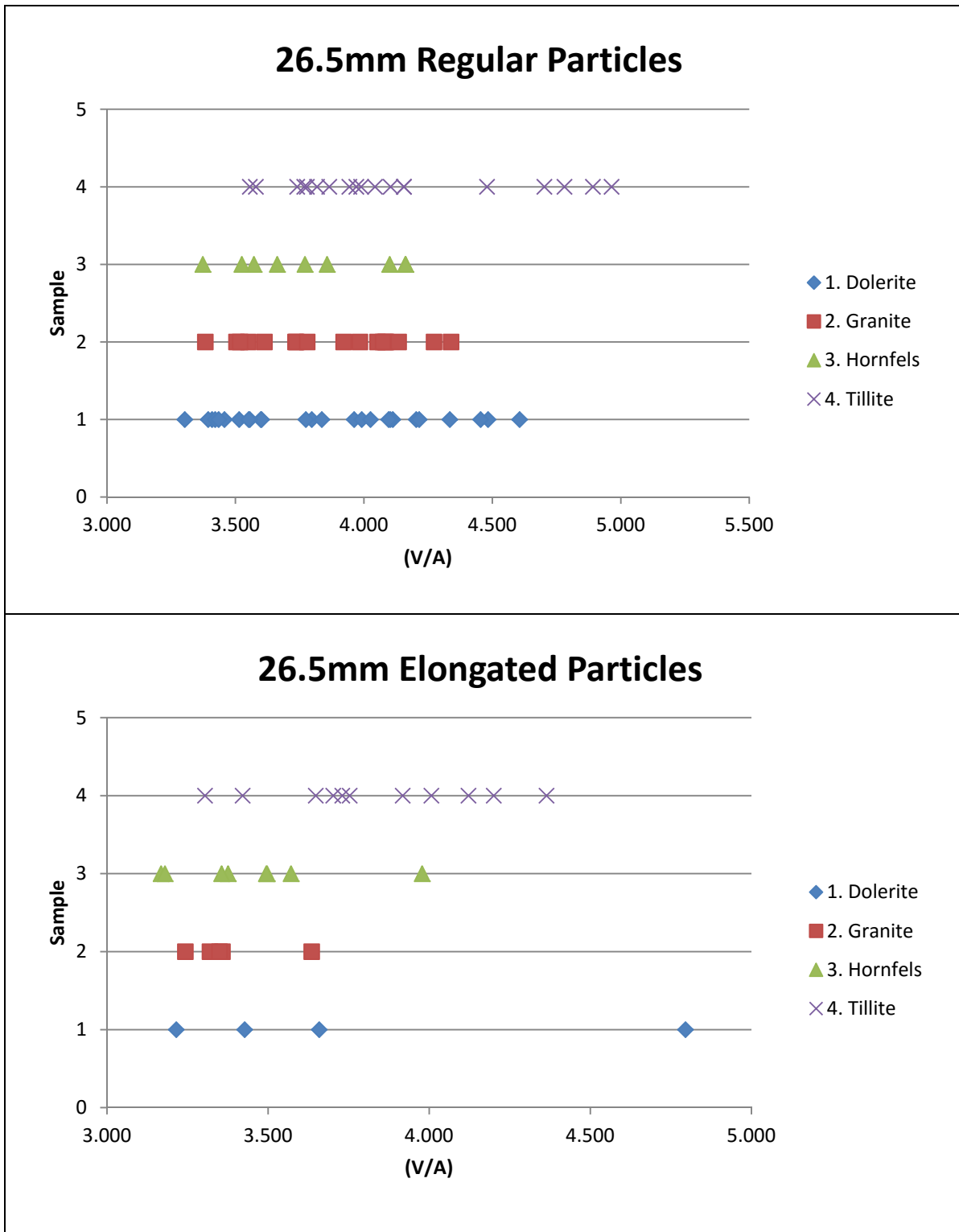


Figure 4.6 Particle ranges for 26.5 mm particles

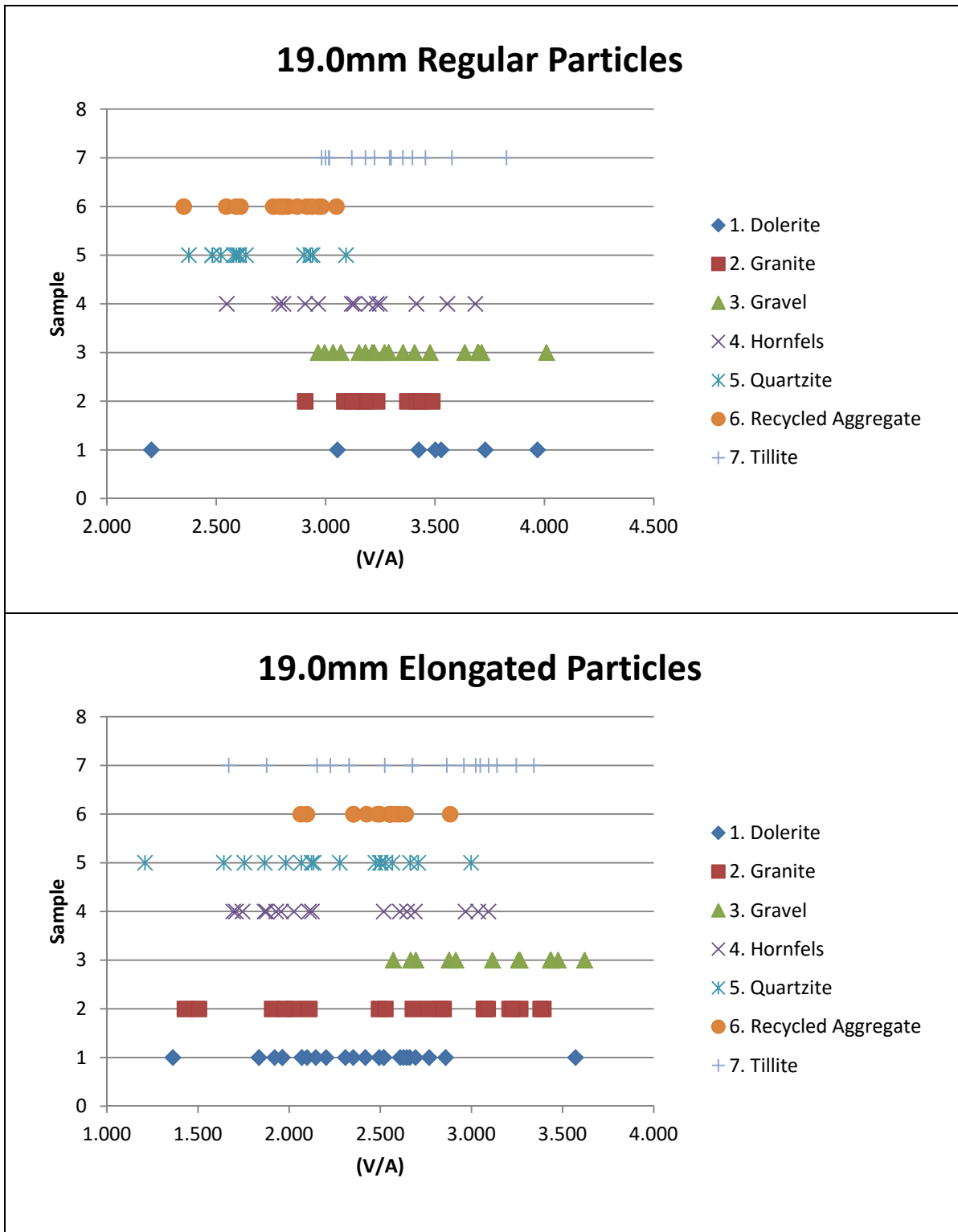


Figure 4.7 Particle ranges for 19.0 mm particles

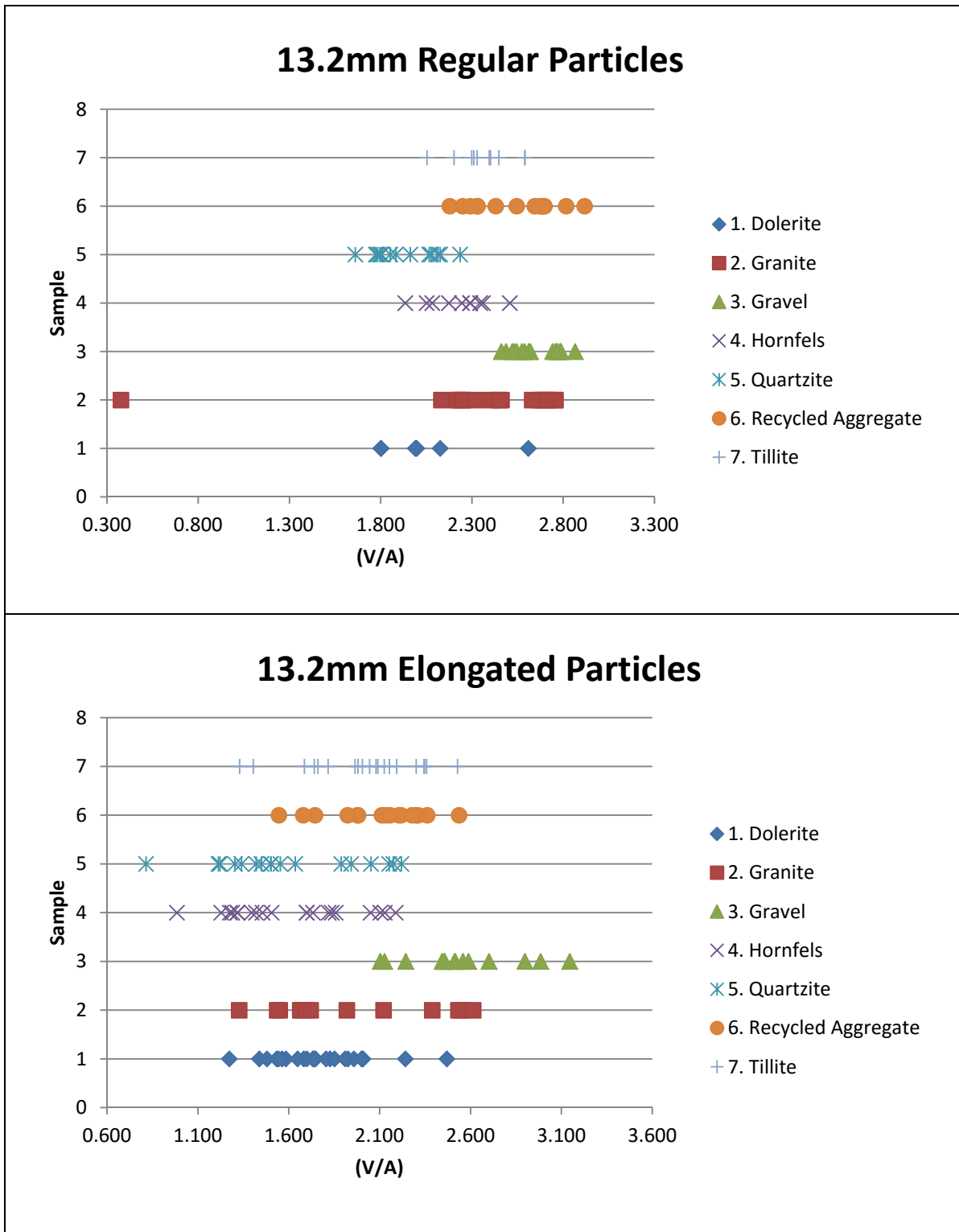


Figure 4.8 Particle ranges for 13.2 mm particles

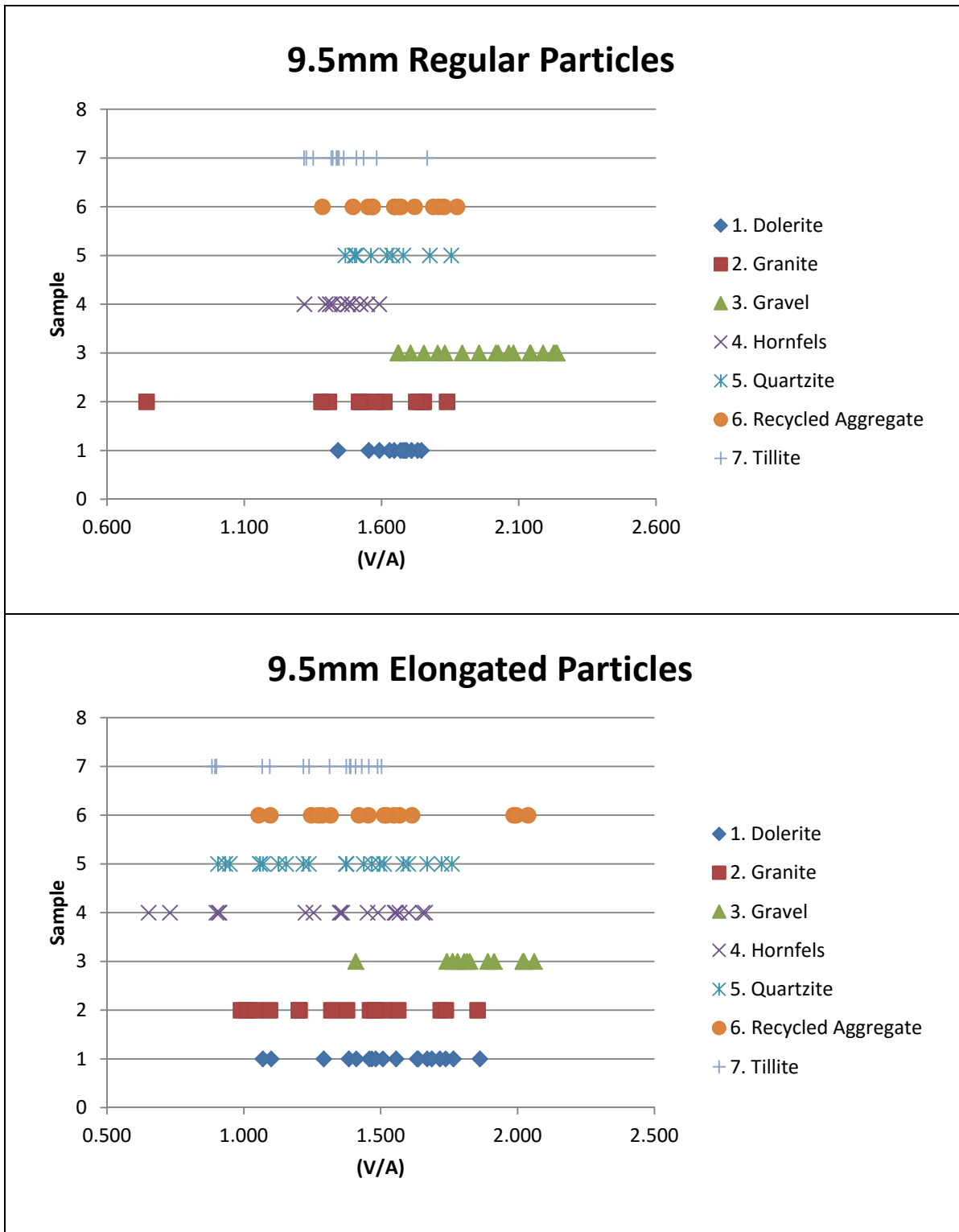


Figure 4.9 Particle ranges for 9.5 mm particles

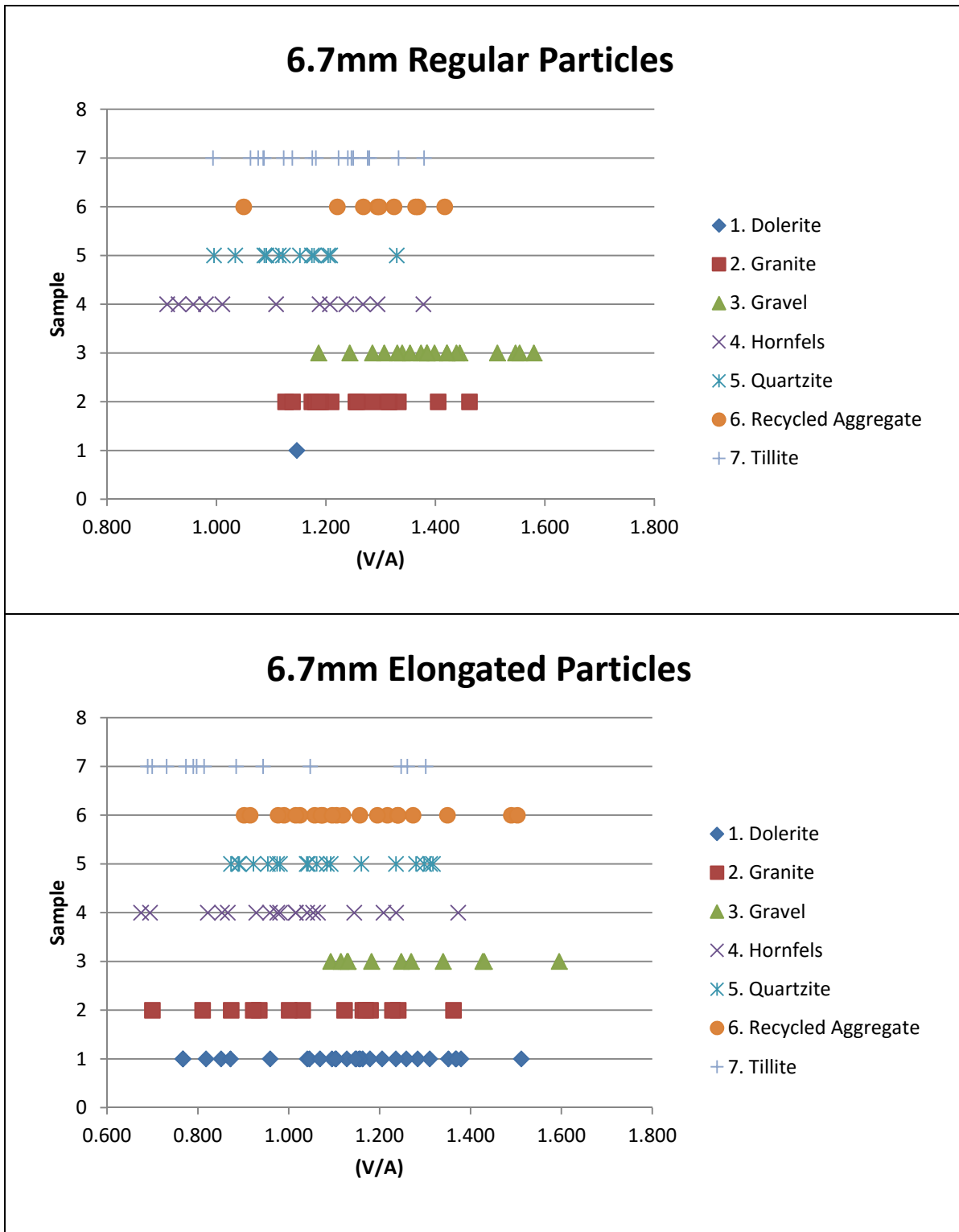


Figure 4.10 Particle ranges for 6.7 mm particles

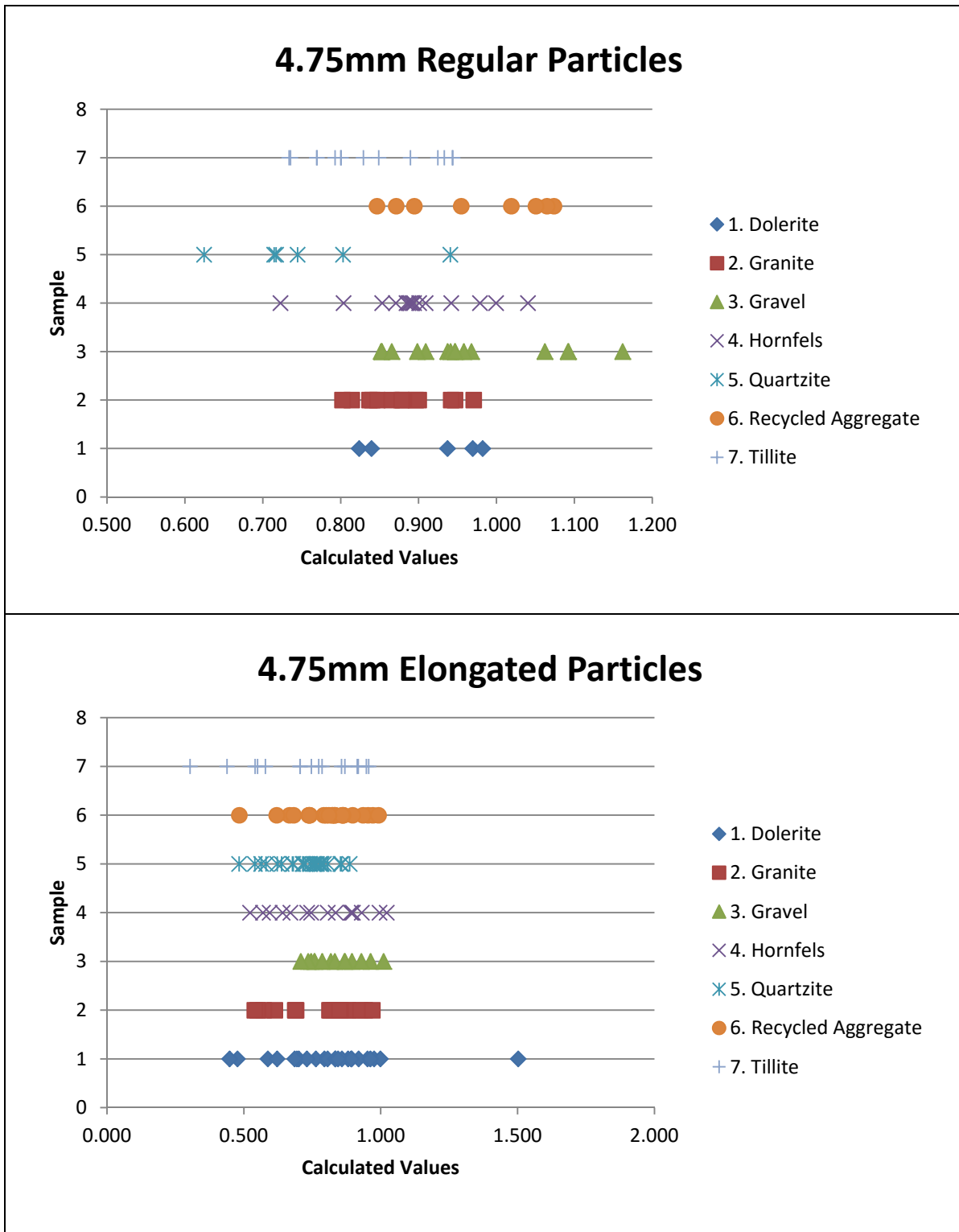


Figure 4.11 Particle ranges for 4.75 mm particles

Additional scatter plots were done for various parameters using a combination of approaches and data sorting methods; however, these produced little useful results. Attempts to analyse data were hampered somewhat by the effects of elongated particles, as was encountered

during early stages of modelling. One observation that was made from scatter plots (and also noted during the modelling procedure) was that elongated particles for a given value had lower (V/A) model values than regular particles from the same origin.

## 4.7 Shear Strength Properties of G1 Aggregate

### 4.7.1 Tri-axial Tests

After initially using multi-stage tri-axial test results to assess shear strength properties, the approach was abandoned in favour of the conventional tri-axial test approach. A comparison between the two approaches will be discussed in section 4.8. All results discussed in this section were derived using the *conventional* tri-axial test method.

### 4.7.2 Mohr-Coulomb Failure Criteria and Mohr Circles

Using the results obtained from the tri-axial tests, the shear strength properties of the samples were assessed using Mohr circles. The measured confining stresses were applied ( $\sigma_3$ ), while  $\sigma_1$  was calculated as follows (Cernica, 1982; Craig, 1997):

$$\sigma_1 = \Delta \sigma_1 + \sigma_3 \quad (\text{Equation 4.3})$$

where

- $\sigma_1$  = maximum principal stress
- $\Delta \sigma_1$  = the force resulting from the deviator load (calculated to kPa)
- $\sigma_3$  = confining pressure

According to Cernica (1982) and Craig (1997) the normal load applied during the test must be added to the confining pressure in order to obtain the  $\sigma_1$  value. Using this approach, three sets of values were calculated (from three individual tri-axial tests) to produce Mohr Circles for each of the six samples, as summarised in Table 4.43. The Mohr circles drawn for each of the listed samples are shown in Figure 4.12 through Figure 4.17 and the cohesion values (i.e. Y-intercepts) are marked on each graph.

**Table 4.43** Load summary for Mohr circles

Sample	$\sigma_3$ (kPa)	$\sigma_1$ (kPa)
1. Quartzite	41.420	684.661
	102.890	1180.786
	138.220	1515.639
2. Granite	41.615	494.435
	104.686	1032.453
	138.430	1336.633
3. Quartz Porphyry	41.615	568.566
	104.680	1040.823
	139.040	1235.667
4. Tillite	41.612	426.753
	105.698*	866.925*
	139.250	1219.240
5. Hornfels	41.620	438.305
	103.680	932.927
	138.490	1247.906
6. Dolerite (modified)	41.614	602.349
	104.686	1058.144
	138.920	1133.292

\* Test did not proceed to completion/failure

A tangent line was drawn to the Mohr circles with the two best fit tangent points marked with a dot on each graph. The internal friction angle was determined from the drawn tangent line. As per convention, the horizontal axis shows the principle stresses (i.e.  $\sigma_1$  and  $\sigma_3$ ) in kPa, while the vertical axis represents the shear stress ( $\tau$ ), also in kPa.

The tri-axial test for tillite, confined at 105.698 kPa, was terminated due to technical reasons and as such, the results of the test must be viewed in this context. The relevant Mohr circle suggests that the sample was near failure when the procedure was halted.



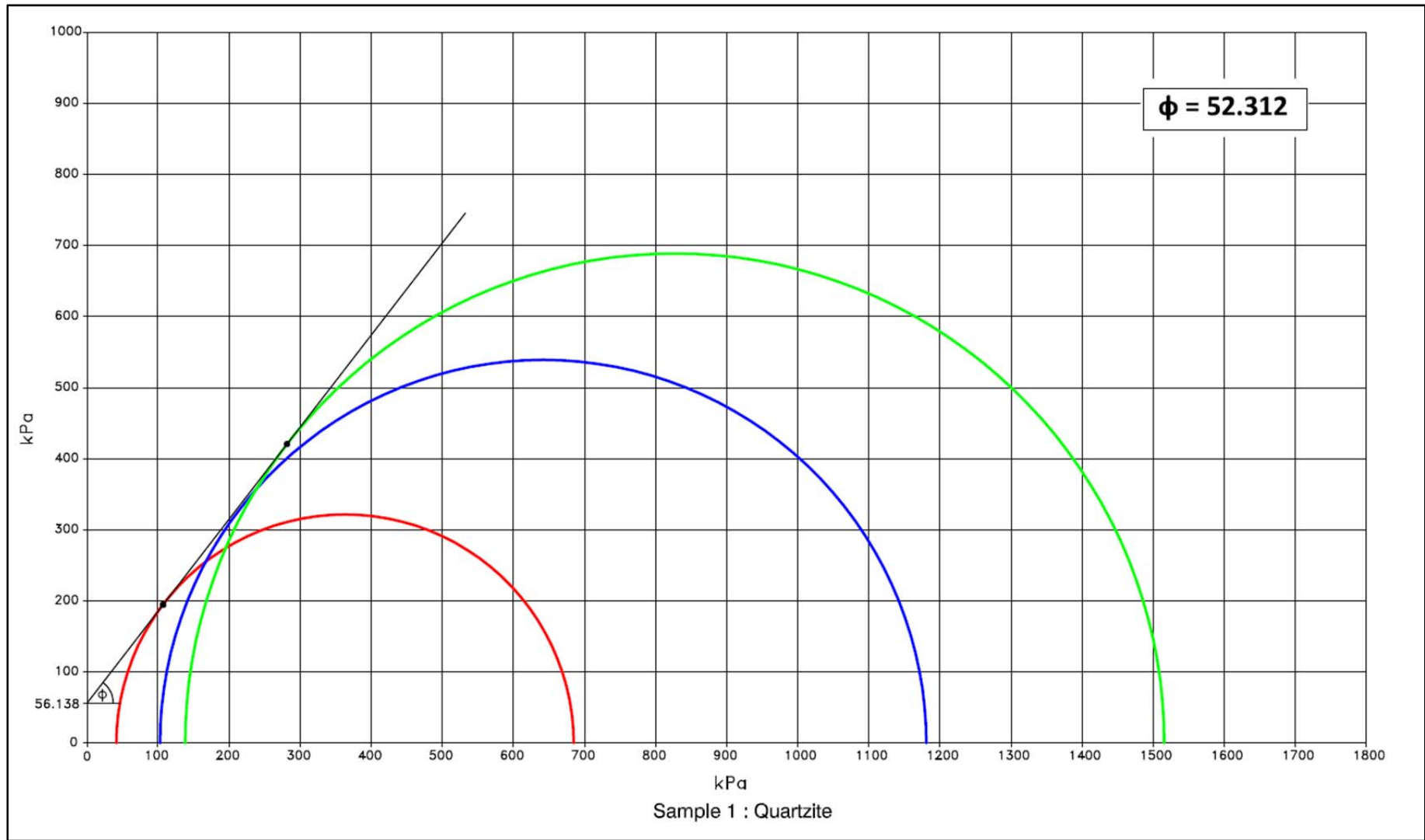
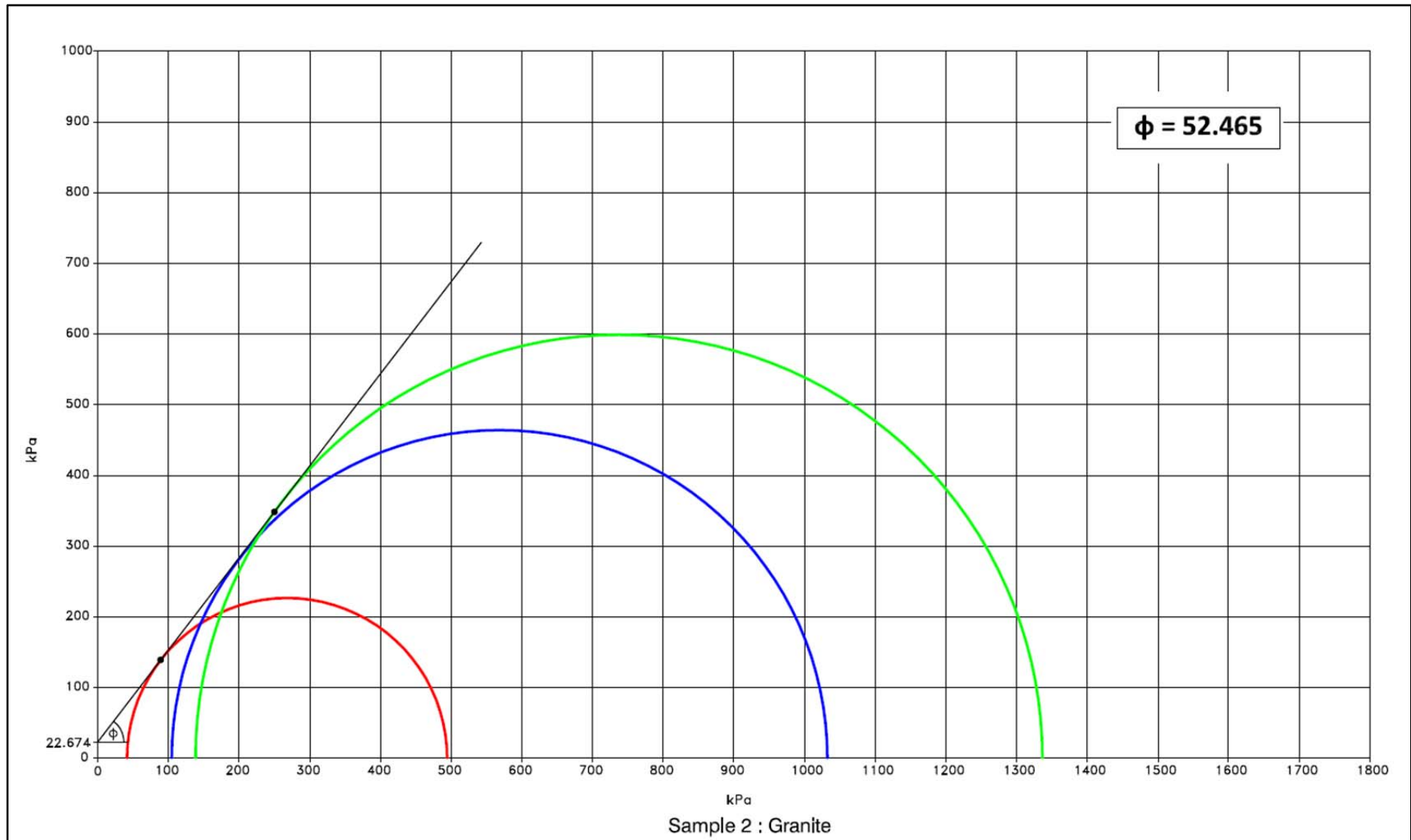


Figure 4.12 Mohr-Coulomb failure criterion for sample 1, quartzite



**Figure 4.13** Mohr-Coulomb failure criterion for sample 2, granite

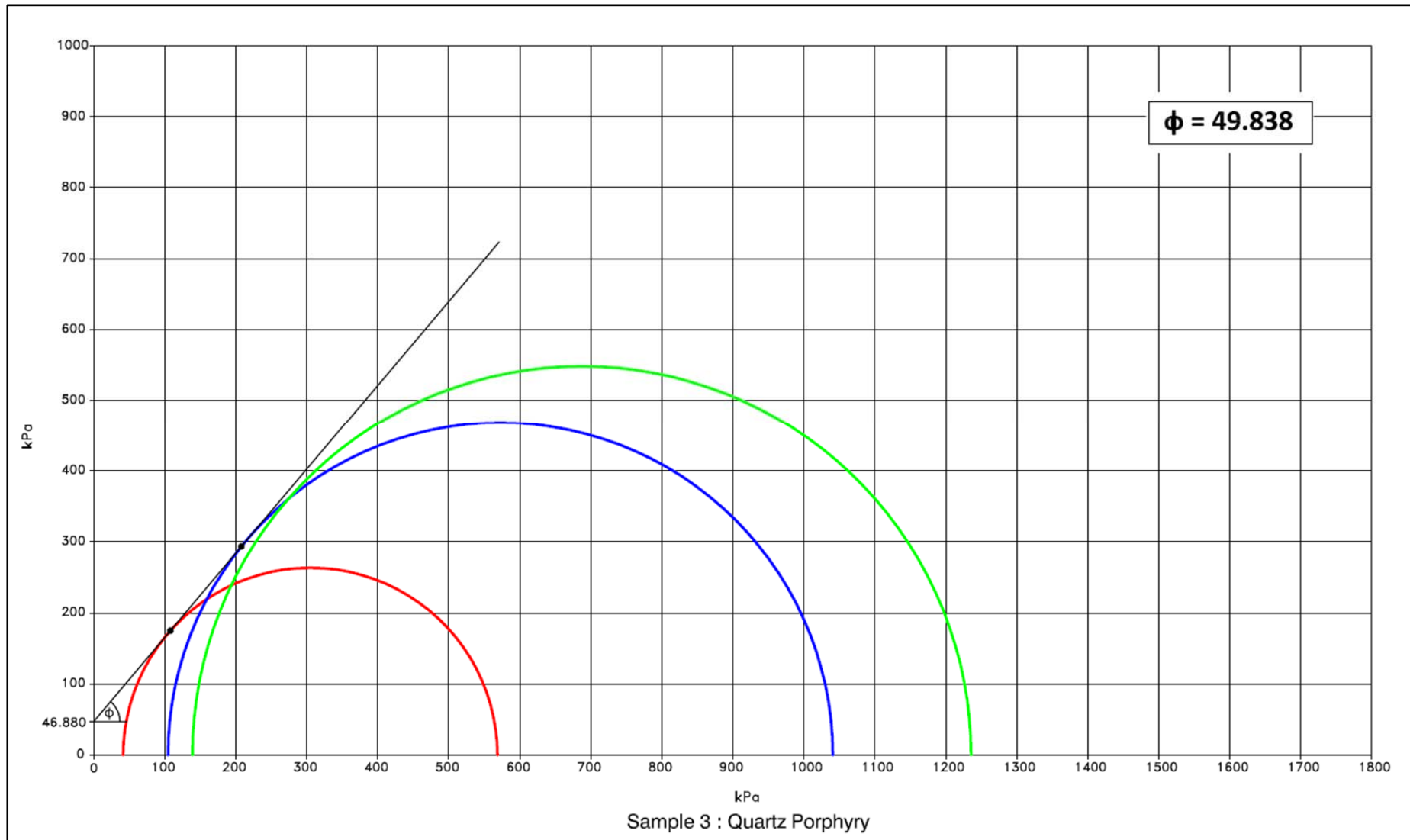


Figure 4.14 Mohr-Coulomb failure criterion for sample 3, quartz porphyry

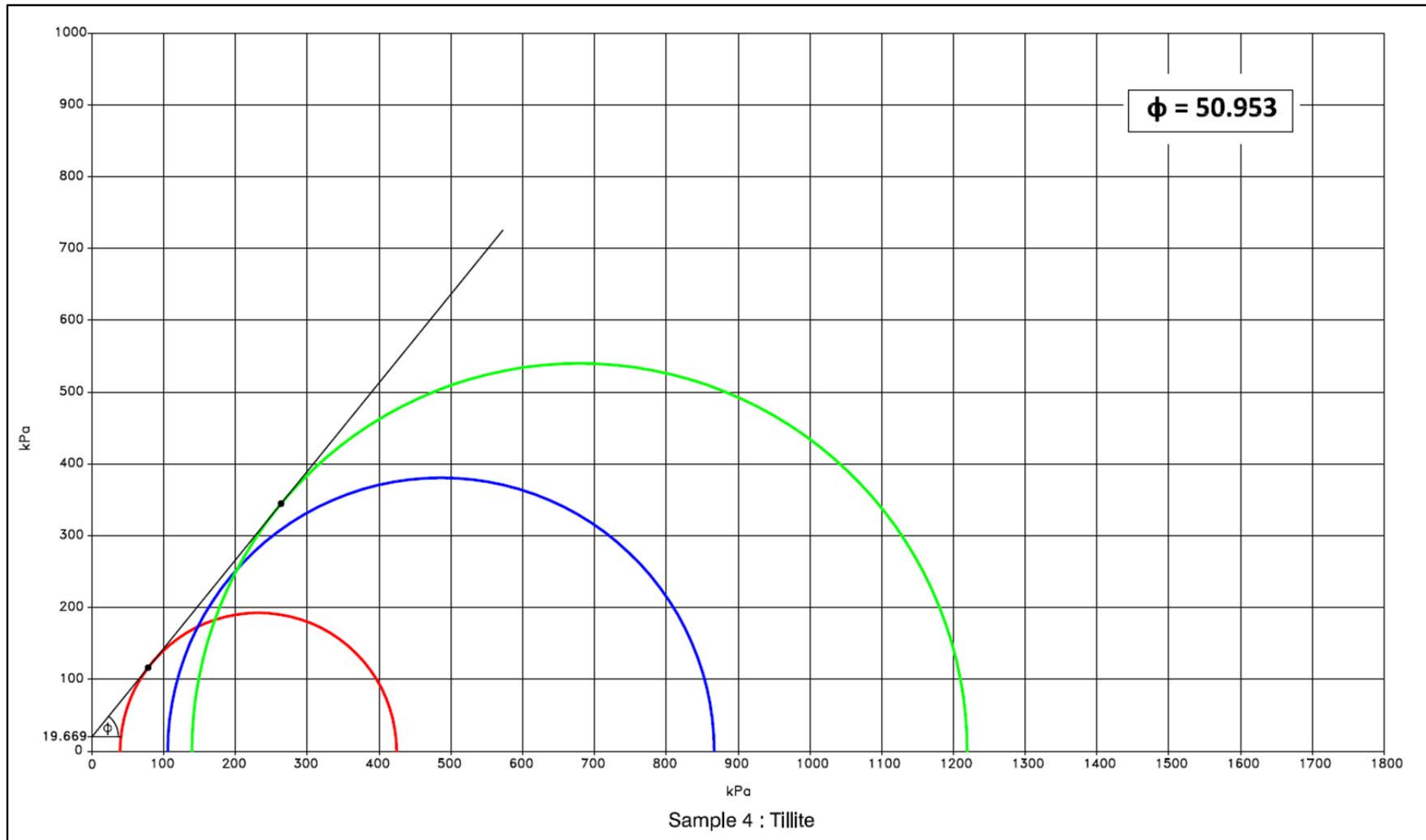


Figure 4.15 Mohr-Coulomb failure criterion for sample 4, tillite

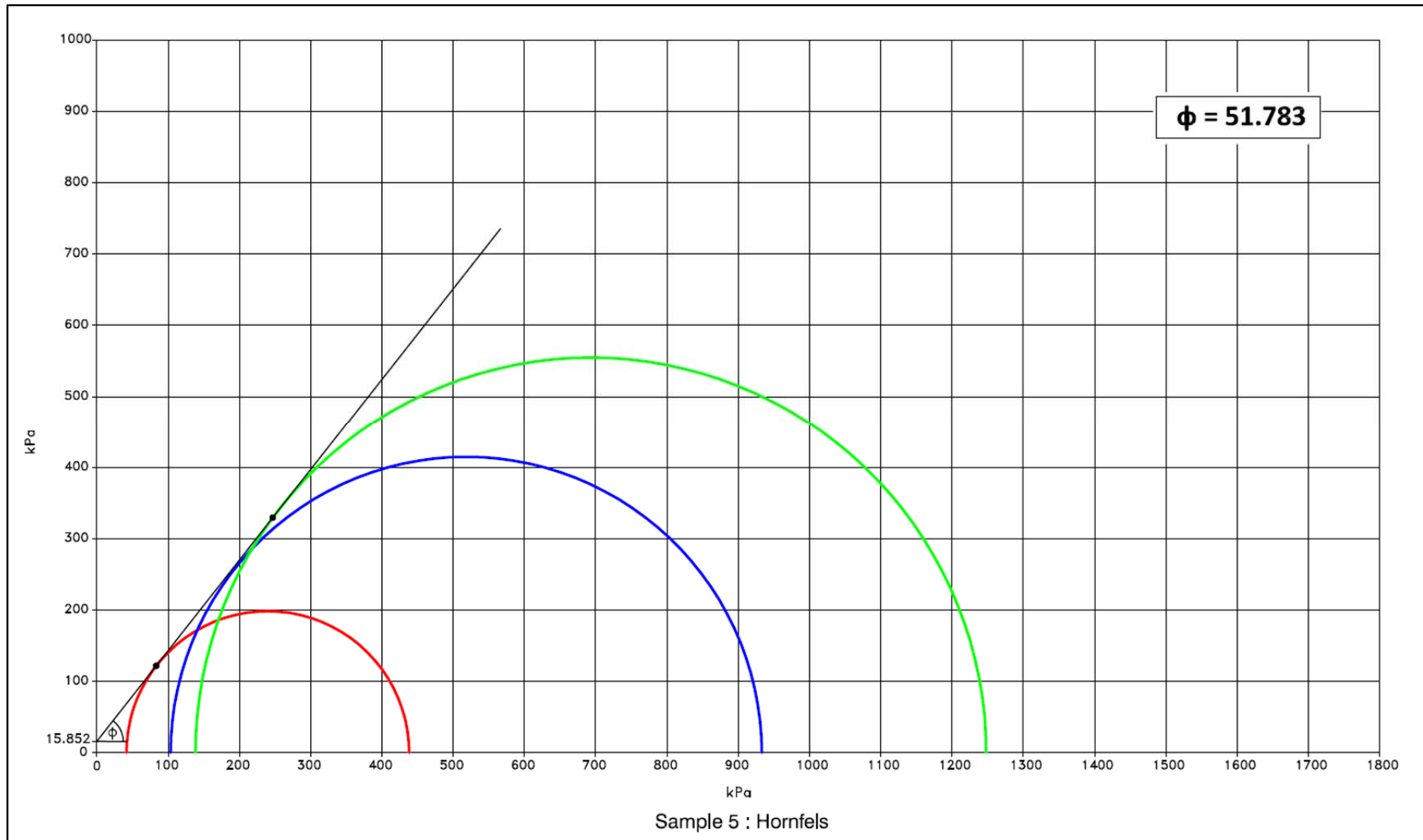


Figure 4.16 Mohr-Coulomb failure criterion for sample 5, hornfels

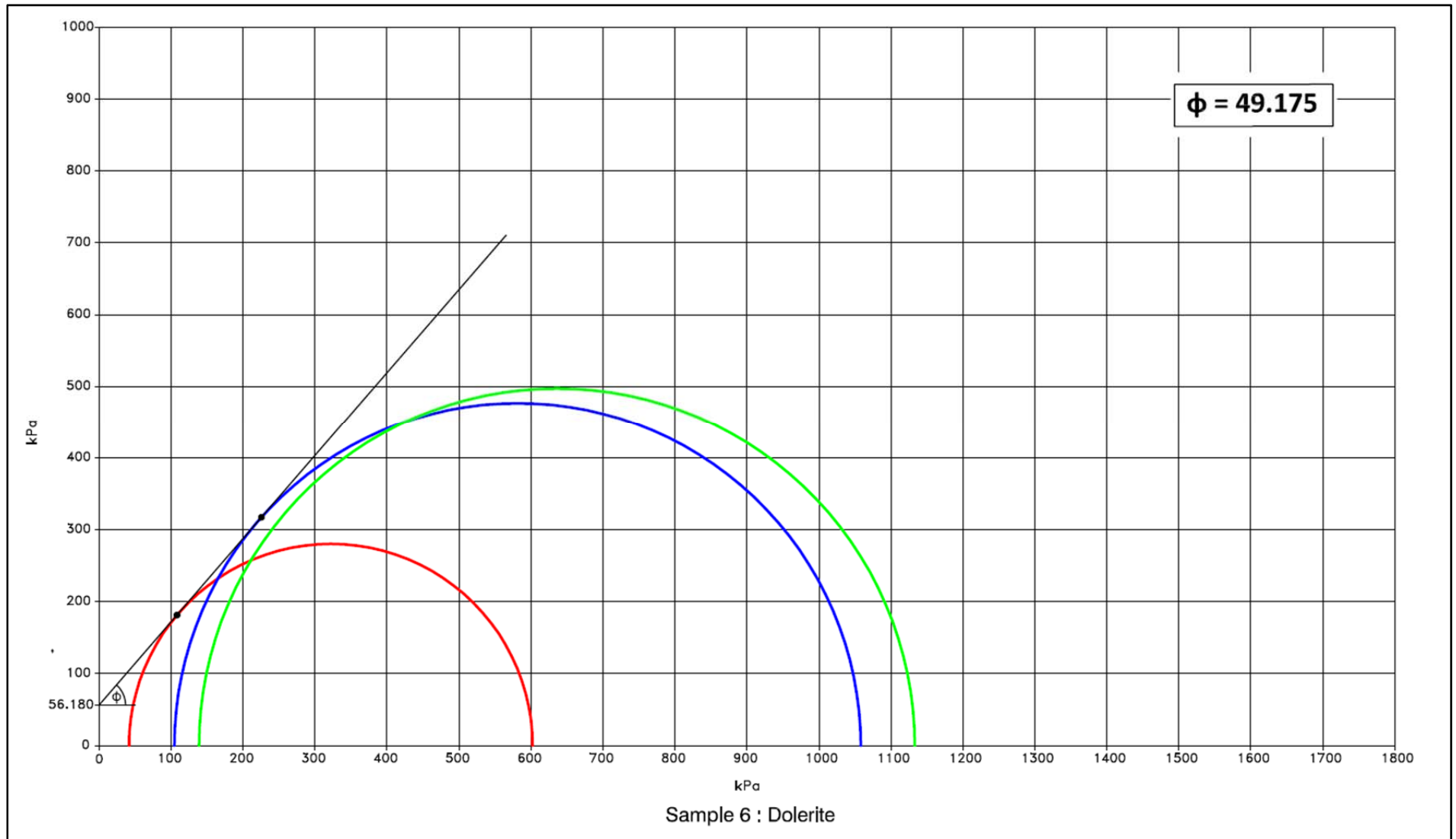


Figure 4.17 Mohr-Coulomb failure criterion for sample 6, dolerite

Initial results were confusing as all of the materials showed notable cohesion values. This was disconcerting, as one of the aims of replacing all the samples' fine constituents (refer to section 3.3.1) with an inert quartzite crusher dust mix was in part to ensure minimal cohesion (assuming minimal effects of suction). It may be argued that the cohesion deduced from the graphs is common in this type of test and is attributed to the strength of the rubber membrane enclosing the sample in the tri-axial test apparatus, though the range in cohesion values seem too variable for this alone to be true. Seeing as the same membranes were used for all samples, it is assumed that the difference in cohesion related to the membranes are minimal and that the variation in cohesion values is attributed to the sample materials. Nevertheless, the cohesion and internal friction angle values are summarised in Table 4.44.

**Table 4.44** Summary of shear strength properties deduced from Mohr circles

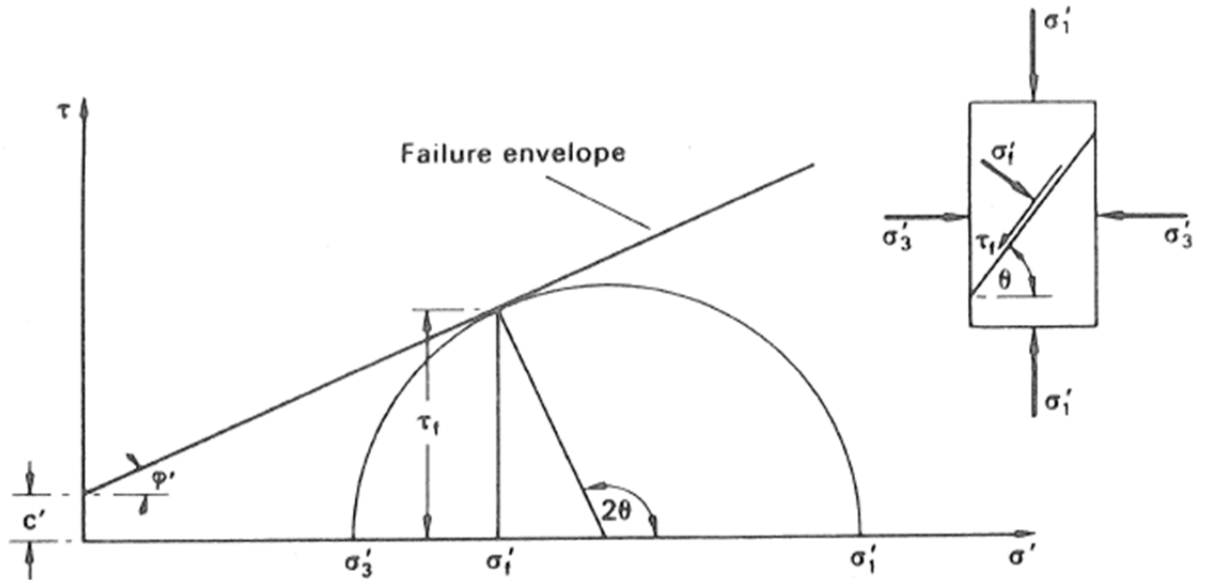
<b>Sample</b>	<b>Cohesion (kPa)</b>	<b>Friction Angle (°)</b>
1. Quartzite	56.138	52.312
2. Granite	22.674	52.465
3. Quartz Porphyry	46.880	49.838
4. Tillite	19.669	50.953
5. Hornfels	15.852	51.783
6. Dolerite	56.180	49.175

The apparent cohesion indicated in the table was disregarded and cohesion of 0 kPa was assumed for all samples. This assumption was made as the emphasis of the research falls on the properties related to the aggregate particles (i.e. the friction angle) and not the fine constituents (i.e. cohesion).

The internal friction angle and cohesion values summarised above correspond well with the range of similar properties found by Theyse (2007) when using a similar test approach and equipment. Theyse (2007) tested similar crushed rock materials, notably a quartzite sample from the same source as tested in this research. The cohesion values determined by Theyse (2007) – as determined for six samples - ranged from 19 kPa to 43 kPa and internal friction angles were between 51° and 56°.



The shear strength ( $\tau_f$ ) and normal stress ( $\sigma'_f$ ) on the failure plane at sample failure (for a specific confining pressure) can be read off the Mohr circles at the point where the tangent line touches the relevant Mohr circle (refer to Figure 4.18)



**Figure 4.18** Mohr-Coulomb failure criteria at sample failure (after Craig, 1997)

Considering the general equation for determining the shear strength of a material (equation 4.4), the shear strength ( $\tau_f$ ) and normal stress ( $\sigma'_f$ ) on the failure plane at sample failure can also be calculated as indicated below:

$$\tau = c + \sigma_n \tan \phi \quad (\text{Equation 4.4})$$

$$\tau_f = \frac{1}{2}(\sigma'_1 - \sigma'_3) \sin 2\theta \quad (\text{Equation 4.5})$$

$$\sigma'_f = \frac{1}{2}(\sigma'_1 + \sigma'_3) + \frac{1}{2}(\sigma'_1 - \sigma'_3) \cos 2\theta \quad (\text{Equation 4.6})$$

where

$\sigma'_1$  = Major principal stress at failure

$\sigma'_3$  = Minor principal stress at failure

$\theta$  = the theoretical angle between the major principal plane and the plane of failure

The theoretical angle between the major principal plane and the plane of failure ( $\theta$ ) can be calculated as follows:

$$\theta = 45^\circ + (\phi'/2) \quad \text{(Equation 4.7)}$$

In order to compare the two methods (i.e. reading off the graph vs calculating values), a comparison was undertaken for sample 1 (quartzite) when considering the test performed at  $\pm 41$  kPa confining pressure. A comparison is summarised in Table 4.45 below.

**Table 4.45** Summary of calculated values and graph values of shear strength parameters

Calculated Values		Values from Mohr Circle	
$T_f$	$\sigma'_f$	$T_f$	$\sigma'_f$
194.787 kPa	107.114 kPa	194.788 kPa	107.116 kPa

The differences in values are very small and can be attributed to rounding off of decimal places during calculations. This confirms that reading the values directly from the Mohr circle diagrams accurately, is acceptable for deriving the shear strength and normal stress on the failure plan at failure.

For the purposes of further analyses in this chapter (i.e. section 4.8), failure data for all samples will be considered for the tests conducted at approximately 41 kPa confining pressure, as this result was the only one that yielded a tangent point throughout all of the tri-axial tests (multi-stage and conventional) conducted during this research. The relevant values are summarised in Table 4.46 below and also include the shear strength assuming no cohesion.

With the majority of the test results correlating fairly well, the dolerite sample (i.e. sample 6) clearly proved unusual. This is evident from the material's Mohr circles, as depicted in Figure 4.17. The Mohr circles of the dolerite samples show that the test with the highest confining pressure (i.e.  $\pm 138$  kPa) did not behave in a similar manner to other samples.

**Table 4.46** Shear strength of samples (at approximately 41 kPa confining pressure)

Sample	$\sigma_n$ (kPa)	$\tau_f$ (kPa)	$\tau_f$ Assuming No Cohesion (kPa)
1. Quartzite	107.116	194.788	138.650
2. Granite	89.110	138.782	116.108
3. Quartz Porphyry	108.075	174.941	128.061
4. Tillite	78.127	116.012	96.343
5. Hornfels	83.469	121.858	106.006
6. Dolerite	108.297	181.506	125.326

At the highest confining pressure, the dolerite sample appeared to have failed at a relatively low deviator stress. The possible reasons for this are:

1. Due to the inclusion of excessive elongated or flattened particles, compaction was less effective, resulting in voids between interlocking particles. The partial interlock was overcome by the (higher) deviator load, resulting in the particles changing orientation or shifting into the unoccupied spaces. This would imply that the deviator load applied to cause individual particle movement of the particles must have exceeded the effort applied during compaction.
2. The deviator load applied at failure exceeded the inherent strength of numerous particles in the sample, causing them to break. The breakage of particles resulted in some movement/settlement in the sample as interlocking was overcome. From here a scenario similar to that described in point 1 above may also have occurred. Audible observations during the tri-axial test suggest that particle breakage did occur during testing, as particles were frequently heard breaking.

#### **4.8 Comparison between Multi-Stage and Conventional Tri-axial Tests**

As discussed earlier in this thesis, tri-axial tests were initially undertaken using the multi-stage tri-axial test approach. However, the test results were eventually abandoned as they appeared to be questionable and inconsistent. This did, however, provide an opportunity to compare the multi-stage tri-axial test results with those of conventional tri-axial test results, as the tests were repeated using the latter approach.

Figures 4.19 to 4.24 show Mohr circle plots for the various material samples, tested using the two different test approaches (i.e. conventional tri-axial tests vs multi-stage tri-axial tests). The Mohr circles depicted in red were derived from tri-axial results obtained using the conventional approach. The Mohr circles depicted in green are the corresponding tests conducted using the multi-stage approach to tri-axial testing. The figures are fairly self-explanatory as far as the influence on shear strength properties is concerned; nevertheless, a number of observations can be made based on these results:

- The multi-stage tri-axial test consistently underestimates the maximum deviator stress (i.e. normal load) that can be applied before sample failure occurs, with the exception of the lowest confining pressure test (i.e. 41 kPa). This can likely be attributed to the fact that the material was first tested at 138 kPa confining pressures, effectively inducing “strain hardening”.
- The effect of underestimating failure points (i.e. the onset of plastic failure during multi-stage testing) appears to become more pronounced with an increasing confining pressure when deviator loads are also higher.
- The point at which loading is terminated (i.e. when the deviator stress increase/application is discontinued) during the multi-stage test is subjective and operator-dependent. The point at which loading is halted becomes a personal matter, rather than a scientific matter, as the operator tends to stop loading prematurely to prevent sample failure.
- The Mohr circles deduced from the multi-stage tri-axial test results correlate very poorly with each other, due to the variability and inconsistency in the method. When comparing any of the multi-stage Mohr circles with conventional test Mohr circles, it is apparent that the Mohr circles often show large discrepancies which sometimes even prevent the sensible fitting of a tangent line.

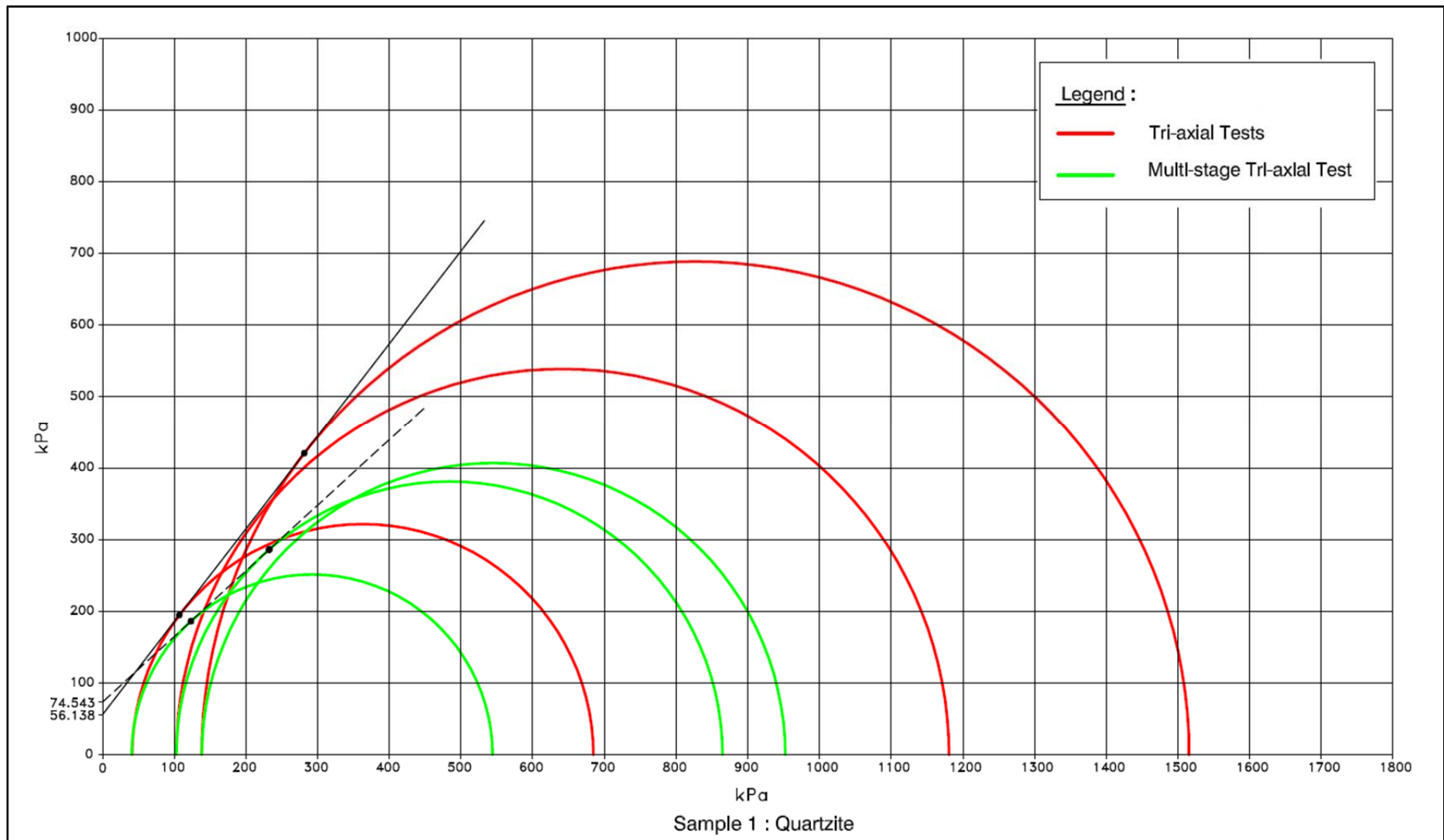


Figure 4.19 Comparative Mohr-Coulomb failure criteria for sample 1, quartzite

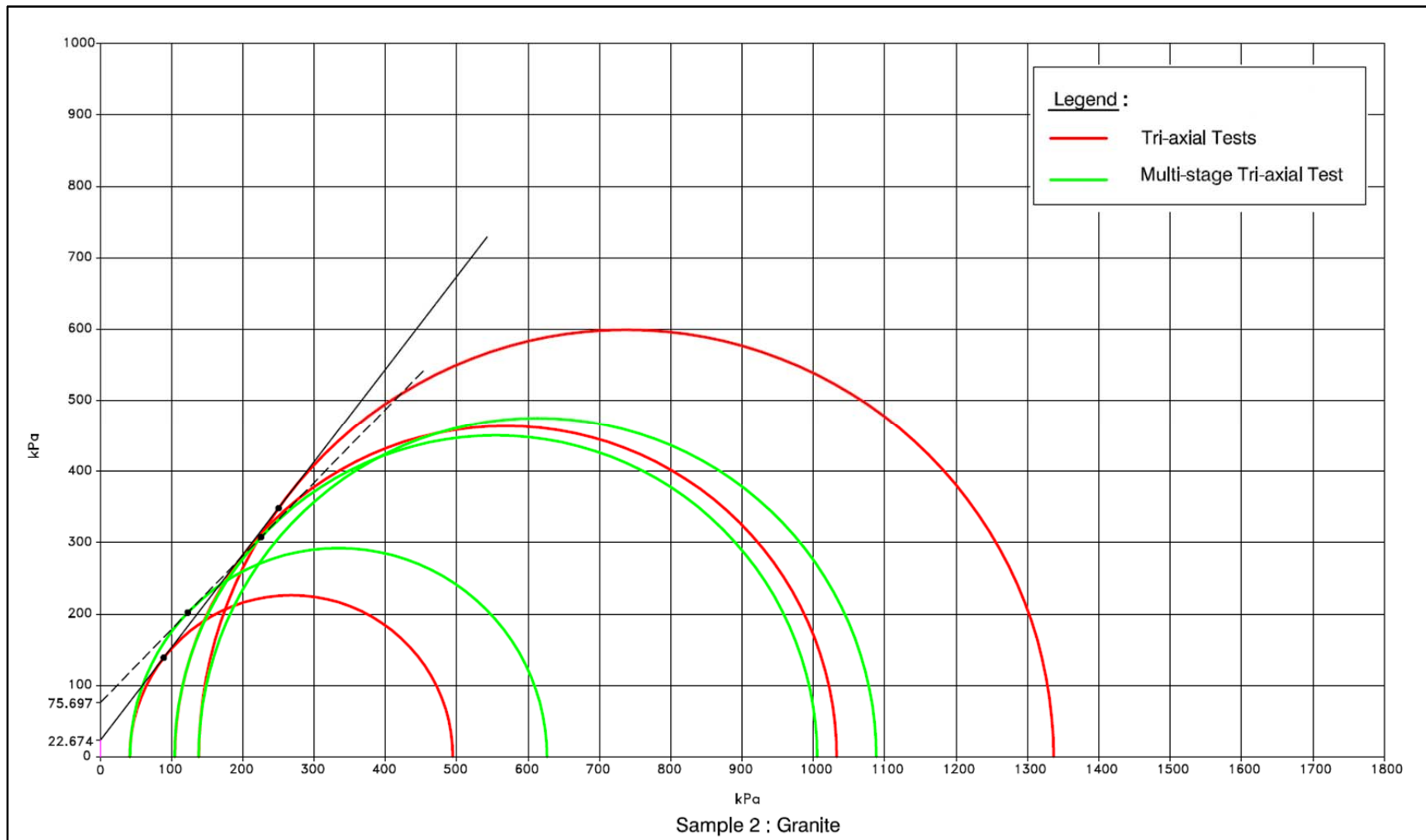


Figure 4.20 Comparative Mohr-Coulomb failure criteria for sample 2, granite

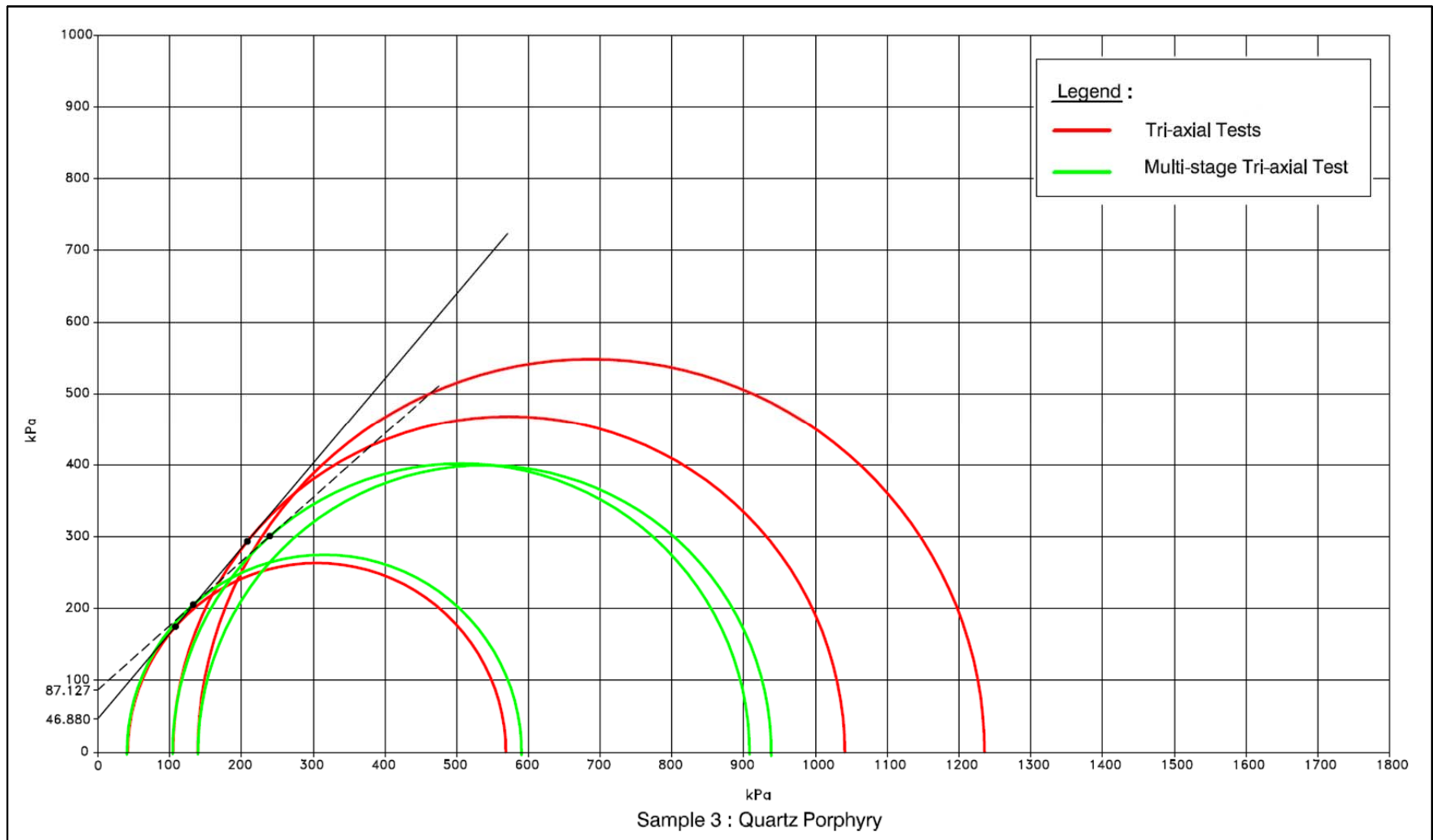


Figure 4.21 Comparative Mohr-Coulomb failure criteria for sample 3, quartz porphyry



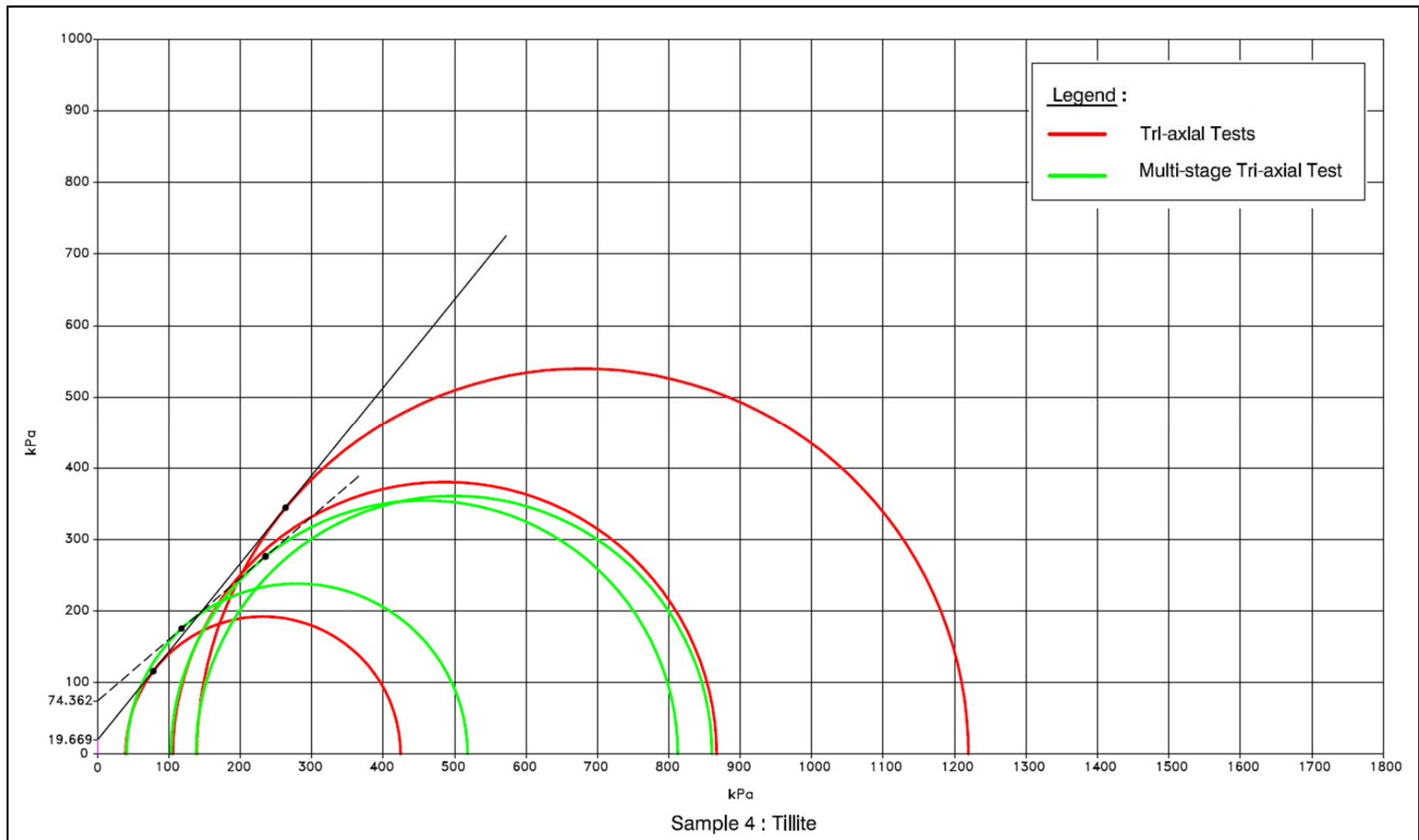


Figure 4.22 Comparative Mohr-Coulomb failure criteria for sample 4, tillite

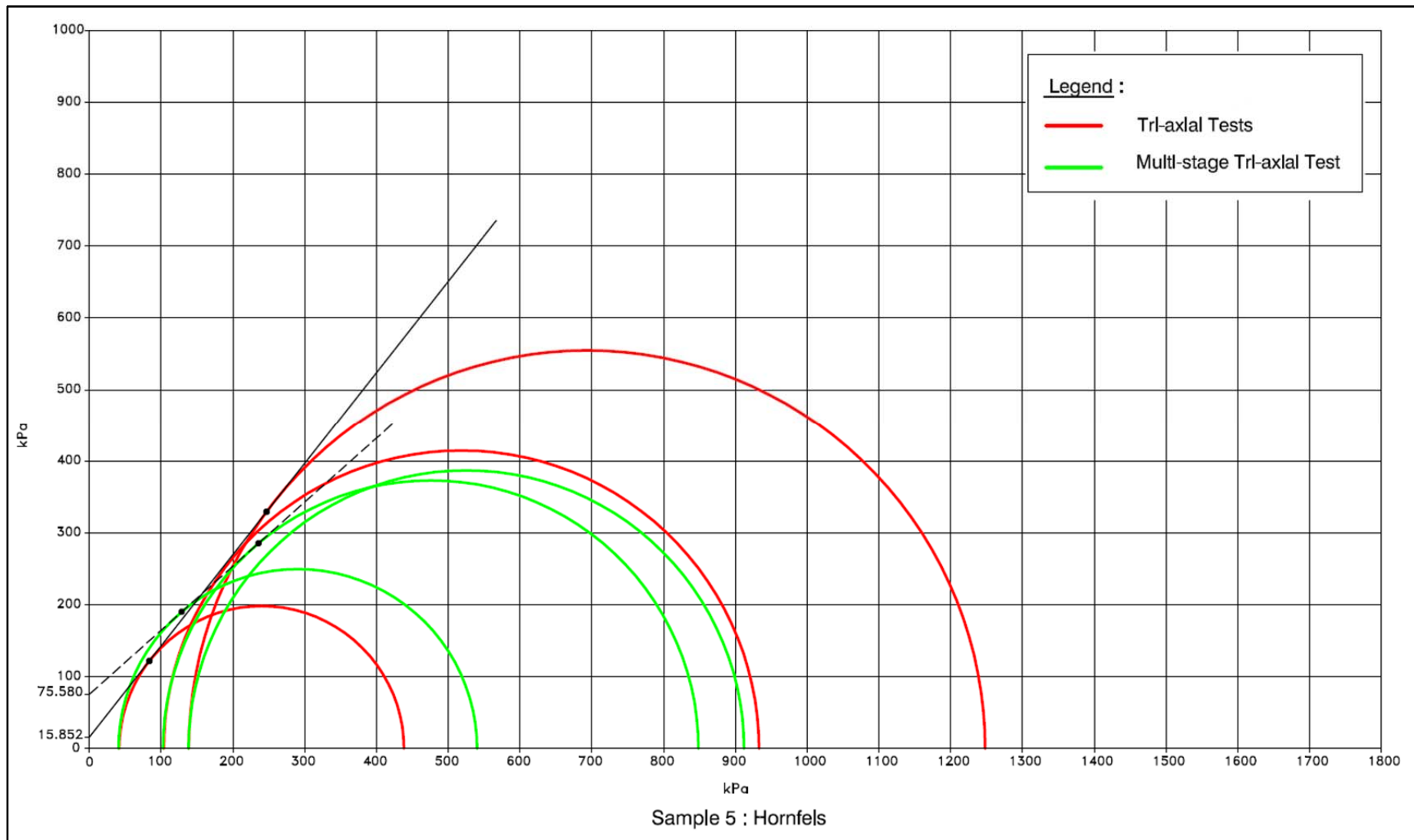


Figure 4.23 Comparative Mohr-Coulomb failure criteria for sample 5, hornfels

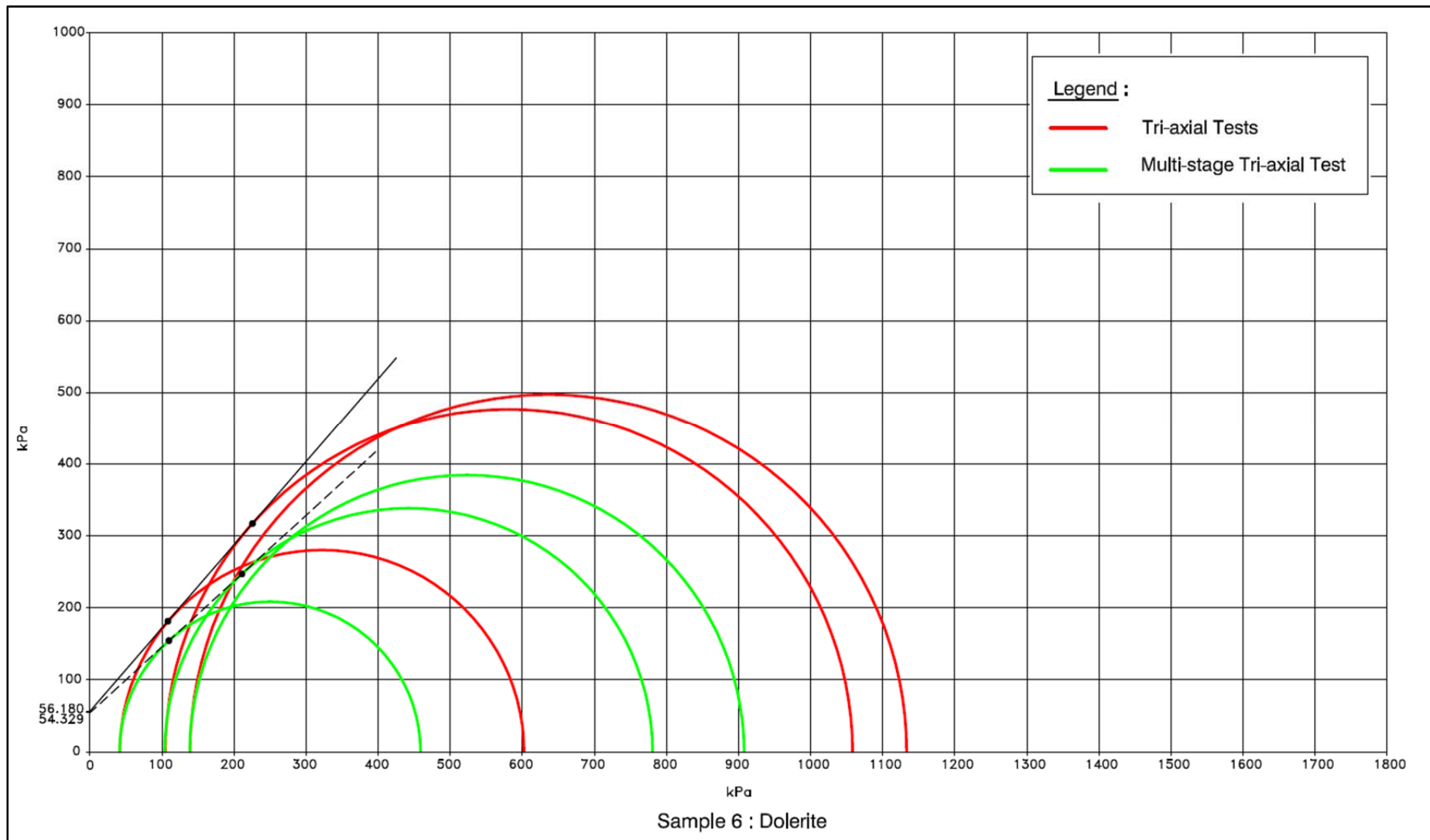


Figure 4.24 Comparative Mohr-Coulomb failure criteria for sample 6, dolerite

- The tangent lines drawn to the Mohr circles of the multi-stage tests and the conventional tests show a different gradient (often very much so), which translates into notable differences in the derivation of the cohesion, internal friction angle and ultimately the shear strength.

In order to illustrate the difference in shear strength parameters (i.e.  $c$  and  $\phi$ ), Table 4.47 summarises the values deduced from the Mohr circles in the preceding figures.

**Table 4.47** Comparative summary of shear strength properties deduced from Mohr circles

Sample	Multi-Stage Tri-Axial Test		Conventional Tri-Axial Test	
	Friction Angle (°)	Cohesion (kPa)	Friction Angle (°)	Cohesion (kPa)
1. Quartzite	42.454	74.543	52.312	56.138
2. Granite	45.804	75.697	52.465	22.674
3. Quartz Porphyry	41.753	87.127	49.838	46.880
4. Tillite	40.661	74.362	50.953	19.669
5. Hornfels	41.708	75.580	51.783	15.852
6. Dolerite	42.431	54.329	49.175	56.180

Shear strengths were determined as discussed in section 4.7.2 to compare the results obtained from the two methods, based on the properties summarised in Table 4.47 above. In this instance, however, the effects of cohesion were dismissed (i.e. zero cohesion was assumed;  $c = 0$ ). Table 4.48 summarises the difference in values for tests conducted at a confining pressure of approximately 41 kPa.

The difference in calculated shear strength (final column of Table 4.48) indicates absolute values and is fairly self-explanatory as to the accuracy – or rather subjectivity – of the multi-stage tri-axial test. These discrepancies fully warrant the repeat of the tri-axial tests

**Table 4.48** Comparative Shear strength of samples (approximately 41 kPa confining pressure)

Sample	Multi-Stage Tri-Axial Test		Conventional Tri-Axial Test		$\Delta$ Shear Strength (kPa)
	$\sigma_n$ (kPa)	Shear Strength (kPa) assuming (c = 0)	$\sigma_n$ (kPa)	Shear Strength (kPa) assuming (c = 0)	
1. Quartzite	123.265	111.765	107.116	138.650	26.885
2. Granite	122.753	126.248	89.110	116.108	10.140
3. Quartz Porphyry	132.887	118.616	108.075	128.061	9.445
4. Tillite	118.036	101.389	78.127	96.343	5.046
5. Hornfels	128.645	114.651	83.469	106.006	8.645
6. Dolerite	109.603	100.194	108.297	125.326	25.132

undertaken in this research and should serve as a warning to others regarding the use of the multi-stage tri-axial test method.

## 5 Application

### 5.1 Model Application – Modified Dolerite

#### 5.1.1 Flakiness Index

This section of the research aims to apply the models and approaches compiled thus far to illustrate their potential benefits and compare the outputs with the flakiness index currently used in industry. This is problematic as the data from the scanned samples is biased to include elongated or flattened particles which, in turn, mean that the data is not fully representative of the actual sample populations. Only the dolerite sample (i.e. sample 6) had representative scan data with randomly selected particles; however, this sample itself was modified to intentionally include an excess of elongated particles compared with the normal crushed aggregate for experimental purposes.

Despite the modified nature of the dolerite sample, it can still be used to illustrate how the flakiness index can be refined using laser scanner results. It must also be borne in mind that the flakiness index of the modified sample (i.e. 44,4 %) is fully representative of the sample as the entire sample (i.e. each particle comprising the sample) was tested with the flakiness index plate. The work of Anochie-Boateng *et al.* (2011a) also has specific reference here, as they applied the laser scanning method to the determination of the flakiness index.

In essence, the conventional flakiness index is a ratio - based on mass - of elongated and regular particles. The approach adopted by Anochie-Boateng *et al.* (2011a, 2011b) used a similar approach to that considered here and also made use of the laser scanning apparatus. The mass of a scanned sample can be calculated (with ease in spread sheet format) if the measured/calculated volumes of the particles are multiplied by the material density. However, in the case of the dolerite, for example, this can yield inaccuracies in the calculation of the masses of small particles. The reason for this is that the material contains randomly but inconsistently distributed amygdales (of different densities) which may be absent in some particles and present in others. Instead, it is considered that the volume alone

can be substituted when calculating the flakiness index using the same procedure and would probably be more accurate as well.

Using a similar approach to the conventional flakiness index, the ratio of regular and elongated particles can be determined, using the cumulative volume of particles, as opposed to mass (as used by the conventional flakiness index method). Whereas Anochie-Boateng *et al.* (2011a) pursued the matter of also factoring in the material's mass (using the density and volume), it is anticipated that using only the volume may actually be beneficial.

A weighting factor (equal to the mass ratio of samples selected for the flakiness index test - refer to Table 2.1, row 5) was used in the analysis in order to compensate for the particle size distribution of the sample. Particle volumes (calculated from laser scans) are readily available as part of the data entered into the original spread sheet. Calculating the flakiness index in this manner (i.e. based on volumes) is not only more accurate (due to the accuracy of scan data vs. the plate method), but the calculation using the volumes is also free of any variability related to the moisture content in the rock particles. A sample which is not completely dry will give inaccurate values using the conventional calculation method of the flakiness index due to mass variations associated with this moisture content. This will not be the case when the volume is used. Table 5.1 summarises the derivation of the flakiness index using the scanner-based, volumetric approach.

In this instance the flakiness index calculated in Table 5.1 is approximately 10 % higher than that calculated using the conventional plate method (i.e. 44.4 %). It is considered that the value obtained from scanning data is more accurate due to the precision of the scanning tool and its ability to identify elongated particles far more accurately than the plate method. Regardless of the anticipated improvement in accuracy, the scanner-based method still suffers from the same fundamental flaw as the normal flakiness index test. Both tests rely on a limited number of randomly selected particles to represent large stockpiles of aggregate to be used in construction.

**Table 5.1** Derivation of the flakiness index using scan data (dolerite)

<b>Particle Size (retained on sieve)</b>	<b>Volume of Elongated Particles (mm<sup>3</sup>)</b>	<b>Total Volume of Particles (mm<sup>3</sup>)</b>	<b>Ratio</b>	<b>Elongated Fraction</b>	<b>Flakiness Index</b>
<b>26.5 mm</b>	61260.87	434675.71	5	14.09 %	4.40 %
<b>19.0 mm</b>	119945.87	184375.13	4	65.06 %	16.27 %
<b>13.2 mm</b>	53452.23	67771.04	3.5	78.87 %	17.25 %
<b>9.5 mm</b>	20540.33	33916.58	2	60.56 %	7.57 %
<b>6.7 mm</b>	14136.03	14486.77	1	97.58 %	6.10 %
<b>4.75 mm</b>	4330.31	5099.34	0.5	84.92 %	2.65 %
<b>Total</b>	273 665.64	740 324.57			<b>54.24 %</b>

### 5.1.2 Particle Texture

The particle texture can be calculated using the *aggregate texture value*, as proposed in this research. Reviewing the data for the modified dolerite sample, it is clear that bigger particles have larger (V/A) values and hence smaller particle sizes should have less influence on the texture value. For this reason the incorporation of the grading (i.e. mass of the particles) into the *aggregate texture value* is considered vital in order to weight the results.

Considering the dolerite sample discussed here, the 26.5 mm fraction is comprised largely of regular particles (refer to Table 5.2). Simultaneously, though, all particle sizes smaller than 26.5 mm were dominated by elongated particles. Factoring in the grading (i.e. particle mass distribution) ensures that the entire composition of the sample is fully represented. This is important because even though the finer particles may be largely elongated, the sample behaviour will be more strongly affected by the quantities of elongated particles and not merely the fact that they are elongated.



It was initially considered that the grading distribution factor should be normalised as particles passing the 4.75 mm screen are not considered in this research or when determining the flakiness index; however, normalising the data would have a limited effect, as the particle size distributions must be within the window range in the COLTO specifications. As such, normalising the grading data was not done.

The *aggregate texture value* can be calculated using equation 5.1 below:

$$\text{Aggregate texture value} = \sum (\text{Weighted V/A}) \times (\% \text{ of Fraction}) \times \text{Grading} \quad (\text{Equation 5. 1})$$

where

- The weighted (V/A) value is calculated from the model data
- The (% of fraction) is the percentage of a particular size fraction which is elongated or regular. This is the percentage calculated based on elongated vs. regular particles and recorded on model tables
- “Grading” is the percentage of a specific size fraction retained on the relevant screen

The weighted (V/A) value is obtained using the procedure described in section 4.5. The percentage of regular or elongated particles comprising the sample also needs to be considered. The result yields two *aggregate texture values* for each sample (i.e. one for elongated particles and one for regular particles).

The calculation for the dolerite material is summarised in Table 5.2. No limits are likely to be specified for the *aggregate texture value*, as it is only considered as a means of quantifying the roughness of a material or particle. Simply stated, the *aggregate texture value* assesses the surface texture of a material and is unlikely to be included in specifications which may exclude material from use as would, for instance, the flakiness index.

**Table 5.2** Analysis of dolerite sample

Particles	Weighted (V/A)	% of Fraction (Regular vs Elongated)	% Retained on Corresponding Screen	Regular Particles	Elongated Particles
26.5 mm Regular	3.856	87 %	10.32	0.346	
26.5 mm Elongated	3.774	13 %			0.051
19.0 mm Regular	3.345	23 %	13.80	0.106	
19.0 mm Elongated	2.374	77 %			0.252
13.2 mm Regular	2.055	20 %	9.27	0.038	
13.2 mm Elongated	1.767	80 %			0.131
9.5 mm Regular	1.648	40 %	3.67	0.024	
9.5 mm Elongated	1.524	60 %			0.034
6.7 mm Regular	1.147	3 %	11.80	0.004	
6.7 mm Elongated	1.133	97 %			0.130
4.75 mm Regular	0.911	17 %	10.13	0.016	
4.75 mm Elongated	0.819	83 %			0.069
<b>Aggregate Texture Value</b>				<b>0.534</b>	<b>0.667</b>

The time and equipment necessary to measure the aggregate texture value would also make it impractical for use as a routine test method. However, it is considered to be a powerful research and analytical tool.

With the relatively limited quantity of scan data currently available, this approach cannot be substantiated or evaluated comprehensively. Subsequently no value ranges can be proposed for the *aggregate texture value*; however as mentioned, it is unlikely that specification limits will be imposed on the index as it is a descriptive parameter.

## **5.2 Correlation Between Shear Strength Properties and Particle Properties**

One of the aims of this project was to assess the relationship between the particle shape/surface texture and the shear strength properties of the sample materials. Bias in the scan data prevented a direct comparison, as particles selected for scanning deliberately included more elongated/flattened particles (i.e. not reflecting the true material properties) for research purposes. Using the scan results obtained would therefore not be a true reflection of the samples used for the tri-axial tests as the scan data would represent a material with more elongated particles (i.e. higher flakiness index) than actually used for the tri-axial tests.

It was ultimately concluded that the texture parameters (i.e. *aggregate texture value*) sourced from the scan data could be used; however the flakiness index derived from the scan data (refer to section 5.1.1) would not be representative, as discussed above. As a result, the flakiness index of the bulk sample (i.e. as tested in the aggregate laboratory) was considered for further use, as this would be more representative of the ratio between elongated and regular particles (despite the ratios being determined by the less accurate plate-based method). The flakiness index was therefor used to correct or weight the *aggregate texture values* for regular and elongated particles, based on the simple premise

that if a material has a flakiness index e.g. 20%, some 20% of the particles (of each size fraction) are elongated. Such a scenario would never occur in real world conditions. The exception here was the modified dolerite (i.e. sample 6), for which the tested flakiness index of the modified sample (i.e. 44.4 %) was used. This value was also determined using the flakiness index plate; hence the results from different materials can be compared directly.

The matter was further complicated by the fact that the 6.7 mm and 9.5 mm fractions were not determined when the tri-axial samples were prepared. This was because these fractions are not standard sizes described in the COLTO grading requirements (refer to Table 4.1), as specified for G1 crushed rock aggregate. This necessitated that certain assumptions be made regarding the grading (and subsequently, the *aggregate texture values*) of the 9.5 mm, 6.7 mm and 4.75 mm fractions. For the purposes of this section it will be assumed that the 9.5 mm, 6.7 mm and 4.75 mm fractions are all equal; hence the fraction retained on the 4.75 mm sieve (as measured for the tri-axial test grading analyses) are divided in three equal parts. The *aggregate texture value* was calculated for regular and elongated particles for each of the samples used, as outlined in section 5.1.2. Addendum H contains the spreadsheet used to calculate the weighted *aggregate texture values*, based on the flakiness indices of bulk samples.

Of all the materials used for tri-axial tests, only the granite, dolerite, tillite and hornfels had representative scan data for all size fractions. The remainder of the samples had no scan data for the 26.5 mm fraction. Thus only the four materials mentioned were utilised for further analyses. However, these materials not only yielded a wide range of results during tri-axial tests, but they also had large variations (between samples) in shape and texture properties.

For the purposes of the analysis, it was deemed sensible to select at least three shear strengths for each of the samples considered. Reverting back to Figures 4.13, 4.15, 4.16

and 4.17, the data were read off and considered for further analysis and adjusted assuming no cohesion (refer to Table 5.3). While it would have been ideal to consider higher ranges of  $\sigma'_f$  data, this would not allow effective comparison due to the tendency of dolerite particles to break, as discussed at the end of section 4.7.2 and depicted in Figure 4.17.

**Table 5.3** Shear strength data considered for analysis

Sample	$\sigma'_f$ (kPa)	$\tau_f$ (kPa)	$\sigma'_f$ (kPa)	$\tau_f$ (kPa)	$\sigma'_f$ (kPa)	$\tau_f$ (kPa)
2 Granite	50	65.868	100	131.493	200	256.493
4 Tillite	50	63.836	100	125.692	200	246.310
5 Hornfels	50	64.148	100	128.148	200	255.865
6 Dolerite	50	57.961	100	114.527	200	232.48

The parameters and values used in the correlation analysis are listed in Table 5.4. The correlation analysis was performed in Excel® and results of the correlation analysis are summarised in Table 5.5.

A number of observations can be made from Table 5.4 and Table 5.5. It must be emphasised that these observations are based on only four data points/sets and *should therefore be interpreted with caution*. The following was noted:

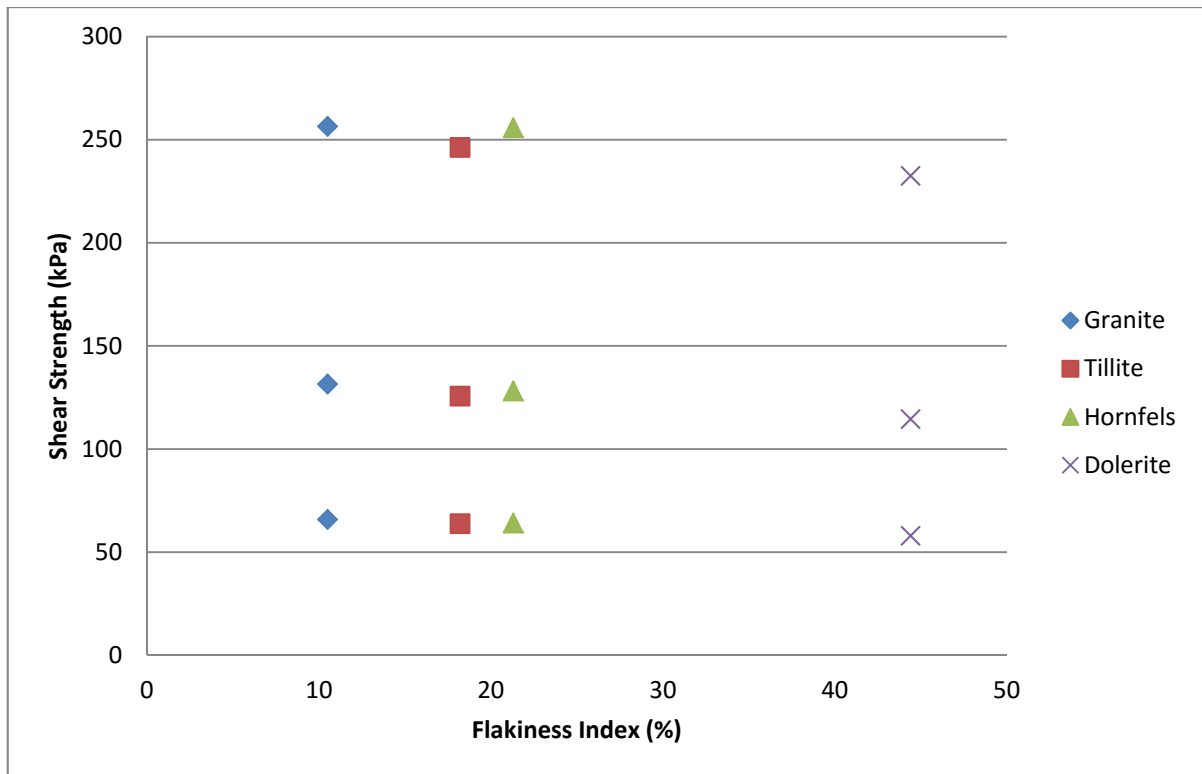
- The lowest flakiness index (i.e. 10.5 %) corresponds with the highest shear strength (i.e. granite sample) at all three normal stresses considered. The opposite is also true in that the highest flakiness index (i.e. 44.4 %) corresponds with the lowest shear strength (i.e. modified dolerite sample). Intermediate flakiness indices did not necessarily follow this tendency consistently. Figure 5.1 plots the flakiness indices against shear strength of each sample analysed for the three normal stresses considered (i.e. 50 kPa, 100 kPa and 200 kPa).

**Table 5.4** Summary data for correlation analysis

Sample	Material	ATV (Regular Particles)	ATV (Elongated Particles)	Flakiness Index (%)	Friction Angle (°)	Shear Strength (kPa) $\sigma'_f = 50$ kPa	Shear Strength (kPa) $\sigma'_f = 100$ kPa	Shear Strength (kPa) $\sigma'_f = 200$ kPa
2	Granite	1.226	0.122	10.5	52.465	65.868	131.493	256.493
4	Tillite	1.144	0.220	18.2	50.953	63.836	125.692	246.310
5	Hornfels	1.019	0.224	21.3	51.783	64.148	128.148	255.865
6	Modified Dolerite	0.744	0.512	44.4	49.175	57.961	114.527	232.480

**Table 5.5** Correlation matrix of test parameters (assuming flakiness index of bulk samples)

	ATV (Regular Particles)	ATV (Elongated Particles)	Flakiness Index (%)	Friction angle (°)	Shear Strength (kPa) $\sigma'_f = 50$ kPa	Shear Strength (kPa) $\sigma'_f = 100$ kPa	Shear Strength (kPa) $\sigma'_f = 200$ kPa
<b>ATV (Regular Particles)</b>	1						
<b>ATV (Elongated Particles)</b>	-0.971040072	1					
<b>Flakiness Index (%)</b>	-0.987004386	0.996807077	1				
<b>Friction angle (°)</b>	0.883586174	-0.963899059	-0.943751218	1			
<b>Shear Strength (kPa) <math>\sigma'_f = 50</math> kPa</b>	0.957549275	-0.99862331	-0.991338953	0.971797637	1		
<b>Shear Strength (kPa) <math>\sigma'_f = 100</math> kPa</b>	0.927441893	-0.989154154	-0.975092129	0.991224976	0.994203932	1	
<b>Shear Strength (kPa) <math>\sigma'_f = 200</math> kPa</b>	0.821427049	-0.933466544	-0.902223464	0.984631941	0.949702651	0.974810801	1



**Figure 5.1** Flakiness index vs. shear strength

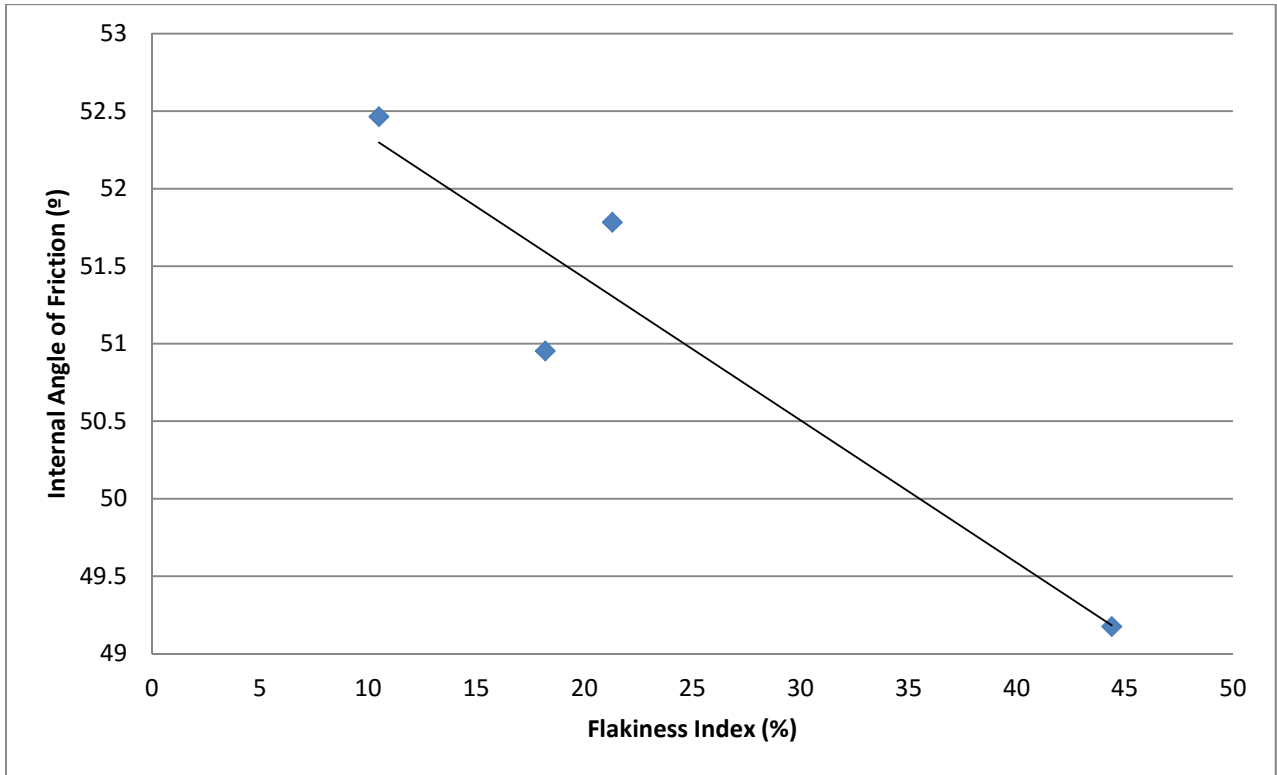
While the graph is based on only four data points, it clearly illustrates that the dolerite sample with its high flakiness index constantly shows lower shear strength than the remaining samples.

- The flakiness index correlates well with the shear strength(s) of samples. However, it appears that the effect of the flakiness index becomes less pronounced as the normal stress at failure ( $\sigma'_f$ ) increases. This is deduced from the fact that the correlation decreased from  $r^2 = 0.983$  ( $r \approx -0.991$ ) at  $\sigma'_f = 50$  kPa to  $r^2 = 0.951$  ( $r \approx -0.975$ ) at  $\sigma'_f = 100$  kPa, and even further to  $r^2 = 0.814$  ( $r \approx 0.902$ ) at  $\sigma'_f = 200$  kPa.
- The shear strength shows a stronger correlation with the *aggregate texture value* for elongated particles ( $r^2 = 0.929$  ;  $r \approx -0.964$ ) than with the *aggregate texture value* for regular particles ( $r^2 = 0.781$  ;  $r \approx 0.884$ ). This suggests that the particle shape has a bigger effect on the shear strength than the particle surface texture. The effects of assessing the surface texture does, however, refine the correlation as the *aggregate texture value* for elongated particles constantly has better correlations with the shear strength than only the flakiness index.

- The preceding point is further supported by the fact that the internal friction angle also shows better correlation with the *aggregate texture value* of elongated particles ( $r^2 = 0.929$  ;  $r \approx 0.964$ ) than the *aggregate texture value* of regular particles ( $r^2 = 0.781$  ;  $r \approx 0.884$ ).
- The *aggregate texture value* for elongated particles shows a strong correlation with the flakiness index. This is not surprising, as the elongated particles are effectively the particles which result in the flakiness index and the two properties are therefore considered to be co-dependent.
- A trend is noticed in the correlation between the shear strengths and the *aggregate texture values* for both regular and elongated particles. The correlations decrease as the normal stress (at failure) increases. This suggests that both the particles shape and surface texture properties become less influential at higher normal stresses. It is anticipated that this effect is accurate, seeing as interlock and surface friction should at some point (during loading) reach a peak. At this point, the shear strength of the material will be affected by the inherent strength of individual aggregate particles and the effective load transfer between them.
- Seeing as the friction angle was used to calculate the shear strength values, one would expect a correlation between these parameters of 1.00; however this proved not to be the case. It is anticipated that this is due to rounding off errors during calculation.
- All things considered, the correlations shown in the results are fairly strong and suggest that the approach used has been successful, though again, it must be emphasised that the correlations are based on very limited data.

In addition to Figure 5.1, further linear relationships were noted between the flakiness index and internal angle of friction (Figure 5.2). In this instance, it is worth noting that the dolerite sample (with its high flakiness index) consistently showed the lowest shear strength of all the materials.





**Figure 5.2** Flakiness index vs. Internal Angle of Friction

## 6 Conclusions and Findings

The research summarised in this thesis proved to deliver results that can be applied to advance the assessment of materials in the road construction industry significantly. Based on the analysis of the data available, the newly derived *aggregate texture value* parameter has been shown to present an opening for continued research in this area.

### 6.1 Particle Grain Crushing

The occurrence of particle crushing was confirmed between the stages of sample preparation and completion of tri-axial tests. The effects were observed as differences in grading analyses before compaction/testing and after testing.

### 6.2 Development and Application of Scanner-based Models

#### 6.2.1 Scanner Properties and Attributes

The laser scanner apparatus and methods applied during this research proved to hold many advantages over conventional methods of particle shape and surface texture analysis; however, a number of disadvantages were also noted. Perhaps the methods most significant advantages are the accuracy with which it measures the target scanned and its ability to supply results which present the scanned particle in three dimensions. The result of the scan procedure is a data set which yields (among other things) the three principal dimensions of the target, as well as the surface area and volume. Conventional methods currently in use do not allow this level of data procurement.

While this new technology holds many advantages over current procedures, it also has limitations. The most obvious limitations can be summarised as follows:

- The approach of sampling a limited number of particles for analysis is flawed in that an assumption is made that the number of particles selected is representative of the entire material population (e.g. stockpile) that it was sampled from. Statistically, this

is a significant flaw. However, the approach currently used to test a material's flakiness index works on the same basis and as such, the laser analysis is seen neither as an improvement, nor a regression in terms of sampling.

- In order to obtain good accuracy from the scan results, the resolution used must be optimised. Higher scan resolution results in longer scanning times. As a result, scanning is time-consuming and often impairs work flow due to the limited pace and capacity that the equipment can accommodate.
- Some difficulties may be encountered when scanning flattened or elongated particles (or even oddly shaped particles that are unstable when placed). Instability or movement during turntable rotation could be problematic for such particles. In addition, flattened particles often do not allow complete direct line of sight for the scanner, resulting in scan “shadows” on the flattened surfaces. These surfaces are then filled (assumed) by the software during processing, ultimately resulting in inaccurate estimates of particle volumes (and to a lesser extent, surface area).
- The scanning equipment is highly sensitive to dust and vibration, both of which are common in a non-research (i.e. commercial) laboratory environment. The effects of CBR compaction equipment, sieve shakers and other general test equipment in a routine testing laboratory mean that the placement of the apparatus would have to be very carefully selected.
- A high degree of computer literacy (and training) is required to perform the tasks associated with scanning and data processing.

### *6.2.2 Preliminary Models*

Two models were initially proposed in an attempt to quantify particle surface textures. The dimensions, surface area and volume of aggregate particles were exploited in this regard. It was immediately noted that any attempts to refine data were affected by the elongation (or flakiness) of the particles. Initial attempts to refine the data in bulk were thus abandoned in favour of subdividing the data into subsets of “elongated” and “regular” particles.

The first model that was proposed considered a parameter which factored in the elongation value of the particle under consideration. While the results initially seemed promising it was soon noted that the model refinement was strongly affected by the particle elongation.

Models exhibited the tendency to include few regularly shaped particles but an abundance of elongated particles. The subsequent model ultimately discerned between different levels of elongation and angularity rather than the particle texture. This model was thus abandoned but not without contributing to a better understanding of particle properties. The model did illustrate two important factors which were beneficially used in the second model:

1. Bulk scan data should preferably be divided into elongated and regular particle subsets before further analysis. While it proved invaluable to separate the data in this way, the first model also showed that factoring the elongation into the model biases the model output significantly.
2. The particle texture, elongation and angularity appear to be interdependent and it was very difficult to separate the three parameters in the data. The angularity and elongation were particularly interdependent and as a result, the angularity could to some extent be managed by dividing the data into regular and elongated particles.

The second preliminary model that was proposed showed more potential than the first. This method used a similar approach to the original model but did not factor the particle elongation into the model calculations. The resulting models were still affected by the angularity of particles, but to a much lesser extent than the first model, as excessive angularity was removed by omitting the elongation values from the model calculations. The method proved satisfactory.

### *6.2.3 Working Scanner-based Models*

The working models compiled to evaluate particle textures were based on the second preliminary model. Two models (i.e. regular and elongated) were derived for each particle size (i.e. 26.5 mm, 19.0 mm, 13.2 mm, 9.5 mm, 6.7 mm and 4.75 mm) using the data of all the scanned materials' for each respective particle size. The models were developed in such a way as to allow a simple mathematical and visual assessment of each particle, based on ten "classes". The models have scope for improvement if a larger data set could be developed and analysed. Nevertheless, even with the data available, the models appeared to present a satisfactory analysis technique.

The models were further adapted in order to allow the reduction of any number of particles of a selected size to a single, seemingly representative, particle. While this approach also makes use of the ten particle “classes” identified, the single representative value can be compared directly with the entire data base in spread sheet form to find a more accurate representation which is not necessarily reflected in the model tables developed. From here the representative values can be used either as a reference or further analysed to derive an *aggregate texture value* for a given material.

The *aggregate texture value* provides two values – one for the elongated particle fraction of the sample and one for the regular particle fraction of the sample – for each sample and is an index weighted by the particle size distribution of the material and the ratio between the regular and elongated particles.

It is not anticipated that the *aggregate texture value* is likely to ever be implemented in any formal guideline or specifications. The parameter is descriptive and not restrictive (i.e. providing a set range with which a sample must comply such as the flakiness index). Instead, it is more likely that the comparative tables and model value approach may prove more usable and can even be applied to replace the somewhat subjective visual description of particle textures. The technique is also expected to be a valuable research tool, with application in research involving the surface texture of aggregate particles. Substituting visual assessment with the proposed models would largely remove any subjectivity and replace it with a scientific approach.

### **6.3 Flakiness Index**

As far as the flakiness index is concerned, it is anticipated that the approach suggested in this research – and described by Anochie-Boateng *et al.* (2011a) - is considerably more accurate than the current method which utilises a flakiness index plate. This approach assumes that the selected particles are representative of an entire material source, an assumption that is flawed but is generally applied for practical reasons.

The scanner-based method has the main advantage that it can assess each aggregate particle based on its exact dimensions (three dimensions), whereas the conventional flakiness index

is far more general and considers only two dimensions. If desired, particles do not have to be screened prior to scanner analyses as the results would discern when particles are elongated. As a direct result of this, the scanner-based approach would accurately identify elongated particles, based on their dimensions, with high accuracy.

Furthermore, assessing the flakiness index in terms of a cumulative volume (as a fraction of the total sample volume) is considered more accurate than the current mass-based approach proposed by Anochie-Boateng *et al.* (2011a). Any variation in the moisture content (i.e. moisture absorption after oven-drying) or relative density of the particles used in the determination of the flakiness index may potentially reflect an inaccurate flakiness index. By comparison, the volume-based method is not susceptible to variations in moisture content or relative density.

It is thus clear that the determination of the flakiness index using a laser scanner is significantly superior (in terms of accuracy and adaptability) to the current plate-based method. Based on a modified sample with an artificially elevated flakiness index, it was found that the plate-based method underestimates the flakiness index by some 10 %, compared with the laser based system. It must be noted, though, that this comparison was derived from a single sample that was deliberately mixed to have a flakiness index exceeding the COLTO specifications and as such, the 10 % underestimation is likely to be less pronounced in conventional G1 materials complying with the specification.

## **6.4 Shear Strength Properties**

### *6.4.1 Shear Strength of Aggregate*

Despite the limited data available for comparison and analysis in this study, the assessment of shear strength properties showed a number of interesting preliminary results. Three of the four samples used in the correlation analyses satisfied the COLTO (1998) specifications (with specific reference to the flakiness index). The fourth sample (dolerite) was intentionally blended to exceed the maximum flakiness index specified by COLTO (1998). The modified sample had a flakiness index of 44.4 % as determined using the conventional plate method. This flakiness index value, however, is fully representative of the sample as

every particle in the sample was tested using the flakiness index plate with the aim of obtaining the most accurate flakiness index possible (by conventional means).

The comparative results showed that the dolerite sample with its high flakiness index consistently had lower shear strength than samples with flakiness indices within the range specified by COLTO (1998). The material appeared to be considerably weaker at higher deviator stresses (associated with higher confining pressures during tri-axial tests) compared with other materials. Conversely, the granite sample had the lowest flakiness index and the highest shear strength. One may therefore assume that a decrease in flakiness index is associated with an increase in shear strength, but this was not necessarily reflected in the remaining data with the remaining samples (which had intermediate flakiness indices). Nevertheless, the conclusion made here was that the material with the elevated flakiness index constantly underperformed when compared with the remaining samples.

The observation above was reflected in the correlation coefficient between the flakiness and the shear strength; however, it must be cautioned that this was based on only four test results and may therefore not be statistically significant.

#### 6.4.2 Aggregate Texture Value and Shear Strength Properties

The correlation between the shear strength data and the *aggregate texture value* was found to be good. It would thus appear then that the *aggregate texture value* is directly related to the shear strength. The following preliminary deductions can be made from the results:

1. The *aggregate texture value* of elongated particles showed a better correlation with the shear strength than the *aggregate texture value* of the regular particles did. As such, it is deduced that the elongation of the particles affects the shear strength properties more significantly than the texture properties.
2. The *aggregate texture value* for elongated particles showed a better correlation with the shear strength properties than the flakiness index did. Considering the fact that the flakiness indices were used to calculate the actual *aggregate texture value* in this instance, the results would suggest that the *aggregate texture value* improved the correlation by considering the influence of the surface texture of the particle. Simply

stated, the *aggregate texture value* refined the flakiness index's correlation with the shear strength properties by also considering the particle textures.

3. The correlation between the shear strength and a number of other properties (i.e. ATV for regular particles, ATV for elongated particles and flakiness index) showed a decrease as principal stresses increased. This suggests that other factors may also have an influence at higher normal loads (e.g. material strength and load transfer between particles).

#### 6.4.3 *The Use of Multi-Stage Tri-Axial Tests*

The results of multi-stage tri-axial tests were proven to be highly variable, as well as largely inaccurate. While it is *theoretically* possible to achieve a close correlation between results of the multi-stage test approach and the conventional test approach, the results are very subjective and strongly operator dependant. The biggest problem appears to stem from the observation that the test is halted prematurely to avoid failing the sample before moving on to the next phase of the test (i.e. the next confining pressure).

### 6.5 Final Conclusion

Considering all the findings and experimental results obtained during this research project, the work is considered to be of an innovative but preliminary nature only. Although the results show promise, they remain to be substantiated by refinement with more data and test trials (i.e. experimental tests and analyses).

The following conclusions were reached:

- The new laser scanning technique was successfully applied to quantify or describe the shape and surface texture properties of aggregate particles. The result is a massive improvement on current methods (i.e. flakiness index) used in the South African industry.
- Descriptive models (tables) were developed which can be used to allow comparison of any aggregate particle, depending on its particle size and elongation. The models



are also capable of arranging/sorting particles based on their shape and surface texture.

- The *aggregate texture value* (ATV) was derived as a parameter which describes/summarises the shape and texture of a given aggregate sample, taking into account all particle size fractions larger than (and including) 4.75mm and (smaller than) 37.5mm.
- A good correlation was identified between shear strength properties (derived from tri-axial tests) and the *aggregate texture value*, although additional testing and comparison is necessary to substantiate this.

## 7 Recommendations and Further Work

After completion of the research conveyed in this thesis, a number of recommendations can be made for additional work to be undertaken. These recommendations are made with the specific intentions of expanding on the findings described here and may be implemented largely to fill in gaps not covered during this research. The following is recommended:

### 7.1 Data Base Compilation

A comprehensive data base containing results of as many South African materials as possible must be compiled. Additional samples including a wider range of material types would be an added bonus as more data would present a better opportunity to develop and refine the models. The present approach of scanning 30 particles per size fraction seems adequate; however it is recommended that 25 particles be randomly chosen for each size fraction, with the remaining five being chosen for specific purposes (e.g. elongated particles). Using this approach the first 25 particles could then be used in analysis as an unbiased sample for real-world sample analysis.

Scanning should preferably be continued using the protocol developed by the CSIR; however it is proposed that a scanning resolution be standardised for various specific applications. For example, analysing railway ballast may not necessarily require the same resolution as that for G1 crushed stone aggregate. For the purposes of road construction aggregate analyses, it is recommended that a resolution of 0.1 mm be applied (vertically and horizontally) in order to obtain maximum resolution when analysing surface textures. Sensitivity analyses have been undertaken in this regard (Pers. Comm., J. Komba, 2013) and should be implemented in the scanning protocol.

Once sufficient additional data has been obtained, the models proposed in this thesis should be revised. Reference tables, data ranges and particle properties should be reassessed in order to produce complete working models.

As this research was of an exploratory nature and concentrated on developing techniques and processes, the findings are based on a limited database and should be applied to a much wider dataset. Although the results show significant promise and usefulness, they remain to be substantiated by refinement with more data and test trials.

## 7.2 Flakiness Index

The findings of this work indicate that it would be beneficial to pursue the assessment of flakiness index determination with the aid of a volume-based approach, using the laser scanner. The initial findings of this research and the work of Anochie-Boateng *et al.* (2011a) show that the flakiness index can be significantly refined and data accuracy can be improved using the scanner.

A comparison is suggested in this regard. A selected number of samples (e.g. 30 different G1 aggregate samples) should be used for evaluating the flakiness index. A test complement of particles must be sampled according to test method B3 described in the TMH1 (1986). The flakiness index should then be determined in accordance with this method, keeping detailed record of each size fraction analysed. Once completed, the same particles used for the conventional flakiness index determination should be scanned. The flakiness index should then be determined using the volume-based approach as described in section 5.1.1 of this document as well as with the method proposed by Anochie-Boateng *et al.* (2011a).

The results of the three methods will allow a direct comparison between the conventional (i.e. plate) approach and the scanner's various approaches. Clearly a wider range of test samples will be beneficial.

## 7.3 Aggregate Texture Value and Shear Strength Properties

It is recommended that additional tests be performed to verify the applicability of the models developed in this research using a wider number of samples and material types. It is recommended that a similar approach be used to the experimental procedure followed in this research (i.e. substitution of material fines with a uniform, inert source). The basic grading analysis used for material classification of the sample must also include (i.e. record) the 9.5

mm and 6.7 mm fractions in addition to the COLTO-specified fractions (i.e. 26.5 mm, 19.0 mm, 13.2 mm and 4.75 mm). Each sample must be tested at three different confining pressures until the sample fails (the same material may be re-used provided particle crushing does not affect the sample adversely). If possible, it would also be preferred if shear box tests could be used in order to assess the friction characteristics of the material more directly.

Once shear tests are completed, the materials can be divided into their size fractions by means of sieving and oven dried. Aggregate particles should be washed and/or brushed and oven dried again. Representative particles should then be selected and scanned with the laser scanner according to the CSIR protocol, using a resolution of 0.1 mm in a vertical and horizontal direction.

From the scanned data, model values, model compositions and grading analyses of the samples, the *aggregate texture values* should be determined. If desired the flakiness index can also be calculated using the volumetric-based approach (derived from scan data). Once the data has been processed, the relationship between the *aggregate texture values*, flakiness index (if applicable) and the shear strength properties can be re-assessed in order to validate the findings of this research. The opportunity should also be used to compile a range of *aggregate texture values* to create a reference system (i.e. range in values) for the parameter.

Aggregate producers should be encouraged to carry out such work on their own products and relate the results to their production methods (i.e. blasting and crushing). This may assist them in providing more uniform, consistent and better controlled products.

#### **7.4 Multi-Stage Tri-Axial Test Method**

While the benefits of the multi-stage tri-axial test approach are very tempting, the use of this approach cannot be recommended. The variability and subjectivity of the test procedure (compared with conventional tri-axial test procedures) simply makes for poor and inaccurate test results.

## 8 References

Anochie-Boateng, J., Komba, J., Mukalenga, N. and Maharaj, A. (2010). *Evaluation of 3D laser device for characterizing shape and surface properties of aggregates used in pavements*. 29th Southern Africa Transportation Conference, Pretoria, South Africa, August 2010.

Anochie-Boateng, J. and Komba, J.J. (2010): Laser scanning protocol for determining aggregate shape and surface properties, Pretoria: CSIR Built Environment. Report number CSIR/BE/IE/IR/2010/0061/B

Anochie-Boateng, J., Komba, J and O'Connell, J. (2011a). *Laser-based approach for determining flakiness index of aggregates used in pavements*. 30th Southern Africa Transportation Conference, Pretoria, South Africa, July 2011.

Anochie-Boateng, J., Komba, J and G.M. Mvelase (2011b). *Advanced and Automated Laser-based Technique to Evaluate Aggregates*. IRF International Road Congress "Innovation in Road Infrastructure", November 2011, Moscow, Russia.

Anochie-Boateng, J.K., Komba, J. and Tutumluer, E. (2012). *Aggregate surface areas quantified through laser measurements for South African asphalt mixtures*. ASCE J Transport Eng 2012; **138** (8):1–11.

Arslan, H., Baykal, G. and Sture, S. (2009). Analysis of the influencing of crushing on the behaviour of granular materials under shear. *Granular Matter*, **11**, 87 - 97

Bouquety, M.N., Descantes, Y., Barcelo, L., de Larrard, F. and Clavaud, B. (2006). Automated measurement of aggregate properties: Part 2 – flakiness index. *Materials and Structures*, **39**(1), 13 – 19

Cernica, J.N. (1982). *Geotechnical Engineering*, Holt-Saunders International Editions, New York, 488pp

COLTO (Committee of Land Transport Officials) (1998). Standard Specifications for Road and Bridge Works for State Road Authorities. South African Institute of Civil Engineers (SAICE)

Craig, R.F. (1997). *Soil Mechanics 6<sup>th</sup> Edition*. Spon Press, London and New York, 485pp

Descantes, Y., Fosse, Y. and Ehret, G. (2003). Automated measurement of aggregate properties: Part 1 – Crushed and broken surfaces in coarse aggregate particles. *Materials and Structures*, **39**(1), 3 - 12

Dunlevey, J.N. and Stephens, D.J. (1994). Crushed Natal Group sandstone used as coarse aggregate. *SAICE Journal*, **36**(3), 11 – 17

Dunlevey, J.N., Stephens, D.J. (1995). The use of Dwyka Group diamictite as crushed aggregate in Natal. *SAICE Journal*, **37**(2), 11 - 16

Dunlevey, J.N. and Stephens, D.J. (1996). The use of crushed Karoo dolerite aggregate in KwaZulu-Natal. *SAICE Journal*, **38**(4), 33 – 40

Fernlund, J.M.R. (2005). Image analysis method for determining 3-D size distribution of coarse aggregates. *Bulletin of Engineering Geology and the Environment*, **64**(2), 159 - 166

Fletcher, T., Chandan, C., Masad, E. and Sivakumar, K. (2002). *Aggregate Imaging System (AIMS) for Characterizing the shape of Fine and Coarse Aggregate*. A paper submitted to the 82<sup>nd</sup> Annual Transportation Research Board for presentation and presentation, submitted July 2002

Griffith, A.A. (1921). The phenomenon of rupture and flow in solids. *Philosophical Transactions of the Royal Society of London*, A 221: 163 - 198

Henderson, R., Herrington, P., Patrick, J., Kathirgamanathan, P. and Cook, S. (2011). Analysis of Particle Orientation in Compacted Unbound Aggregate. *Road Materials and Pavement Design*, **12**(1), 115 - 127

- Ken, C., Pan, Z. and Xuemei, Z. (2009). A description method for arbitrarily shaped and sized granules in 2D image. *Journal of Electronics (China)*, **26**(3), 423 – 427
- Kim, H., Haas, C.T. and Rauch, A.F. (2003). 3D Image Segmentation of Aggregates from Laser Profiling. *Computer-Aided Civil and Infrastructure Engineering*, **18**(4), 254 - 263
- Kujundžić, T., Bedeković, G., Kuhinek, D. and Korman, T. (2008). Impact of Rock Hardness on Fragmentation by Hydraulic Hammer and Crushing in Jaw Crusher. *The Mining Geological Petroleum Engineering Bulletin*, **20**(1), 83 – 90 (English translation)
- Ling, P.A.N.G., Shaopeng, W.U., Jiqing, Z.H.U. and Lu, W.A.N. (2010). Relationship between Retrographical and Physical Properties of Aggregates. *Journal of Wuhan University of Technology – Material Science Edition*, **25**(4), 678 – 681
- Maree, J.H. (1979). *Die gedrag en gebruik van korrlemateriaalkroonlae in plaveisel met dun bitumineuse oppervlaklae*. Proc. 3<sup>rd</sup> Conference on asphalt pavements for Southern Africa, Durban
- Mgangira, M.B. (2008). *Microstructural Pavement Material Characterization : Some Examples*. Southern African Transport Conference July 2008, Pretoria. ISBN 978-1-920017-34-7
- Miskovsky, K., Taborda Duarte, M., Kou, S. Q. and Linsqvist, P.-A. (2004). Influence of the Mineralogical Composition and Textural Properties on the Quality of Coarse Aggregate. *Journal of Materials Engineering and Performance*, **13**(2), 144 – 150
- Räisänen, M. and Mertamo, M. (2004). An evaluation of the procedure and results of laboratory crushing in quality assessment of rock aggregate raw materials. *Bulletin of Engineering Geology and the Environment*, **63**(1), 33 - 39
- Rao, C., Tutumluer, E. and Kim, I.T. (2002). *Quantification of Coarse Aggregate Angularity based on Image Analysis*. Transportation Research Record, No. 1787, TRB, National Research Council, Washington D.C., pp. 117 – 124

Rao, C., Pan, T. and Tutumluer, E. (2003). *Determination of Coarse Aggregate Surface Texture Using Image Analysis*. Proceedings of the Pavement Mechanics Symposium at the 16<sup>th</sup> ASCE Engineering Mechanics Division Conference, University of Washington, Seattle, July 2003

Semmelink, C.J. (1991). *The effect of material properties on the compactability of some untreated road building materials*. PhD thesis. University of Pretoria

Theyse, H.L. (2007). *A mechanistic-empirical design model for unbound granular pavement layers, Volume I*. PhD thesis. University of Johannesburg

TMH1 (Technical Methods for Highways) (1986). *Standard Methods of Testing Road Construction Materials*. 2<sup>nd</sup> Edition. National Institute for Transport and Road Research of the Council for Scientific and Industrial Research, Pretoria, South Africa, 232pp

Tons, E. and Goetz, W.H. (date unknown, presumably 1967). *Packing Volume Concept for Aggregates*. Purdue University (publishing information not supplied)

Weinert, H.H. (1980). *The Natural Road Construction Materials of Southern Africa*. Academia, Pretoria, 298pp

Zeghal, M. (2009). The Impact of Grain Crushing on Road Performance. *Geotechnical and Geological Engineering*, **27**(4), 549 - 558



## List of Addenda

The following Addenda are contained on a compact disc is the rear cover of this thesis:

Addendum A: CSIR Laboratory Results for Bulk Sample Analyses

Addendum C: Scan Data (Rapidform Software required to view data)

Addendum D: Master Data Set

Addendum E: Data for “6.7mm Example”

Addendum F: Data for “9.5mm Example”

Addendum G: Data for “Tillite Comparison”

Addendum H: Data for *aggregate texture value* calculation

## **Addendum B: Thin Section Review of Rock Structures**

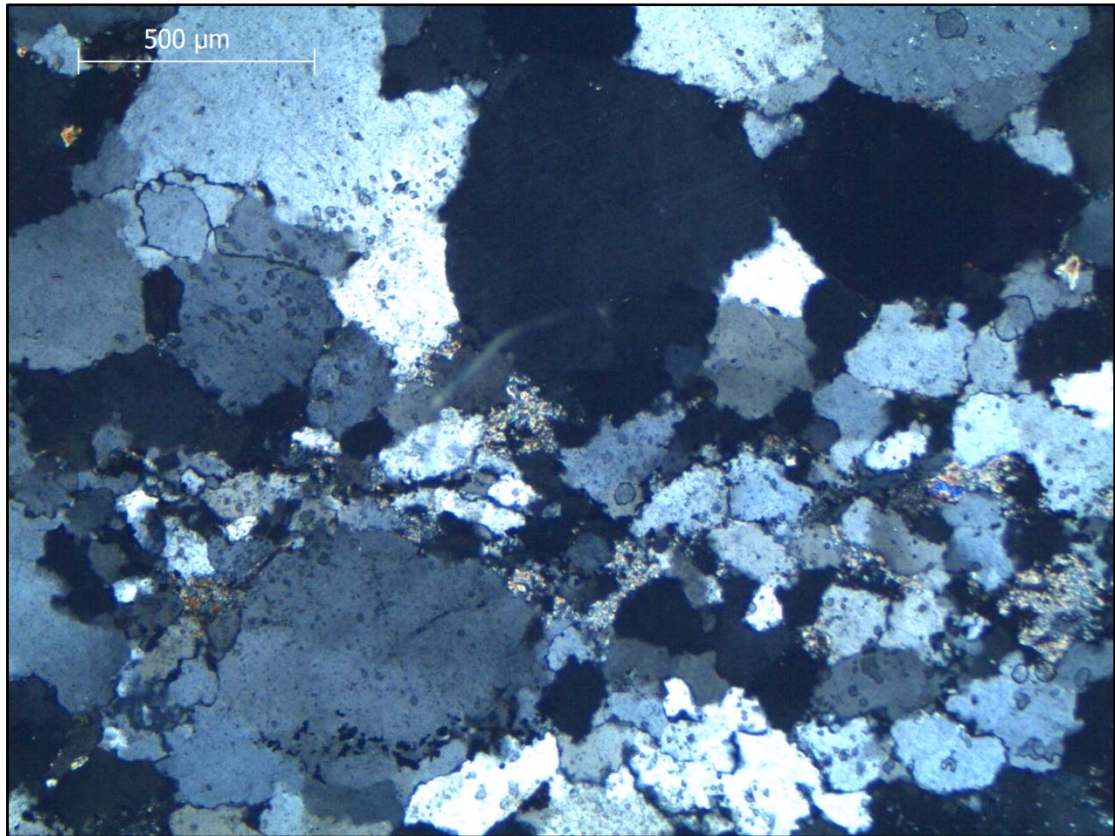
A short description of the thin sections made of each material selected for the research is provided. The emphasis of the thin section study was not focussed on a detailed analysis of mineralogical composition or alteration, but rather on any grain properties or other structural features that could be observed and may potentially affect fracturing of particles.

### *B.1 Sample 1 - Quartzite*

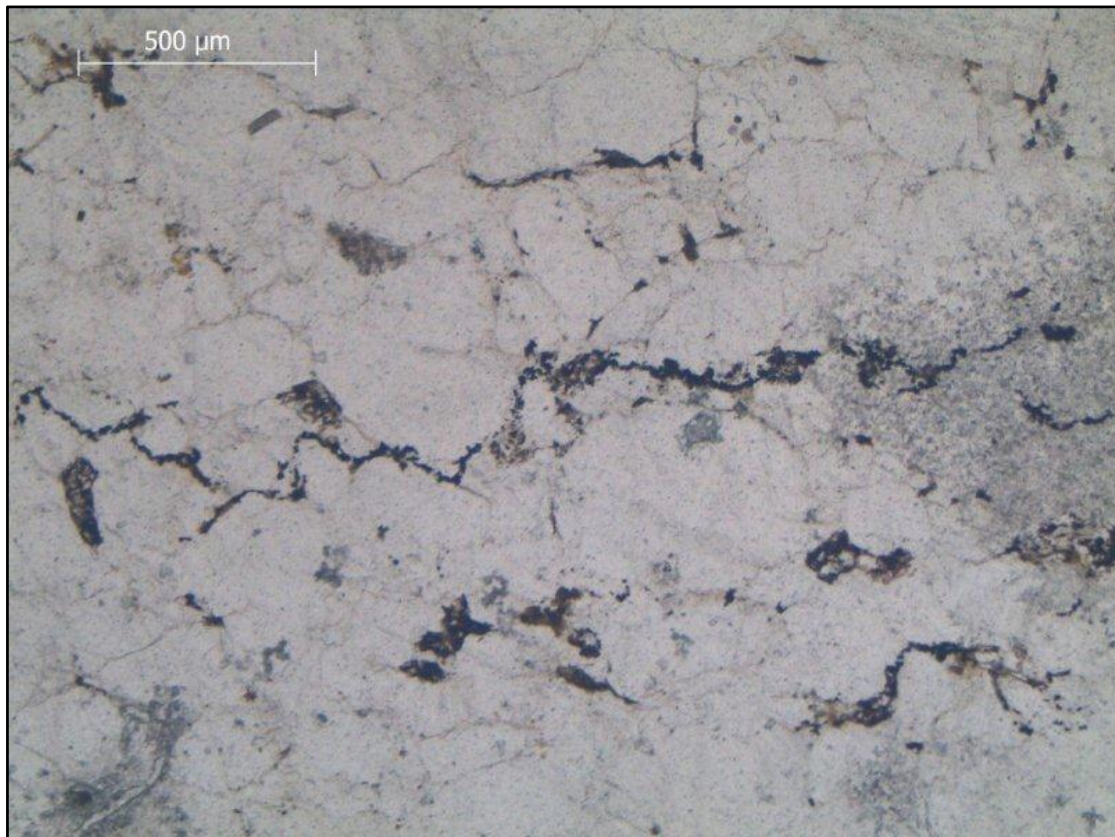
As is to be expected, the quartzite material consisted largely of amorphous, interlocking quartz grains. The quartzite had two predominant structural features, the first being occasional laminations and the second micro-cracks.

The laminations are ascribed to the depositional process of the grains. Laminations are usually observed in hand specimen as stripes or bands in the sample which mostly occur as alternating darker and lighter “layers”. Under magnification it is clear that the laminations also differ significantly in different grain size. Figure B.1 illustrates the difference in grain sizes in one of the laminations under magnification. The photo was taken under cross-polarised light to better emphasise the mineral grains.

The second feature observed was clearly visible under plain light and is illustrated in Figure B.2. Certain mineral boundaries were found to be cracked and subsequently filled with likely hydrothermal minerals which are clearly visible as black and dark grey lines following the mineral boundaries. Light grey areas (centre right border and bottom left border) resulted from air bubbles forming in the sealed thin section and have no relevance here. It must be emphasised that the cracks and hydrothermal filling are related to the genesis or later metamorphism of the material. The fact that micro-cracks contained filling materials suggests that they formed as part of the genesis of the rock and not as a result of blasting. It is probable that such micro-cracks will present a preferred failure plane during blasting and crushing, as they are weak in comparison with the interlocking mineral mass of the remaining material.



**Figure B.1** Grain size differences in quartzite laminations



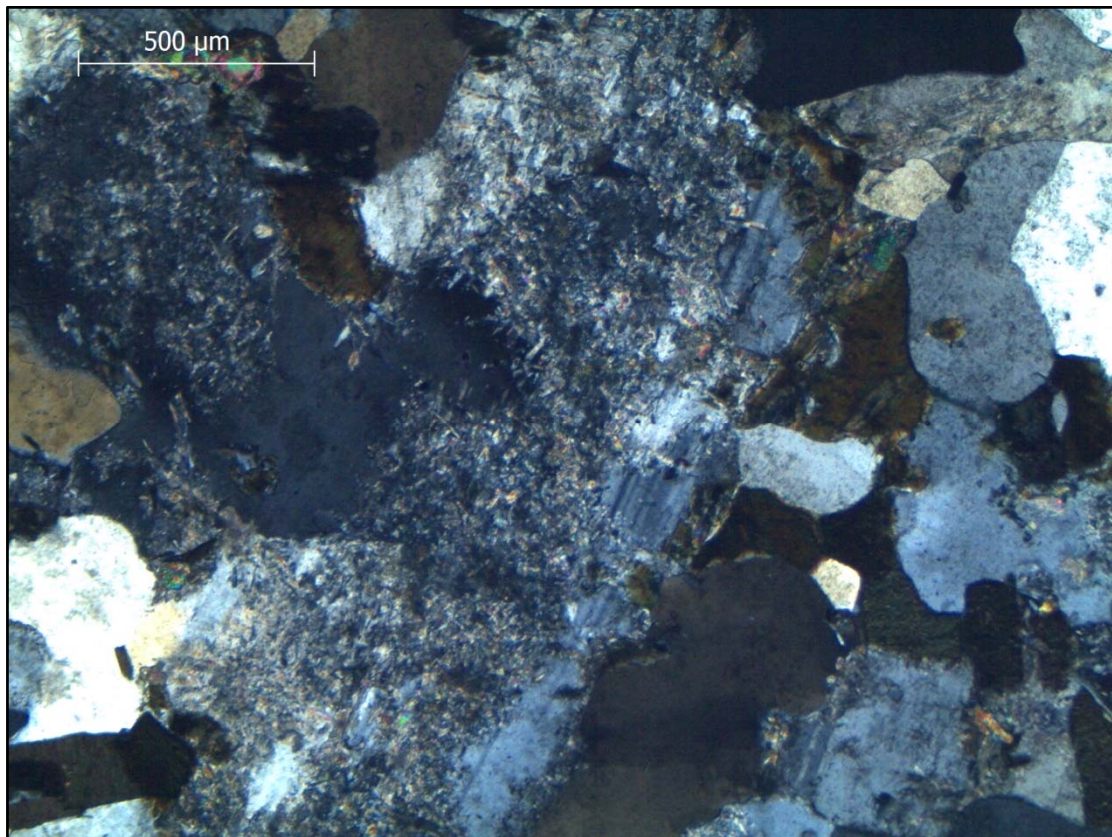
**Figure B.2** Micro-cracks in quartzite



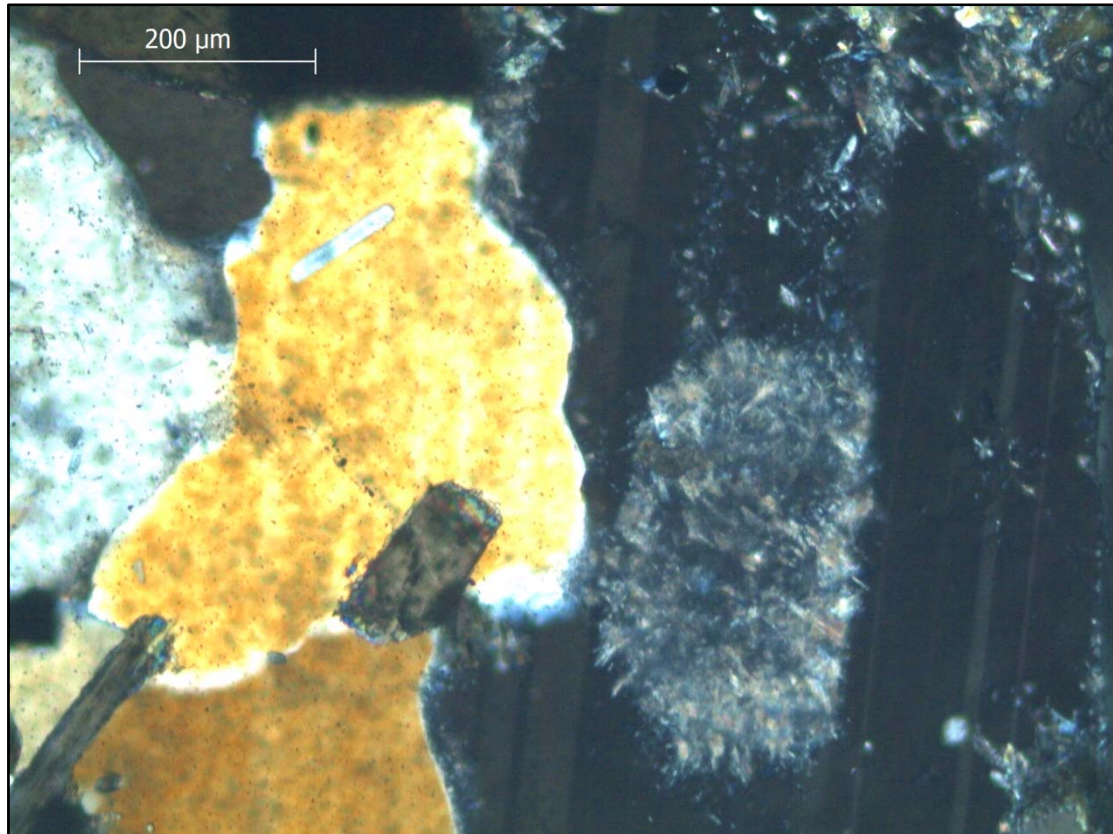
## B.2 Sample 2 - Granite

The granite sample did not reveal significant micro-cracking or any signs of preferential breaking; however, there was clear alteration in much of the plagioclase. Preferential alteration had progressed significantly in the plagioclase minerals, while the remaining minerals showed significantly less weathering (and quartz grains were unweathered). The alteration (or weathering) of the plagioclase minerals was not limited to the mineral boundaries, but frequently occurred in the centre of the mineral body. Figure B.3 illustrates plagioclase which has been significantly weathered in the centre of the mineral, whilst Figure B.4 shows the clear difference between the (peripheral) weathering of plagioclase and the unweathered quartz.

With the above properties considered, it is likely that aggregate breakage may be more pronounced through the (weaker) weathered plagioclase minerals or mineral boundaries.



**Figure B.3** Preferential weathering of plagioclase



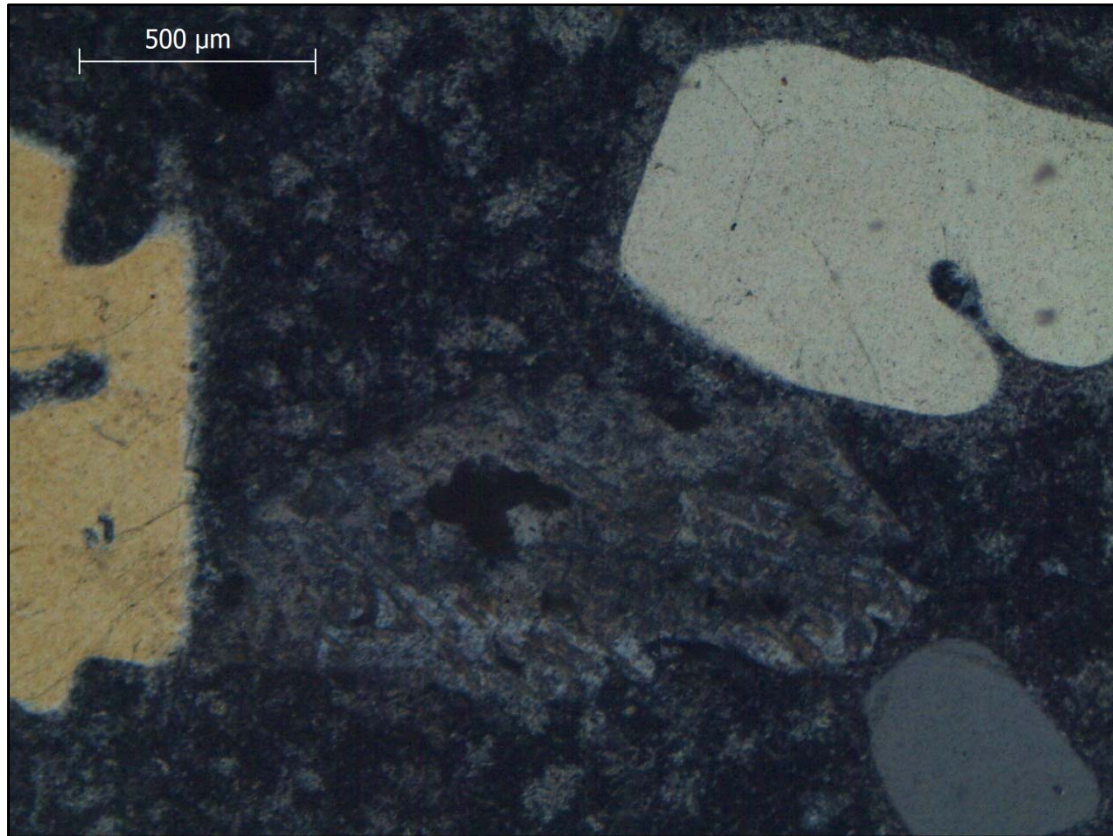
**Figure B.4** Weathered plagioclase and unweathered quartz

Observations made in hand specimen very often (but not always) showed that particles broke preferentially along mineral grain boundaries. Clearly the random orientation of minerals in the rock matrix does not allow for absolutely clean breaks along all mineral boundaries.

### *B.3 Sample 3 - Quartz porphyry*

The quartz porphyry was found to have a very fine matrix with predominantly quartz minerals and lesser plagioclase. The quartz particles were fairly rounded or euhedral. As with the granite sample, plagioclase showed some alteration, while the quartz particles were unaltered. It is likely that the smooth particle boundaries of the quartz will result in propagation of any cracks induced by crushing or blasting, resulting in material breakage along particle borders (this was also visible in hand specimen). Figure B.5 shows the shape of some quartz particles, as well as a poorly defined plagioclase particle which has been altered.

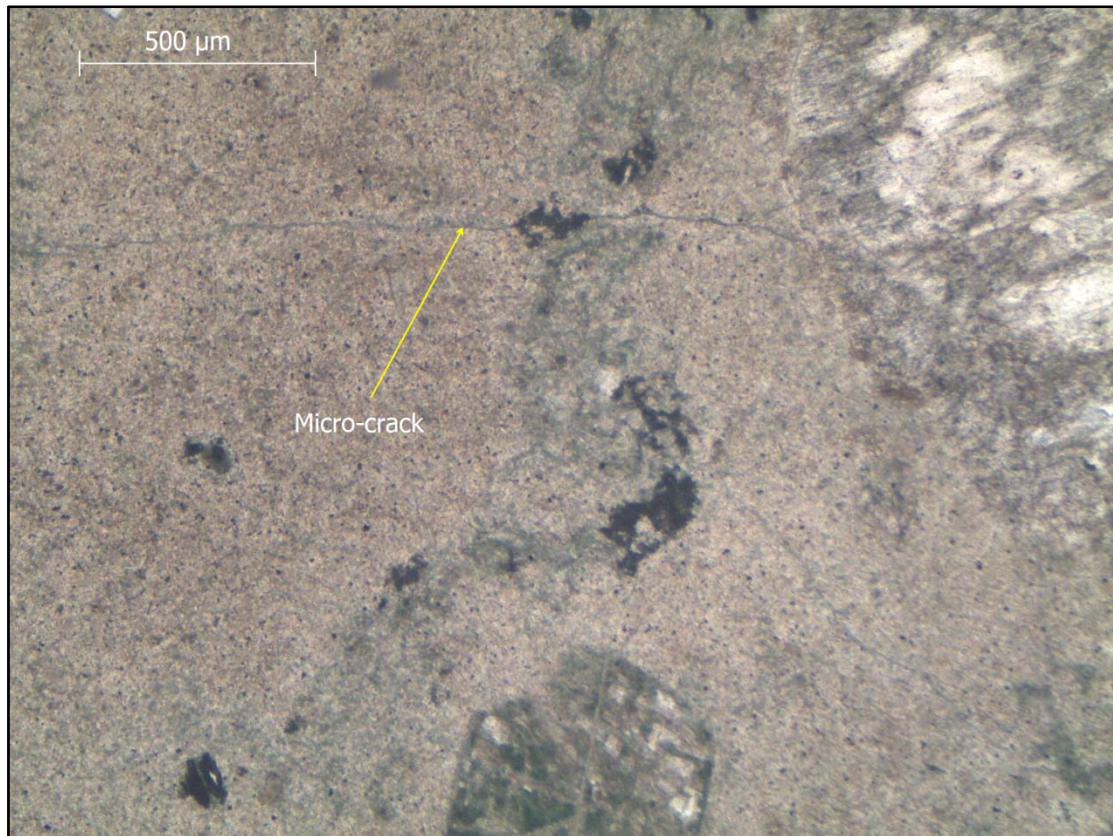




**Figure B.5** Quartz particles in a fine matrix

The thin section of the quartz porphyry also revealed a very distinctive micro-crack which runs through the matrix itself. The crack appears to have been subjected to some weathering and alteration as is evident by the green discolouration shown in Figure B.6 and may possibly have been a thermal fracture formed during the cooling of the magma.

It was notable in hand specimen that particles mostly broke through the fine matrix and did not show any particular preference to break along the larger mineral boundaries. In fact, broken hand specimens mostly showed that particles broke right through discernible minerals. (The opposite trend was later observed in the dolerite where breakage along amygdale borders resulted in small pits in one particle and the inclusion of the entire amygdale in the separated particle).



**Figure B.6** Micro-crack in the quartz porphyry matrix

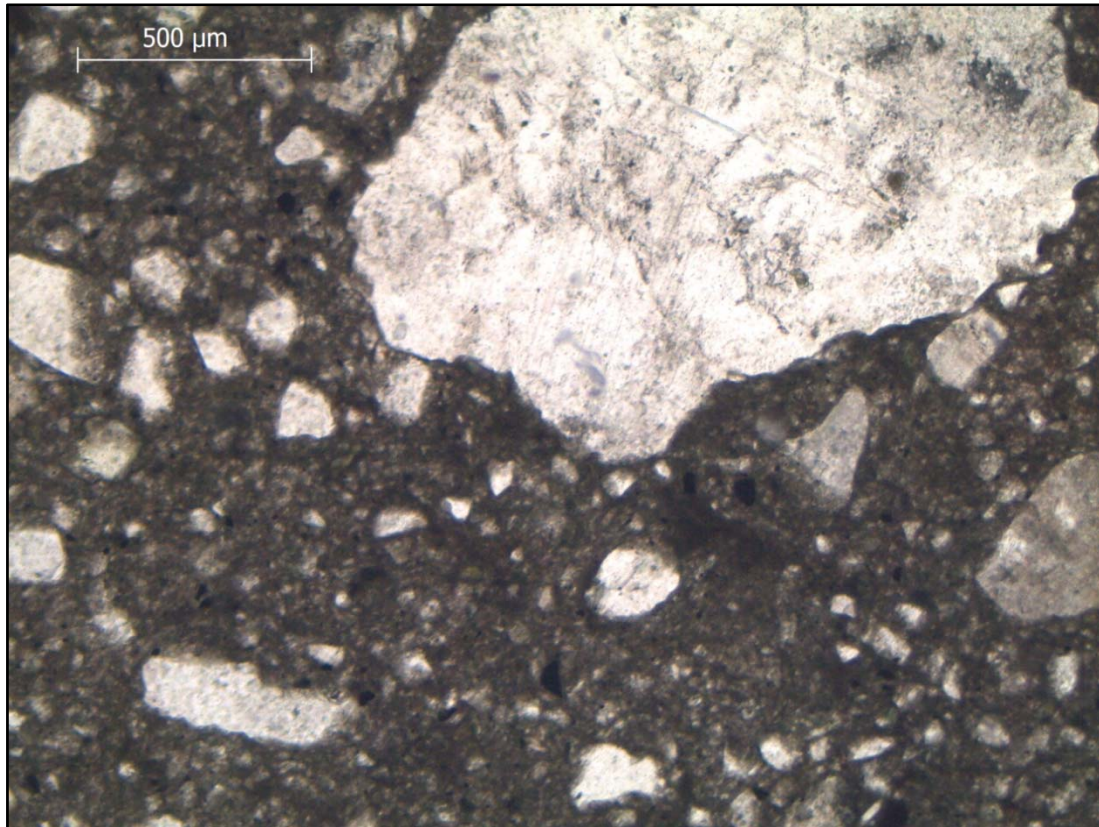
#### *B.4 Sample 4 - Tillite*

The tillite sample had a fine matrix with random mineral inclusions. The shape and size of minerals varied significantly and is a function of the depositional environment (glacial) from which the tillite originated. The matrix contained what appeared to be quartz fragments and scattered plagioclase fragments (a single granite erratic was found in one tillite particle during a later stage of the research). Of interest is that the plagioclase particles tended to be larger than the quartz particles. Figure B.7 shows the material as magnified under normal light. The fine matrix is clearly visible with quartz grains (smaller white minerals) and plagioclase (large white mineral). No structural features were discernible.

#### *B.5 Sample 5 - Hornfels*

The hornfels sample revealed a fine matrix with an array of minerals in its make-up. The metamorphic material showed no structural features, but instead comprised only a mass of





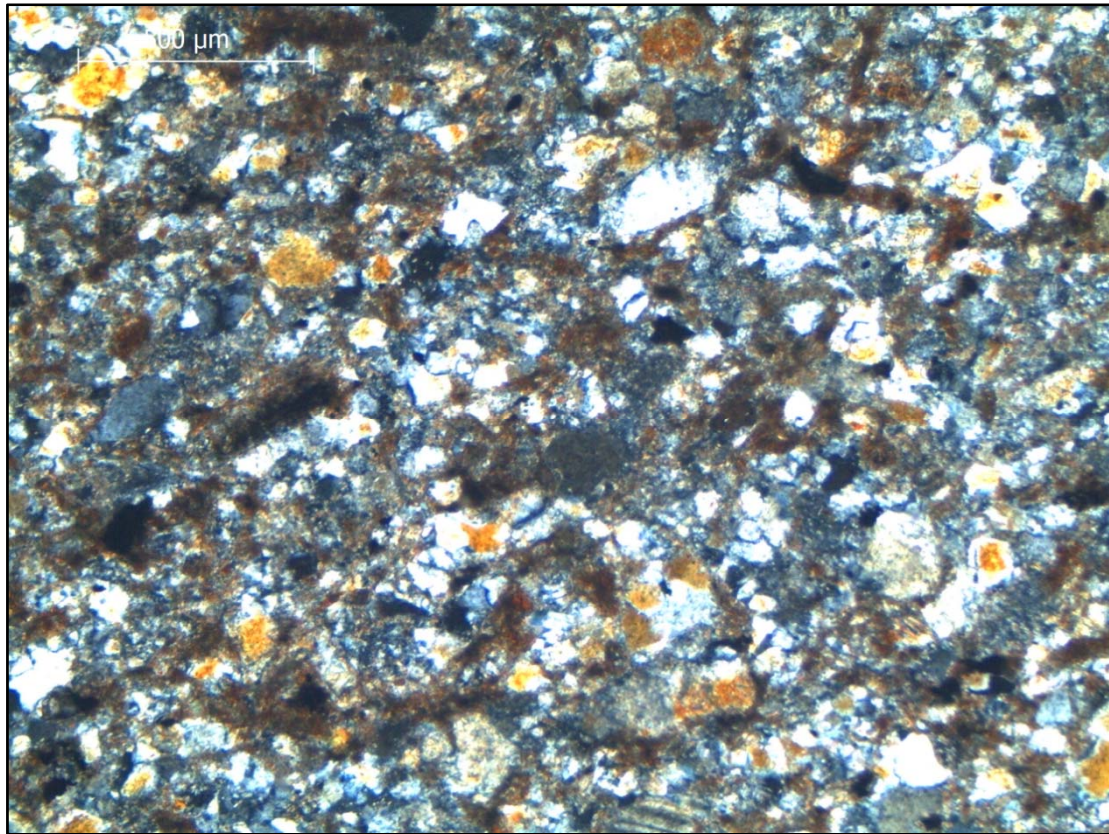
**Figure B.7** Typical tillite matrix

accumulated particles from random origins in random orientations. The lack of any continuous structural features is illustrated in Figure B.8.

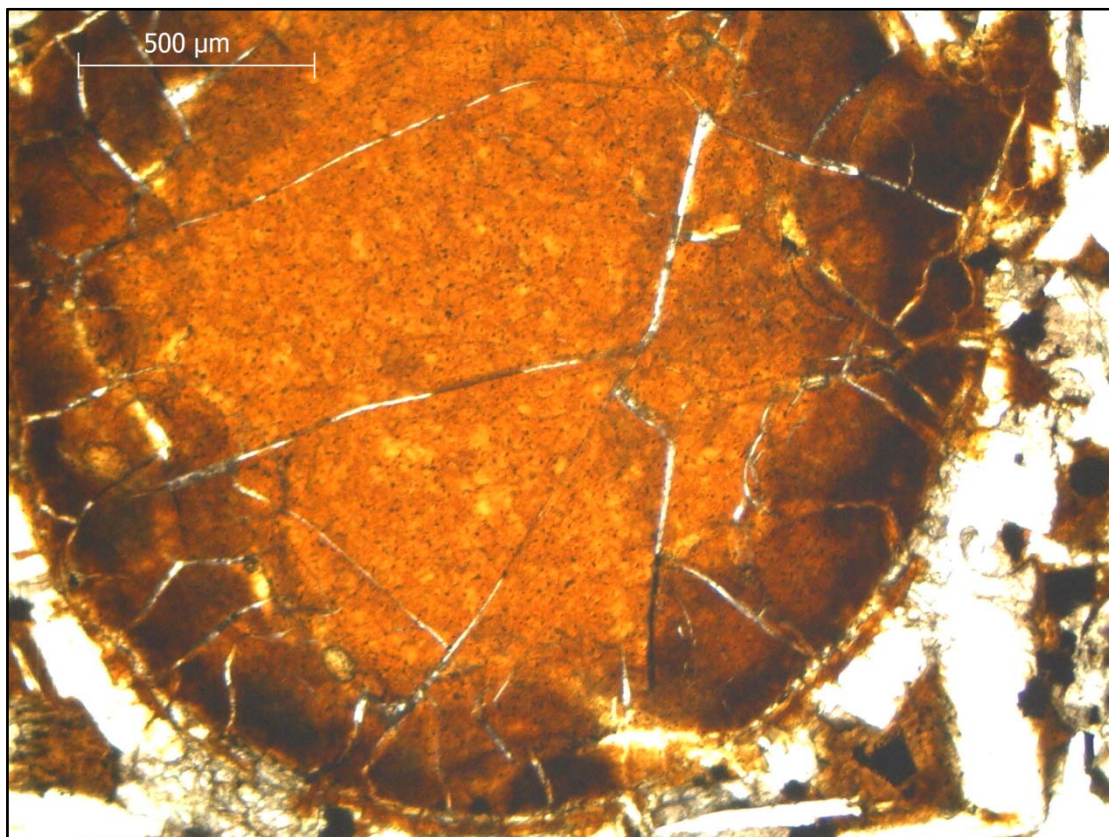
#### *B.6 Sample 6 - Dolerite*

Two main influencing features were identified in the thin section cut from the dolerite sample. The first feature (which was also noted in hand specimen) is the occurrence of amygdales in the rock matrix. From the hand specimens it was clear that breaking or cracking in the rock frequently propagates along the boundaries of the amygdales, often resulting in a pitted texture in the broken face. The thin section analysis showed that the amygdales were largely broken out of the sample during polishing; however a few structures were retained. Figure B.9 shows one such feature which is clearly cracked throughout the centre and less so along the periphery. It can, however, not be substantiated whether these cracks are the result of sample preparation or whether the cracks were inherent in the amygdales due to hydration-related shrinkage.





**Figure B.8** No structural features in the hornfels sample

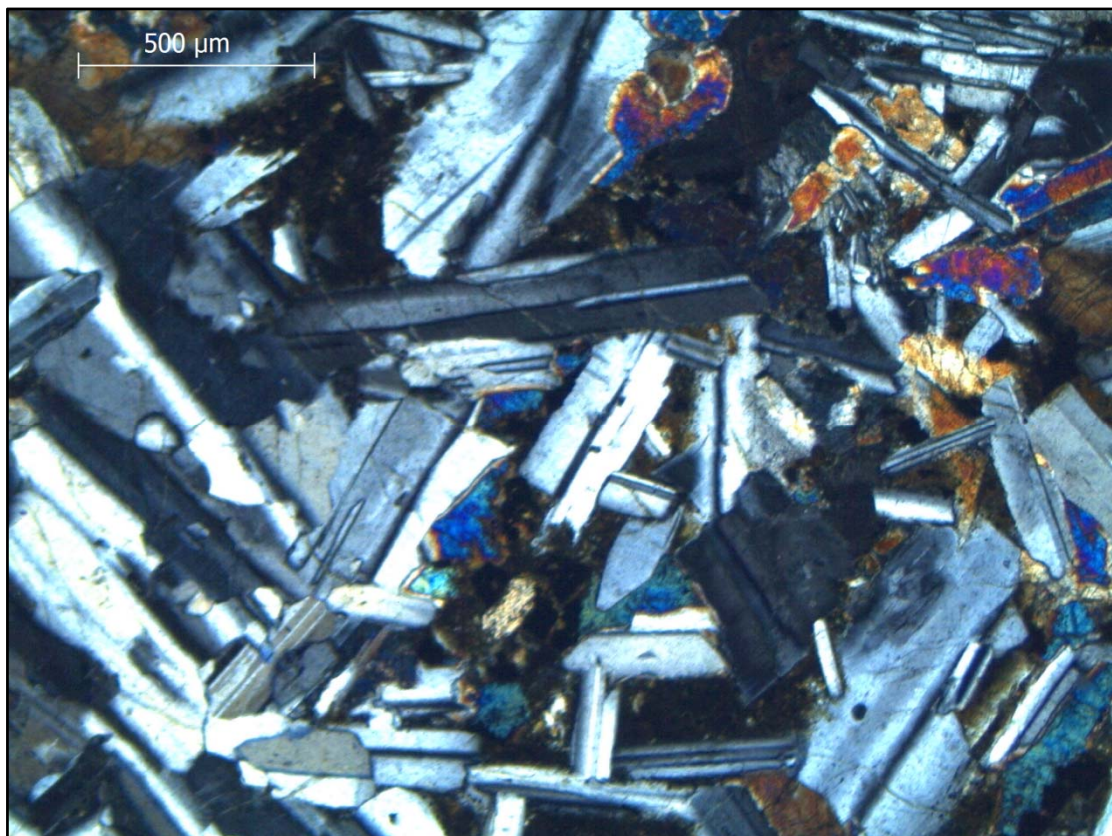


**Figure B.9** Cracked amygdale in dolerite matrix

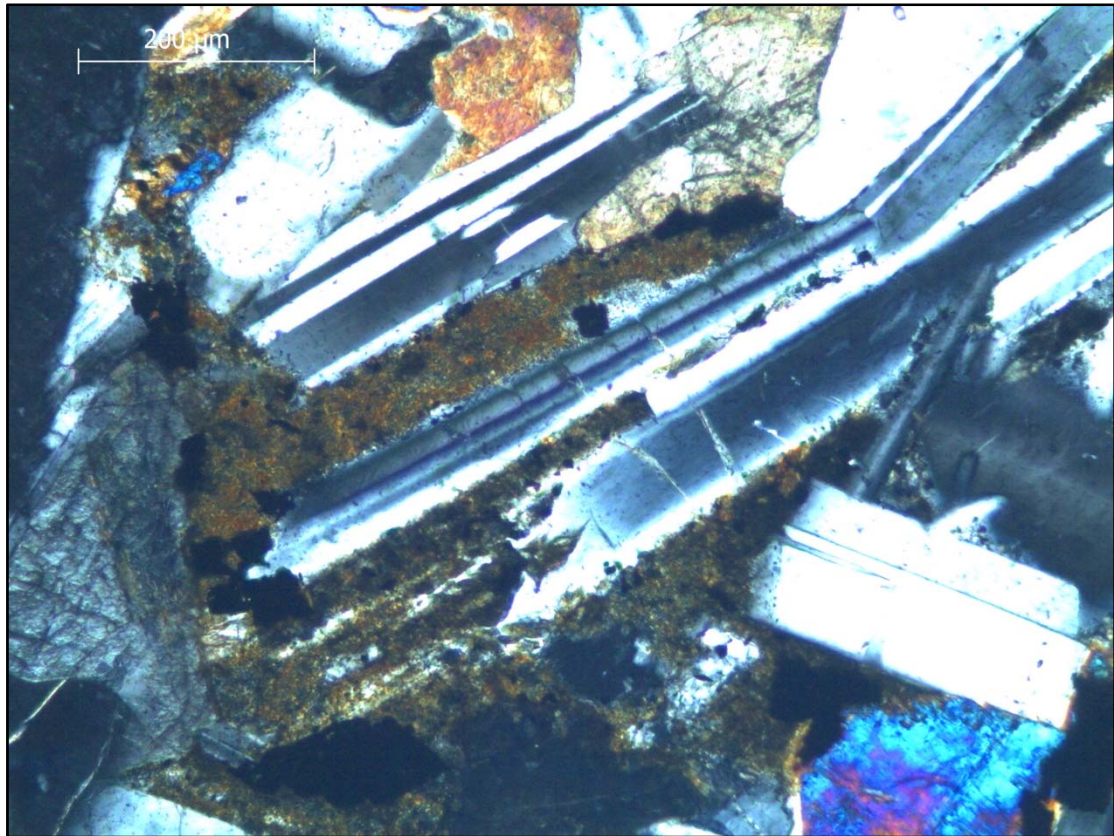


Apart from the amygdales, the rock texture is largely dictated by the characteristic elongated plagioclase crystals (Figure B.10). These elongated crystal structures were visible even to the naked eye or with the aid of a hand lens, but were not as pronounced as for example a spinifex texture would be. In many places the plagioclase showed preferential weathering, as also observed with other materials (Figure B.11). It was sometimes found that one particular blade of the plagioclase's lamina showed extensive weathering, while the second showed virtually none. The reason for this is not clear (possibly related to its orientation or exposure to the elements), but such a preferentially weathered plane would present a preferred (i.e. weaker) area along which particle breakage would occur.

Note: Any localised weakness in the rocks, weathering, fractures, disconnected amygdales, weak particle contacts, etc. would facilitate fracture according to Griffith's failure criterion and theory of crack propagation.



**Figure B.10** Elongated plagioclase crystals in dolerite



**Figure B.11** Preferential weathering of plagioclase in dolerite